Aqueous SOA formation from the <u>direct</u> photo<u>sensitized</u> ~~-~~oxidation of vanillin <u>in the absence and presence of ammonium nitrate</u>~~: Direct photosensitized reactions and nitrate-mediated reactions~~

Beatrix Rosette Go Mabato[1], Yan Lyu[1], Yan Ji[1], Yong Jie Li[2], Dan Dan Huang[3], Xue Li[4], Theodora Nah[1], Chun Ho Lam[1], and Chak K. Chan[1]*

[1]School of Energy and Environment, City University of Hong Kong, Hong Kong, China
[2]Department of Civil and Environmental Engineering, and Centre for Regional Ocean, Faculty of Science and Technology, University of Macau, Macau, China
[3]Shanghai Academy of Environmental Sciences, Shanghai 200233, China
[4]Institute of Mass Spectrometry and Atmospheric Environment, Jinan University No. 601 Huangpu Avenue West, Guangzhou 510632, China

Correspondence to: Chak K. Chan (Chak.K.Chan@cityu.edu.hk)

Abstract. Vanillin (VL), a phenolic aromatic carbonyl abundant in biomass burning emissions, forms triplet excited states (^{3}VL*) under simulated sunlight leading to aqueous secondary organic aerosol (aqSOA) formation. <u>Nitrate and ammonium are among the main components of biomass burning aerosols and cloud/fog water. Under atmospherically relevant cloud and fog conditions, solutions composed of either VL only or VL with ammonium nitrate were subjected to simulated sunlight irradiation to compare aqSOA formation via the direct photosensitized oxidation of VL in the absence and presence of ammonium nitrate. The reactions were characterized</u> ~~This direct photosensitized oxidation of VL was compared with nitrate-mediated VL photo-oxidation under atmospherically relevant cloud and fog conditions through~~<u>by</u> examining the VL decay kinetics, product compositions, and light absorbance changes. ~~The majority of the most abundant products from both VL photo-oxidation pathways were potential Brown carbon (BrC) chromophores. In addition,~~ <u>B</u>~~B~~oth ~~pathways~~ <u>conditions</u> generated oligomers, functionalized monomers, and oxygenated ring-opening products, <u>and ammonium</u> ~~but~~ nitrate promoted functionalization and nitration, ~~which can be ascribed~~<u>likely due</u> to its photolysis products ($^•$OH, $^•$NO$_2$, and ~~N(III),~~ <u>NO$_2^-$ or</u> HONO). Moreover, a potential imidazole derivative observed ~~from nitrate-mediated VL photo-oxidation~~<u>in the presence of ammonium nitrate</u> suggested that ammonium ~~may be involved~~<u>participated</u> in the reactions. <u>The majority of the most abundant products from both conditions were potential Brown carbon (BrC) chromophores.</u> The effects of oxygen (O$_2$), pH, and reactants concentration and molar ratios on ~~VL photo-oxidation~~<u>the reactions</u> were also explored. Our findings show that O$_2$ plays an essential role in ~~VL photo-oxidation,~~<u>the reactions,</u> and oligomer formation was enhanced at pH < 4. Also, functionalization was dominant at low VL concentration, whereas oligomerization was favored at high VL concentration. Furthermore, <u>oligomers and hydroxylated products were detected from the oxidation of</u> ~~comparisons of the apparent quantum efficiency of~~ guaiacol <u>(a non-carbonyl phenol) via VL photosensitized reactions</u> ~~photodegradation indicate that in this study, guaiacol~~

33 ~~oxidation by photosensitized reactions of VL is less efficient relative to nitrate-mediated photo-oxidation~~. Lastly, potential

34 aqSOA formation pathways via the direct photosensitized oxidation of VL in the absence and presence of ammonium nitrate

35 ~~VL photo-oxidation~~ were proposed. This study indicates that the direct photosensitized oxidation of VL ~~and nitrate-mediated~~

36 ~~VL photo-oxidation~~ may be an important aqSOA source~~s~~ in areas influenced by biomass burning ~~emissions~~ and underscores

37 the importance of nitrate in the aqueous-phase processing of aromatic carbonyls.

38

39

40

1 Introduction

42 Aqueous reactions can be an important source of secondary organic aerosols (SOA) (Blando and Turpin, 2000; Volkamer et

43 al., 2009; Lim et al., 2010; Ervens et al., 2011; Huang et al., 2011; Lee et al., 2011; Smith et al., 2014) such as highly-

44 oxygenated and low-volatility organics (Hoffmann et al., 2018; Liu et al., 2019) which may affect aerosol optical properties

45 due to contributions to Brown Carbon (BrC) (Gilardoni et al., 2016). BrC refers to organic aerosols that absorb radiation

46 efficiently in the near-ultraviolet (UV) and visible regions (Laskin et al., 2015). The formation of aqueous SOA (aqSOA) via

47 photochemical reactions involves oxidation, with hydroxyl radical ($^{\bullet}$OH) usually considered as the primary oxidant (Herrmann

48 et al., 2010; Smith et al., 2014). The significance of photosensitized chemistry in atmospheric aerosols has recently been

49 reviewed (George et al., 2015). For instance, triplet excited states of organic compounds (^{3}C*) from the irradiation of light-

50 absorbing organics such as non-phenolic aromatic carbonyls (Canonica et al., 1995; Anastasio et al., ~~1996~~1997; Vione et al.,

51 2006; Smith et al., 2014) have been reported to oxidize phenols at higher ~~faster~~ rates and with greater~~higher~~ aqSOA yields

52 compared to $^{\bullet}$OH (Sun et al., 2010; Smith et al., 2014; Yu et al., 2014; Smith et al., 2016). Aside from being an oxidant, ^{3}C*

53 can also be a precursor of singlet oxygen (^{1}O$_2$), superoxide (O$_2^{\bullet-}$) or hydroperoxyl ($^{\bullet}$HO$_2$) radical, and $^{\bullet}$OH (via HO$_2^{\bullet}$/O$_2^{\bullet-}$

54 formation) upon reactions with O$_2$ and substrates (e.g., phenols) (George et al., 2018). The ^{3}C* concentration in typical fog

55 water has been estimated to be > 25 times than that of $^{\bullet}$OH, making ^{3}C* the primary photo-oxidant for biomass burning phenolic

56 compounds (Kaur and Anastasio, 2018; Kaur et al., 2019). Recent works on triplet-driven oxidation of phenols have mainly

57 focused on changes of physicochemical properties (e.g., light absorption) and aqSOA yield (e.g., Smith et al., 2014, 2015,

58 2016), with few reports on reaction pathways ~~mechanisms~~ and ~~characterization of reaction~~ products (e.g., Yu et al., 2014; Chen

59 et al., 2020; Jiang et al., 2021).

60 Inorganic salts such as ammonium nitrate are~~is a~~ major component~~s~~ of aerosols and cloud/fog water. In cloud and fog

61 water, the concentrations of inorganic nitrate can vary from 50 μM to > 1000 μM, with higher levels typically noted under

62 polluted conditions (Munger et al., 1983; Collett et al., 1998; Zhang and Anastasio, 2003; Li et al., 2011; Giulianelli et al.,

63 2014; Bianco et al., 2020). Upon photolysis (Vione et al., 2006; Herrmann, 2007; Scharko et al., 2014), inorganic nitrate in

64 cloud and fog water can contribute to BrC (Minero et al., 2007) and aqSOA formation (Huang et al., 2018; Klodt et al., 2019;

65　Zhang et al., 2021) by generating $^\bullet$OH and nitrating agents (e.g., $^\bullet$NO$_2$). For example, the aqSOA yields from the photo-

66　oxidation of phenolic carbonyls in ammonium nitrate are twice as high as that in ammonium sulfate solution (Huang et al.,

67　2018). Nitration is a significant process in the formation of light-absorbing organics or BrC in the atmosphere (Jacobson, 1999;

68　Kahnt et al., 2013; Mohr et al., 2013; Laskin et al., 2015; Teich et al., 2017; Li et al., 2020). Moreover~~Furthermore~~, nitrate

69　photolysis has been proposed to be a potentially important process for SO$_2$ oxidation and SOA formation via the generation of

70　$^\bullet$OH, $^\bullet$NO$_2$, and N(III) within particles (Gen et al., 2019a, 2019b; Zhang et al., 2020, 2021), and it can also potentially change

71　the morphology of atmospheric viscous particles (Liang et al., 2021). Furthermore, ammonium (NH$_4^+$) can react with carbonyls

72　producing light-absorbing compounds and highly oxygenated oligomers, as well as catalyze different reactions (De Haan et

73　al., 2009, 2011; Nozière et al., 2009, 2010, 2018; Shapiro et al., 2009; Yu et al., 2011; Lee et al., 2013; Powelson et al., 2014;

74　Gen et al., 2018; Mabato et al., 2019). Accordingly~~Therefore~~, ~~both~~ ^{3}C* and inorganic nitrate can contribute to aqSOA and BrC

75　formation.

76　　　　Biomass burning (BB) is a significant atmospheric source of both phenolic and non-phenolic aromatic carbonyls

77　(Rogge et al., 1998; Nolte et al., 2001; Schauer et al., 2001; Bond et al., 2004). Upon exposure to sunlight, aromatic carbonyls

78　are excited to their triplet excited states, which can initiate oxidation leading to aqSOA formation (e.g., Smith et al., 2014;

79　2015, 2016). ~~For~~ An example ~~is~~, vanillin (VL) (Henry's law constant of 4.56×10^5 M atm^{-1}; Yaws, 1994), a phenolic aromatic

80　carbonyl that has been used as a model compound for methoxyphenols, ~~~which~~ which are abundant in BB emissions (Li et al., 2014;

81　Pang et al., 2019a). The aqueous $^\bullet$OH oxidation and direct photodegradation of VL~~,~~ ~~has~~ have been shown to yield low-volatility

82　products, although these findings were based on 254-nm irradiation (Li et al., 2014) ~~via aqueous $^\bullet$OH oxidation and direct~~

83　~~photodegradation~~. Photodegradation kinetics and aqSOA yields have been reported for direct VL photodegradation under

84　simulated sunlight (Smith et al., 2016), with oxygenated aliphatic-like compounds (high H:C, $\geq$ 1.5 and low O:C, $\leq$ 0.5 ratios)

85　~~reported~~ noted as the most likely products (Loisel et al., 2021). Additionally, aqueous-phase reactions of phenols with reactive

86　nitrogen species have been proposed to be a significant source of nitrophenols and SOA (Grosjean, 1985; Kitanovski et al.,

87　2014; Kroflič et al., 2015, 2021; Pang et al., 2019a; ~~Kroflič et al., 2021;~~ Yang et al., 2021). For instance, nitrite-mediated VL

88　photo-oxidation can generate nitrophenols, and the reactions are influenced by nitrite/VL molar ratios, pH, and the presence

89　of $^\bullet$OH scavengers (Pang et al., 2019a). Nitrate and ammonium are also among the main biomass burning aerosol components

90　(Xiao et al., 2020; Zielinski et al., 2020). As BB aerosols are typically internally mixed with other aerosol components

91　(Zielinski et al., 2020), VL may coexist with ammonium nitrate in BB aerosols. The ~~aqueous-phase photo-oxidation~~ direct

92　photosensitized oxidation of VL in the absence and presence of ammonium nitrate may then reveal insights into the

93　atmospheric processing of BB aerosols. Moreover, the ^{3}C* of non-phenolic aromatic carbonyls (e.g., 3,4-

94　dimethoxybenzaldehyde, DMB; a non-phenolic aromatic carbonyl) (Smith et al., 2014; Yu et al., 2014; Jiang et al., 2021) and

95　phenolic aromatic carbonyls (e.g., acetosyringone, vanillin) (Smith et al., 2016) have been shown to oxidize phenols, but the

96　reaction products from the latter are unknown.

97

98   Previous works on aqSOA formation via triplet-mediated oxidation are mostly based on reactions between phenols
99   and a non-phenolic aromatic carbonyl as triplet precursor (e.g., Smith et al., 2014; Yu et al., 2014; Jiang et al., 2021). Also,
100 studies examining the effects of inorganic nitrate on aqSOA formation and properties remain limited. The present study aimed
101 to evaluate aqSOA formation via the direct photosensitized oxidation of a triplet precursor (VL) alone. Furthermore, aqSOA
102 formation via the direct photosensitized oxidation of VL in the presence of ammonium nitrate was also examined. Accordingly,
103 the main goals of this study are (1) to compare aqSOA formation in cloud/fog water via the direct photosensitized oxidation
104 of VL in the absence and presence of ammonium nitrate, (2) to evaluate the influences of O_2, solution pH, and reactants
105 concentration and molar ratios on the reactions, (3) to investigate the participation of ammonium in the direct photosensitized
106 oxidation of VL in the presence of ammonium nitrate, and (4) to examine aqSOA formation from the oxidation of guaiacol, a
107 non-carbonyl phenol, via photosensitized reactions of VL. To achieve these goals, solutions composed of either VL only or
108 VL in the presence of ammonium nitrate were subjected to simulated sunlight irradiation under atmospherically relevant cloud
109 and fog conditions. Solutions composed of VL in the presence of sodium nitrate were also examined for comparison with the
110 presence of ammonium nitrate. To evaluate the potential significance of VL and its reactions with nitrate in aqSOA formation
111 in cloud/fog water, we studied the direct photosensitized oxidation of VL and nitrate-mediated VL photo-oxidation under
112 atmospherically relevant conditions. In this work,The reactions were characterized based on VL decay kinetics, light
113 absorbance changes, and detected products, and light absorbance changes. The influences of O_2, solution pH, and reactants
114 concentration and molar ratios on these two photo-oxidation pathways were also assessed. The $^3C^*$ of non-phenolic aromatic
115 carbonyls (e.g., 3-4 dimethoxybenzaldehyde, DMB; a non-phenolic aromatic carbonyl) (Smith et al., 2014; Yu et al., 2014;
116 Jiang et al., 2021) and phenolic aromatic carbonyls (e.g., acetosyringone, vanillin) (Smith et al., 2016) have been shown to
117 oxidize phenols, but the reaction products from the latter are unknown. We then examined the photo-oxidation of guaiacol,
118 another non-carbonyl phenol, in the presence of VL and compared it with nitrate-mediated photo-oxidation. Finally, we
119 proposed aqSOA formation pathways via the direct photosensitized oxidation of VL in the absence and presence of ammonium
120 nitrateVL photo-oxidation. This work presents a comprehensive comparison of aqSOA formation from the direct
121 photosensitized oxidation of VL photo-oxidation in the absence and presence of ammonium nitrateby VL photosensitization
122 and in the presence of inorganic nitrate.
123
124
125 **2 Methods**
126 **2.1 Aqueous-_-phase photo-oxidation experiments**
127 Photo-oxidation experiments were performed in a custom-built quartz photoreactor. The solutions (initial volume of 500 mL)
128 were continuously mixed throughout the experiments using a magnetic stirrer. The solutions were bubbled with synthetic air
129 or nitrogen (N_2) (> 99.995%) (0.5 dm^3/min) for 30 min before irradiation to achieve air- orand N_2-saturated conditions,
130 respectively, and the bubbling was continued throughout the reactions (Du et al., 2011; Chen et al., 2020). The aim of the air-

4

131 saturated experiments was to enable the generation of secondary oxidants ($^1O_2$, $O_2^{\bullet-}$/$^\bullet HO_2$, $^\bullet OH$) from $^3VL^*$ as O_2 is present.

132 Conversely, the N_2-saturated experiments would inhibit the formation of these secondary oxidants, which can lead to $^3VL^*$-

133 driven reactions (Chen et al., 2020). Comparison of results of air and N_2-saturated experiments can yield information on the

134 reaction pathways that require O_2 involved in the direct photosensitized oxidation of VL. Solutions were irradiated through

135 the quartz window of the reactor using a xenon lamp (model 6258, Ozone free xenon lamp, 300 W, Newport) equipped with

136 a longpass filter (20CGA-305 nm cut-on filter, Newport) to eliminate light below 300 nm. Cooling fans positioned around the

137 photoreactor and lamp housing maintained reaction temperatures at 27 ± 2 °C. The averaged initial photon flux in the reactor

138 from 300 to 380 nm measured using a chemical actinometer (2-nitrobenzaldehyde) was 2.6×10^{15} photons cm^{-2} s^{-1} nm^{-1} (Fig.

139 S1). Although the concentration of VL in cloud/fog water has been estimated to be < 0.01 mM (Anastasio et al., ~~1996~~1997), a

140 higher VL concentration (0.1 mM) was used in this study to guarantee sufficient signals for product identification (Vione et

141 al., 2019). The chosen ammonium nitrate (AN) or sodium nitrate (SN) concentration (1 mM) was based on values observed in

142 cloud and fog water (Munger et al., 1983; Collett et al., 1998; Zhang and Anastasio, 2003; Li et al., 2011; Giulianelli et al.,

143 2014; Bianco et al., 2020). It should be noted that this study is not intended to identify the concentrations of ammonium nitrate

144 that would affect the kinetics but to examine the effect of ammonium nitrate on aqSOA formation from the direct

145 photosensitized oxidation of VL. Moreover, ~~comparisons were made between~~ the photo-oxidation of guaiacol (GUA) (0.1

146 mM), a non-carbonyl phenol, in the presence of VL (0.1 mM) was studied~~or AN (1 mM)~~. The GUA experiments allowed us

147 to examine aqSOA formation from the oxidation of phenols by $^3VL^*$. Samples (10 mL) were collected hourly for a total of 6

148 h for offline ~~optical and~~ chemical and optical analyses. ~~Absorbance measurements,~~ VL (and GUA) decay kinetics

149 measurements (calibration curves for VL and GUA standard solutions; Fig. S2), ~~small organic acids measurements, and~~

150 product characterization, small organic acids measurements, and a~~Absorbance measurements,~~ were conducted using ultra-

151 high-performance liquid chromatography with photodiode array detector (UHPLC-PDA), UHPLC coupled with quadrupole

152 time-of-flight mass spectrometry (UHPLC-qToF-MS) equipped with an electrospray ionization (ESI) source and operated in

153 the positive ion mode (the negative ion mode signals were too low for our analyses), ion chromatography (IC), and UV-Vis

154 spectrophotometry, ~~ultra-high-performance liquid chromatography with photodiode array detector (UHPLC-PDA), ion~~

155 ~~chromatography (IC), and UHPLC coupled with quadrupole time-of-flight mass spectrometry (UHPLC-qToF-MS) equipped~~

156 ~~with an electrospray ionization (ESI) source and operated in the positive ion mode (the negative ion mode signals were too~~

157 ~~low for our analyses),~~ respectively. Each experiment was repeated independently at least three times and measurements were

158 done in triplicate. The reported decay rate constants and absorbance enhancement are the average of results from triplicate

159 experiments, and the corresponding errors represent one standard deviation. The mass spectra are based on the average of

160 results from duplicate experiments. The Supporting Information (Text S1 to S6~~7~~) provides details on the materials and

161 analytical procedures. The pseudo-first-order rate constant (k') for VL decay was determined using the following equation

162 (Huang et al., 2018):

163

164 $$ln\,([VL]_t/[VL]_0) = -k't \qquad\qquad (Eq.\ 1)$$

5

165

166

where [VL]$_t$ and [VL]$_0$ are the concentrations of VL at time t and 0, respectively. Replacing VL with GUA in Eq. 1 enabled

the calculation of GUA decay rate constant. The decay rate constants were normalized to the photon flux measured for each

experiment through dividing k' by the measured 2-nitrobenzaldehyde (2NB) decay rate constant, j(2NB) (see Text S6 for more

details).

2.2 Calculation of normalized abundance of products

Comparisons of peak abundance in mass spectrometry have been used in many recent studies (e.g., Lee et al., 2014;

Romonosky et al., 2017; Wang et al., 2017; Fleming et al., 2018; Song et al., 2018; Klodt et al., 2019; Ning et al., 2019) to

show the relative importance of different types of compounds (Wang et al., 2021). However, ionization efficiency may greatly

vary for different classes of compounds (Kebarle, 2000; Schmidt et al., 2006; Leito et al., 2008; Perry et al., 2008; Kruve et

al., 2014), and so uncertainties may arise from comparisons of peak areas among compounds. In this work, we assumed equal

ionization efficiency of different compounds, which is commonly used to estimate O:C ratios of SOA (e.g., Bateman et al.,

2012; Lin et al., 2012; Laskin et al., 2014; De Haan et al., 2019), to calculate their normalized abundance. The normalized

abundance of a product, [P] (unitless), was calculated as follows:

$$[P] = \frac{A_{P,t}}{A_{VL,t}} \cdot \frac{[VL]_t}{[VL]_0} \qquad\qquad (Eq.\ 2)$$

where $A_{P,t}$ and $A_{VL,t}$ are the extracted ion chromatogram (EIC) peak areas of the product P and VL from UHPLC-qToF-MS

analyses at time t, respectively; [VL]$_t$ and [VL]$_0$ are the VL concentrations (μM) determined using UHPLC-PDA at time t and

0, respectively. Here, we relied on the direct quantification of [VL] using UHPLC-PDA (see Fig. S2 for VL calibration curve).

It should be notedWe emphasize that the normalized abundance of products in this study is a semi-quantitative analysis

intended to provide an overview of how the signal intensities changed under different experimental conditions but not to

quantify the absolute concentration of products. Also, as it is based on comparisons of peak abundance from UHPLC-qToF-

MS analyses, the normalized abundance of products in this study is associated with intrinsic uncertainties due to the variability

in ionization efficiencies for various compounds. Moreover, the major products detected in this study are probably those with

high concentration or high ionization efficiency in the positive ESI mode. The use of relative abundance (product peaks are

normalized to the highest peak) (e.g., Lee et al., 2014; Romonosky et al., 2017; Fleming et al., 2018; Klodt et al., 2019) would

yield the same major products reported. Typical fragmentation behavior observed in MS/MS spectra for individual functional

groups from Holčapek et al. (2010) are outlined in Table S1.

194

6

3 Results and Discussion

3.1 Kinetics, mass spectrometric, and absorbance changes analyses during the direct photosensitized oxidation of VL in the aqueous -phase photo-oxidation of vanillin

For clarity purposes, the reactions involving reactive species referred to in the following discussions are provided in Table 1. Table 2 summarizes the reaction conditions, initial VL (and GUA) decay rate constants, normalized abundance of products, and average carbon oxidation state ($<OS_c>$) (of the 50 most abundant products). In general, the 50 most abundant products contributed more than half of the total normalized abundance of products and can serve as representative products for discussions of reaction pathways and calculation of the $<OS_c>$.

As shown in Figure S3, VL underwent oxidation both directly and in the presence of ammonium (and sodium) nitrate upon simulated sunlight illumination. VL absorbs light and is promoted to its excited singlet state ($^1VL^*$), then undergoes intersystem crossing (ISC) to the excited triplet state, $^3VL^*$. In principle, $^3VL^*$ can oxidize ground-state VL (Type I photosensitized reactions) via H-atom abstraction/electron transfer and form $O_2^{\bullet-}$ or $HO_2^\bullet$ in the presence of O_2 (George et al., 2018), or react with O_2 (Type II photosensitized reactions) to yield $^1O_2$ via energy transfer or $O_2^{\bullet-}$ via electron transfer (Lee et al., 1987; Foote et al., 1991). The disproportionation of $HO_2^\bullet/O_2^{\bullet-}$ (Anastasio et al., ~~1996~~1997) form hydrogen peroxide (H_2O_2), which is a photolytic source of $^\bullet OH$. Overall, air-saturated conditions, in which O_2 is present, enable the generation of secondary oxidants ($^1O_2$, $O_2^{\bullet-}/HO_2$, $^\bullet OH$) from $^3VL^*$ ~~($^1O_2$, $O_2^{\bullet-}/HO_2$, $^\bullet OH$)~~. Moreover, $^\bullet OH$, $^\bullet NO_2$, and NO_2^-/HNO_2, i.e., N(III), generated via nitrate photolysis (Reactions 1–3; Table 1), can also oxidize or nitrate VL. In this work, the direct photosensitized oxidation of VL in the absence (VL only experiments) and ~~nitrate-mediated VL photo-oxidation~~ presence of ammonium nitrate are referred to as VL* and VL+AN, respectively.

3.1.1 VL photo--oxidation under N_2 and air-saturated conditions

As previously stated, the N_2-saturated experiments would inhibit the formation of secondary oxidants ($^1O_2$, $O_2^{\bullet-}/HO_2$, $^\bullet OH$) from $^3VL^*$, facilitating $^3VL^*$-driven reactions (Chen et al., 2020). In contrast, the air-saturated experiments can enable the generation of these secondary oxidants from $^3VL^*$ as O_2 is present. Moreover, for experiments conducted under three saturated gases (air, O_2, and N_2), the rate constant for 4-ethylguaiacol (a non-carbonyl phenol) loss by $^3DMB^*$ decreased in the order of air > N_2 > O_2. This was attributed to the presence of O_2, resulting in a synergistic effect of $^1O_2$ and $^3C^*$ under air-saturated conditions (Chen et al., 2020). The differences in air and N_2-saturated experiments can then be used to infer the role of reaction pathways that require O_2 in the direct photosensitized oxidation of VL. The photosensitized -oxidation of VL under both N_2- and air-saturated conditions (Fig. S3a) were carried out at pH 4, which is representative of moderately acidic aerosol and cloud pH values (Pye et al., 2020). No significant VL loss was observed for dark experiments. The oxidation of ground-state VL by $^3VL^*$ via H-atom abstraction or electron transfer can form phenoxy (which is in resonance with a carbon-centered

7

226 cyclohexadienyl radical that has a longer lifetime) and ketyl radicals (Neumann et al., 1986a, 1986b; Anastasio et al.,

227 ~~1996~~1997). The coupling of phenoxy radicals or phenoxy and cyclohexadienyl radicals can form oligomers as observed for

228 both N_2- and air-saturated experiments (see discussions later). However, the minimal~~little~~ decay of VL under N_2-saturated

229 condition indicates that these radicals probably ~~predominantly~~ decayed via back-hydrogen transfer to regenerate VL (Lathioor

230 et al., 1999). A possible explanation for this is the involvement of O_2 in the secondary steps of VL decay. For instance, a major

231 fate of the ketyl radical is reaction with O_2 (Anastasio et al., ~~1996~~1997). In the absence of O_2, radical formation occurs, but the

232 forward reaction of ketyl radical and O_2 is blocked, leading to the regeneration of VL as suggested by the minimal VL decay.

233 Aside from potential inhibition of secondary oxidants generation (Chen et al., 2020), N_2 purging may have also hindered the

234 secondary steps for VL decay.

235 Contrastingly, the VL~~*~~ decay rate constant for VL* ~~~~under air-saturated conditions was 4 times higher than under

236 N_2-saturated conditions (Table 2). As mentioned earlier, secondary oxidants ($^1O_2$, $O_2^{\bullet-}$/$^{\bullet}HO_2$, $^{\bullet}OH$) can be generated from $^3VL^*$

237 when O_2 is present (~~e.g.,~~under air-saturated conditions). However, the direct photosensitized ~~~~oxidation of VL in this study is

238 likely ~~mainly~~ governed by $^3VL^*$ and that these secondary oxidants have only minor participation. $^1O_2$ is also a potential oxidant

239 for phenols (Herrmann et al., 2010; Minella et al., 2011; Smith et al., 2014), but $^1O_2$ reacts much faster (by ~60 times) with

240 phenolate ions ~~compared to~~than neutral phenols (Tratnyek and Hoigne, 1991; Canonica et al., 1995; McNally et al., 2005).

241 Under the pH values (pH 2.5 to 4) considered in this study, the amount of phenolate ion is negligible (pK_a of VL = 7.9), so the

242 reaction between VL and $^1O_2$ should be slow. Interestingly, however, both $^3C^*$ and $^1O_2$ ha~~ve~~s been shown to be important in

243 the photo-oxidation of 4-ethylguaiacol (pK_a = 10.3) by $^3DMBC^*$ ~~of 3,4-dimethoxybenzaldehyde~~ (solution with pH of ~3)

244 (Chen et al., 2020). Furthermore, while the irradiation of other phenolic compounds can produce H_2O_2, a precursor for $^{\bullet}OH$

245 (Anastasio et al., ~~1996~~1997), the amount of H_2O_2 is small. Based on this, only trace amounts of H_2O_2 were likely generated

246 from VL* (Li et al., 2014) under-air saturated conditions, suggesting that contribution from $^{\bullet}OH$ was minor. Overall, these

247 suggest that the direct photosensitized oxidation of VL in this study is mainly driven by $^3VL^*$. ~~Further study on the impact of~~

248 ~~O_2 on the reactive intermediates involved is required to understand the exact mechanisms occurring under air-saturated~~

249 ~~conditions. Nonetheless, the VL* decay trends clearly indicate that O_2 is important for efficient VL photo-oxidation.~~

250 The VL decay rate constant for VL+AN under air-saturated conditions was also higher (6.6 times) than under N_2-

251 saturated conditions, ~~which may be~~possibly~~~~ due to reactions facilitated by nitrate photolysis products that may have been

252 enhanced in the presence of O_2 (Vione et al., 2005; Kim et al., 2014; Pang et al., 2019a). As shown later, more ~~nitrogen-containing~~N-containing species were observed for VL+AN under air-saturated conditions than under N_2-saturated conditions.

254 An example is enhanced VL nitration likely from increased $^{\bullet}NO_2$ formation such as from the reaction of $^{\bullet}OH$ and $O_2^{\bullet-}$ with

255 NO_2^- (Reactions 4 and 5, respectively; Table 1) or the autoxidation of $^{\bullet}NO$ from NO_2^- photolysis (Reactions 6–9; Table 1) in

256 aqueous solutions (Pang et al., 2019a). Nevertheless, the comparable decay rate constants for VL* and VL+AN imply that

257 $^3VL^*$ chemistry still dominates even at 1:10 molar ratio of VL/AN~~nitrate~~. This can be attributed~~ probably due~~ to the much

258 higher molar absorptivity of VL compared to that of nitrate (Fig. S1) and the high VL concentration (0.1 mM) used in this

259 study. ~~Although we have no~~ The quantification of the oxidants in our reaction systems is not explored here and require
260 additional work ~~as it is outside the scope of this study, these observations clearly substantiate that photosensitized oxidation~~
261 ~~of VL and nitrate-mediated VL photo-oxidation are more efficient in the presence of O_2. In essence, the N_2-saturated~~
262 ~~experiments suggest that the secondary steps for VL decay via $^3VL*$ may require to O_2 proceed. Nonetheless,~~ Ffurther study
263 on the impact of O_2 on the reactive intermediates involved is required to understand the exact mechanisms occurring under air-
264 saturated conditions.

265   The products from VL* under N_2-saturated conditions were mainly oligomers (e.g., $C_{16}H_{14}O_4$) (Fig. 1a), consistent
266 with triplet-mediated oxidation forming higher molecular weight products, ~~probably~~ with less fragmentation relative to
267 oxidation by $^\bullet OH$ (Yu et al., 2014; Chen et al., 2020). A threefold increase in the normalized abundance of products was noted
268 upon addition of ANnitrate (VL+AN under N_2-saturated conditions; Fig. 1b), and in addition to oligomers, functionalized
269 monomers (e.g., $C_8H_6O_5$) and ~~nitrogen-containing~~N-containing compounds (e.g., $C_8H_9NO_3$; No. 3~~2~~, Table S2) were also
270 observed, in agreement with $^\bullet OH$-initiated oxidation yielding more functionalized/oxygenated products compared to triplet-
271 mediated oxidation (Yu et al., 2014; Chen et al., 2020). Oligomers, functionalized monomers (e.g., demethylated VL; Fig. S4),
272 and ~~nitrogen-containing~~N-containing compounds (e.g., $C_{16}H_{10}N_2O_9$; No. 4~~3~~, Table S2) (for VL+AN) had higher normalized
273 abundance under air-saturated conditions (Figs. 1c-d), attributable ~~likely due~~ to efficient $^3VL*$-initiated oxidation and enhanced
274 VL nitration in the presence of O_2. For both VL* and VL+AN under air-saturated conditions, the most abundant product was
275 $C_{10}H_{10}O_5$ (No. 5~~4~~, Table S2), a substituted VL. Irradiation of VL by 254-nm lamp has also been reported to lead to VL
276 dimerization and functionalization via ring-retaining pathways, as well as small oxygenates formation but only when $^\bullet OH$ from
277 H_2O_2 were involved (Li et al., 2014). In this work, small organic acids (e.g., formic acid) were observed from both VL* and
278 VL+AN under air-saturated conditions (Fig. S5) due to simulated sunlight that could access the 308-nm VL band (Smith et al.,
279 2016). Interestingly, we observed a potential imidazole derivative ($C_5H_5N_3O_2$; No. 6 ~~5~~, Table S2) from VL+AN under air-
280 saturated conditions (Fig. 1d), which may have formed from reactions induced by ammonium. This compound was not
281 observed in a parallel experiment in which AN was replaced with ~~sodium nitrate (~~SN~~)~~ (Fig. S6a; see Sect. 3.1.3 for discussion).
282   The potential aqSOA formation pathways via the direct photosensitized oxidation of VL in the absence and presence
283 of AN ~~photo-oxidation~~ in this study are summarized in Fig. 2. At pH 4, $^3VL*$-initiated reactions yielded oligomeric species
284 such as $C_{16}H_{12}O_6$ and $C_{22}H_{22}O_6$. Earlier works on phenolic aqSOA formation have reported that oligomers can form via the
285 coupling of phenoxy radicals or phenoxy and cyclohexadienyl radicals (Sun et al., 2010; Yu et al., 2014; Vione et al., 2019).
286 In this work, phenoxy radicals (in resonance with a carbon-centered cyclohexadienyl radical) can be generated from several
287 processes such as the oxidation of ground-state VL by $^3VL*$ via H-atom abstraction or electron transfer coupled with proton
288 transfer from the phenoxyl radical cation or from solvent water (Neumann et al., 1986a, 1986b; Anastasio et al., ~~1996~~1997)
289 and photoinduced O-H bond-breaking (Berto et al., 2016). Also, similar reactions can be initiated by $^\bullet OH$ (Gelencsér et al.,
290 2003; Hoffer et al., 2004; Chang and Thompson, 2010; Sun et al., 2010), which in this study can be generated from the reaction
291 between $^3VL*$ and O_2, as well as nitrate photolysis. Trace amounts of H_2O_2 could be ~~were likely~~ formed during VL
292 photodegradation (Li et al., 2014), similar to the case of other phenolic compounds (Anastasio et al., ~~1996~~1997). In addition,

9

293 ring-opening products (Fig. S5) from fragmentation in both VL* and VL+AN may have reacted with VL or dissolved ammonia

294 to generate $C_{10}H_{10}O_5$ (No. ~~4~~5, Table S2) (Pang et al., 2019b) or a potential imidazole derivative ($C_5H_5N_3O_2$; No. ~~5~~6, Table

295 S2), respectively. Moreover, nitrate photolysis products promoted functionalization and nitration (e.g., $C_{16}H_{10}N_2O_9$; No. ~~3~~4,

296 Table S2).

297   The molecular transformation of VL upon photo~~sensitized~~-oxidation was examined using the van Krevelen diagrams

298 (Fig. S7). For all experiments (A1-1~~4~~5; Table 2) in this study, the O:C and H:C ratios of the products were ~~mainly~~ similar to

299 those observed from the aging of other phenolic compounds (Yu et al., 2014) and BB aerosols (Qi et al., 2019). Under N$_2$-

300 saturated conditions, oligomers with O:C ratios ≤ 0.6 were dominant in VL*, while smaller molecules (n_c ≤ 8) with higher O:C

301 ratios (up to 0.8) were also observed for VL+AN. In contrast, more products with higher O:C ratios (≥ 0.6) were noted under

302 air-saturated conditions for both VL* and VL+AN. For experiments A5 to A8, H:C ratios were mostly around 1.0 and double

303 bond equivalent (DBE) values were typically (58% of the 50 most abundant products) > 7, indicating that the products were

304 mainly oxidized aromatic compounds (Xie et al., 2020). Compounds with H:C ≤ 1.0 and O:C ≤ 0.5 are common for aromatic

305 species, while compounds with H:C ≥ 1.5 and O:C ≤ 0.5 are typical for more aliphatic species (Mazzoleni et al., 2012;

306 Kourtchev et al., 2014; Jiang et al., 2021). In contrast, Loisel et al. (2021) reported mainly oxygenated aliphatic-like compounds

307 from the direct irradiation of VL (0.1 mM), attributable ~~probably due~~ to their use of ESI in the negative ion mode, which has

308 higher sensitivity for detecting compounds such as carboxylic acids (Holčapek et al., 2010; Liigand et al., 2017), and solid-

309 phase extraction (SPE) procedure causing the loss of some oligomers (LeClair et al., 2012; Zhao et al., 2013; Bianco et al.,

310 201~~9~~8). Among experiments A5 to A8, VL+AN under air-saturated conditions (A7) had the highest normalized abundance of

311 products and <OS_c>, probably due to the combined influence of ^{3}VL* and enhanced VL nitration in the presence of O$_2$. Our

312 measured <OS_c> for all experiments range from -0.28 to +0.12, while other studies on phenolic aqSOA formation reported

313 <OS_c> ranging from -0.14 to +0.47 (Sun et al., 2010) and 0.04 to 0.74 (Yu et al., 2014). The <OS_c> in this study likely were

314 lower estimates since ~~This is likely because~~ we excluded contributions from ring-opening products, which may have higher

315 OS$_c$ values as these products are not detectable in the positive ion mode. ~~Thus, the <OS_c> in this study likely were lower~~

316 ~~estimates.~~ In brief, more oxidized aqSOA and higher ~~the presence O_2 increased the~~ normalized abundance of products such

317 as oligomers and functionalized monomers were noted under air-saturated conditions due to efficient VL oxidation by ^{3}VL*

318 ~~in~~ and ~~promoted the formation of more oxidized aqSOA~~the presence of O$_2$. Compared to N$_2$-saturated condition, the higher

319 normalized abundance of ~~nitrogen-containing~~N-containing products under air-saturated condition for VL+AN (at pH 4)

320 suggests a potential enhancement of VL nitration in the presence of O$_2$.

321   Illumination of phenolic aromatic carbonyls with high molar absorptivities ($\varepsilon_{\lambda max}$) (~8 to 22 × 10^3 M^{-1} cm^{-1}) leads to

322 an overall loss of light absorption but increased absorbance at longer wavelengths (> 350 nm), where the carbonyls did not

323 initially absorb light (Smith et al., 2016). Fig. 3a illustrates the changes in total absorbance from 350 to 550 nm of VL* and

324 VL+AN under N$_2$- and air-saturated conditions. The absorption spectra of VL* under air- and N$_2$- saturated conditions (pH 4)

325 at different time intervals are shown in Fig. S8. For both VL* and VL+AN, evident absorbance enhancement was observed

326 under air-saturated conditions, while the absorbance changes under N$_2$-saturated conditions were minimal, consistent with the

327 VL decay trends. Dimers and functionalized products have been shown to contribute to chromophore formation for the aqueous

328 photo-oxidation of guaiacyl acetone (another aromatic phenolic carbonyl) by ^{3}DMB* (Jiang et al., 2021). Based on this, the

329 higher normalized abundance of ~~This absorbance enhancement can be explained by the formation of~~ oligomers, ~~which~~ith have

330 large, conjugated π-electron systems (Chang and Thompson, 2010), and hydroxylated products (Li et al., 2014; Zhao et al.,

331 2015)~~, in agreement with the observed reaction products~~ observed under air-saturated conditions have contributed to the

332 absorbance enhancement. However, it is worth noting that the products detected may not have contributed significantly to the

333 total products formed and hence may not be the primary contributors to the absorbance enhancement. As mentioned earlier,

334 the major products detected in this study are probably those with high concentration or high ionization efficiency in the positive

335 ESI mode. In other words, the absorbance enhancement may not necessarily correlate directly with the products detected.

336 Correlating speciated chromophores with absorbance changes may be useful in demonstrating how aqSOA influence

337 the Earth's radiative balance and identifying chemical reactions that can affect the overall light absorption by aqSOA. This

338 can be accomplished by using liquid chromatography coupled with photodiode array (PDA) detector and high-resolution mass

339 spectrometry (LC/PDA/HRMS platform) (e.g., Lin et al., 2017; Jiang et al., 2021; Misovich et al., 2021). In our experiments,

340 VL (and GUA) concentration measurements, product characterization, and absorbance measurements were performed using

341 UHPLC-PDA, UHPLC-qToF-MS, and UV-Vis spectrophotometry, respectively. A similar approach is then possible using the

342 current methods in this work by matching the retention time (RT) of the products detected using UHPLC-ToF-MS with that

343 in the PDA. However, the concentration of the chromophores in this study is below the detection limit of the PDA based on

344 the lack of distinct PDA signals from the products. ~~In this work, phenoxy radicals (in resonance with a carbon-centered~~

345 ~~cyclohexadienyl radical) can be generated from several processes such as the oxidation of ground-state VL by ^{3}VL* via H-~~

346 ~~atom abstraction or electron transfer coupled with proton transfer from the phenoxyl radical cation or from solvent water~~

347 ~~(Neumann et al., 1986a, 1986b; Anastasio et al., 1996) and photoinduced O-H bond-breaking (Berto et al., 2016). Also, similar~~

348 ~~reactions can be initiated by ·OH (Gelencsér et al., 2003; Hoffer et al., 2004; Chang and Thompson, 2010; Sun et al., 2010),~~

349 ~~which in this study can be generated from the reaction between ^{3}VL* and O$_2$, as well as nitrate photolysis. Trace amounts of~~

350 ~~H$_2$O$_2$ were likely formed during VL photodegradation (Li et al., 2014), similar to the case of other phenolic compounds~~

351 ~~(Anastasio et al., 1996). Oligomers can then form via the coupling of phenoxy radicals or phenoxy and cyclohexadienyl radicals~~

352 ~~(Sun et al., 2010; Yu et al., 2014; Vione et al., 2019).~~ Absorbance increase at > 350 nm has also been reported for the

353 photosensitized oxidation of phenol and 4-phenoxyphenol (De Laurentiis et al., 2013a, 2013b) and direct photolysis of tyrosine

354 and 4-phenoxyphenol (Bianco et al., 2014) in which dimers have been identified as initial substrates. The continuous

355 absorbance enhancement throughout 6 h of irradiation correlated with the observation of oligomers and nitrated compounds

356 after irradiation. However, the increasing concentration of small organic acids (Fig. S5) throughout the experiments suggests

357 that fragmentation, which results in the decomposition of initially formed oligomers and formation of smaller oxygenated

358 products (Huang et al., 2018), is important at longer irradiation times. Overall, these trends establish that compared to N$_2$-

359 saturated conditions, VL oxidation by ^{3}VL* under air-saturated conditions (O$_2$ is present) enabled ~~O$_2$ is necessary for~~ the

360 efficient formation of light-absorbing compounds from both VL* and VL+AN.

11

3.1.2 VL photo-oxidation under varying ~~Effect of~~ pH conditions

The reaction~~vity~~s of ^{3}C* (Smith et al., 2014, 2015, 2016), aromatic photonitration by nitrate (Machado and Boule, 1995; Dzengel et al., 1999; Vione et al., 2005; Minero et al., 2007), and N(III)-mediated VL photo-oxidation (Pang et al., 2019a) have been demonstrated to be pH-dependent. In this study, the effect of pH on the direct photosensitized oxidation of VL ~~photo-oxidation~~ was investigated over ~~within~~ the pH range of 2.5 to 4, which is within ~~corresponding to~~ typical cloud pH values (2-7) (Pye et al., 2020). The decay rate constants for both VL* and VL+AN increased by 1.6 and 1.4 times, respectively, as pH decreased from 4 to 2.5 ~~(VL* and VL+AN at pH 2.5: 1.6 and 1.4 times faster than at pH 4, respectively)~~ (~~Fig. S3b~~Table 2). These differences in decay rate constants are small but statistically significant ($p < 0.05$). The pK_a for the ^{3}VL* ~~triplet~~ has been reported to be 4.0 (Smith et al., 2016). As there ~~are~~ is a greater fraction of ^{3}VL* ~~triplets~~ that are protonated at pH 2.5 (0.96) than at pH 4 (0.5~~0~~), it is possible that the pH dependence of the VL decay rate constants observed in this study is due to ^{3}VL* being more reactive in its protonated form. Smith et al. (2016) also observed a pH dependence for the direct photodegradation of VL (0.005 mM) (rate constants at pH $\leq$ 3 are ~two times lower than at pH $\geq$ 5) which ~~they~~ has been attributed to the sensitivity of the excimer of VL (i.e., the charge-transfer complex formed between an excited state VL molecule and a separate ground state VL molecule; Birks, 1973, Turro et al., 2010) to acid-base chemistry. The opposite trend observed in this study for 0.1 mM VL may be due to the reactivities of the protonated and neutral forms of ~~the~~ ^{3}VL* being dependent on ~~the~~ VL concentration (Smith et al., 2016). ~~It has been reported that T~~the quantum yield for direct VL photodegradation is higher at pH 5 than at pH 2 for 0.005 mM VL, but they are not statistically different for 0.03 mM VL (Smith et al., 2016). As pH decreases, the higher reactivity of ^{3}VL* and sensitivity of the excimer of VL to acid-base chemistry may have led to faster VL photo-oxidation. Similar to pH 4 experiments, comparable decay rate constants between VL* and VL+AN were also noted at pH < 4, again suggesting the predominant role of ^{3}VL* chemistry compared to nitrate, likely due to the high VL concentration (0.1 mM) used in this study.

As pH decreased, the normalized abundance of products, particularly oligomers and functionalized monomers, was higher for both VL* and VL+AN, consistent with~~further indicating that~~ ^{3}VL* potentially being ~~may be~~ more reactive in ~~their~~ its protonated form. The most abundant products observed were a substituted VL ($C_{10}H_{10}O_5$; No. 54, Table S2) and VL dimer ($C_{16}H_{14}O_6$; No. 76, Table S2) at pH 4 and pH < 4, respectively (Figs. 1c-h). Furthermore, a tetramer ($C_{31}H_{24}O_{11}$) was observed only in VL* at pH 2.5. For VL+AN, the normalized abundance of ~~nitrogen-containing~~N-containing compounds was also higher at lower pH (Table 2), likely due to increased $^{\bullet}OH$ and $^{\bullet}NO_2$ formation, which may be caused by the dependence of N(III) (NO_2^- + HONO) speciation on solution acidity (Pang et al., 2019a). At pH 3.3, half of N(III) exists as HONO (Fischer and Warneck, 1996; Pang et al., 2019a), which has a higher quantum yield for $^{\bullet}OH$ formation than that of NO_2^- in the near-UV region (Arakaki et al., 1999; Kim et al., 2014). Also, NO_2^-/HONO can generate $^{\bullet}NO_2$ via oxidation by $^{\bullet}OH$ (Reactions 4 and 10; Table 1) (Pang et al., 2019a). At pH < 4, ^{3}VL* likely have higher reactivity as suggested by the increased normalized abundance of oligomers (e.g., $C_{16}H_{14}O_6$; No. 76, Table S2 and $C_{31}H_{24}O_{11}$) and N-containing compounds (e.g., $C_{16}H_{10}N_2O_9$; No. 43, Table S2 and $C_{13}H_{14}N_2O_{10}$) (Fig. 2). The most abundant product at pH < 4, $C_{16}H_{14}O_6$ (No. 7, Table S2), is likely a C−

12

394 O coupled dimer. In previous studies on phenolic aqSOA formation, the generation of phenolic dimers has been proposed to
395 occur via C−C or C−O coupling of phenoxy radicals (Sun et al., 2010; Yu et al., 2014; Huang et al., 2018; Chen et al., 2020;
396 Misovich et al., 2021). Similarly, functionalized monomers such as $C_7H_6O_3$ (demethylated VL; No. 8, Table S2) and
397 hydroxylated products (e.g., $C_8H_8O_4$; No. 9, Table S2) also had increased normalized abundance for both VL* and VL+AN.
398 The formation of $C_7H_6O_3$ (No. 8, Table S2), which varies from the structure of VL by CH_2, can be explained by ˙OH addition
399 at the carbon containing the methoxy group, succeeded by the elimination of a methoxy radical (˙OCH_3) (Yee et al., 2013).
400 This reaction has also been postulated for the ˙OH oxidation of syringol (2,6-dimethoxyphenol) (Yee et al., 2013) and
401 transformation of DMB in a system composed of guaiacyl acetone and [3]DMB* (Misovich et al., 2021). The potential imidazole
402 derivative ($C_5H_5N_3O_2$; No. 6̶5, Table S2) was observed only at pH 4, following ~~possibly due to~~ the pH dependence of
403 ammonium speciation (pK_a = 9.25). Imidazole formation requires the nucleophilic attack of ammonia on the carbonyl group
404 (Yu et al., 2011), and at pH 4, the concentration of dissolved ammonia in VL+AN was about 10 or 30 times higher than that
405 at pH 3 or pH 2.5, respectively. ~~At different pH~~For the pH values considered in this study, the O:C and H:C ratios in VL* and
406 VL+AN had no significant differences (Figs. S7c–d and S9), but molecules with higher O:C ratios (> 0.6) were more abundant
407 at pH < 4. ~~Accordingly~~In addition, the <OS$_c$> at pH < 4 for both VL* and VL+AN were higher than that at pH 4, consistent
408 with higher <OS$_c$> observed at pH 5 compared to pH 7 for the ˙OH-mediated photo-oxidation of syringol (Sun et al., 2010).
409 Essentially, the higher reactivity of [3]VL* and predominance of HONO over nitrite at lower pH may have resulted in ~~increased~~
410 ~~formation~~higher normalized abundance of products mainly composed of oligomers and functionalized monomers.

411   Higher absorbance enhancement for both VL* and VL+AN (Fig. 3b) was observed as pH increased. To determine
412 whether the pH dependence is due to the acid-base chemistry of the products or of the reactions, ~~we measured~~ the changes in
413 the UV-Vis absorption spectra ~~pH dependence~~ of the aqSOA formed from VL* at pH 4 and 2.5 were measured over a range
414 of pH conditions from 1.5 to 10.5 (Fig. S10). For both cases, the intensity of absorption at longer wavelengths significantly
415 increased as the pH of the solutions was raised. Moreover, the ~~comparable pH dependence of~~changes in the UV-Vis absorption
416 spectra for the two solutions of varying pH are comparable, suggest~~ings~~ that the observed pH dependence ~~may be attributed~~
417 ~~to the~~ is rooted in acid-base chemistry of the reactions involving ~~, which may involve~~ [3]VL* or the excimer of VL (Smith et al.,
418 2016), as discussed earlier.

419 **3.1.3 Participation of ammonium in the direct photosensitized oxidation of VL in the presence of AN**

420 Ammonium salts are an important constituent of atmospheric aerosols particles (Jimenez et al., 2009), and reactions between
421 dicarbonyls (e.g., glyoxal) and ammonia or primary amines form BrC (De Haan et al., 2009, 2011; Nozière et al., 2009; Shapiro
422 et al., 2009; Lee et al., 2013; Powelson et al., 2014; Gen et al., 2018; Mabato et al., 2019). Imidazole and imidazole derivatives
423 are the major products of glyoxal and ammonium sulfate reactions at pH 4 (Galloway et al., 2009; Yu et al., 2011; Sedehi et
424 al., 2013; Gen et al., 2018; Mabato et al., 2019). Here, we compared VL+AN and VL+SN at pH 4 under air-saturated conditions
425 to confirm the participation of ammonium in the photosensitized oxidation of VL. The presence of ammonium did not appear
426 to influence the kinetics of VL decay and light absorbance changes based on VL+AN and VL+SN having no statistically

427 significant difference ($p > 0.05$) with respect to VL decay rate constants (Table 2) and yielding comparable absorbance

428 enhancement (Fig. 3a), respectively. However, it is important to note that this may not be the case for lower concentrations of

429 VL. As previously stated, the reactions in this study were dominated by $^3VL^*$ chemistry, likely due to the higher molar

430 absorptivity of VL than that of nitrate and the high VL concentration used. Similarly, the normalized abundance of products

431 was comparable in both experiments (A7 and A9; Table 2) with $C_{10}H_{10}O_5$ (No. 5, Table S2) as the most abundant product

432 (Figs. 1d and S6a), but in VL+SN, there was a significant amount of a VL dimer ($C_{15}H_{12}O_8$; No. 10, Table S2). The normalized

433 abundance of N-containing compounds was also similar for VL+AN and VL+SN but the detected N-containing compounds

434 were distinct. Aside from the potential imidazole derivative ($C_5H_5N_3O_2$; No. 6, Table S2), $C_8H_9NO_3$ (No. 3, Table S2), possibly

435 an aminophenol, was also observed from VL+AN but only under N_2-saturated conditions (Fig. 1b), probably due to further

436 oxidation by $^3VL^*$. Relative to VL+AN, the products from VL+SN had higher O:C ratios (e.g., $C_7H_4N_2O_7$; No. 11, Table S2),

437 OS_C, and $<OS_C>$ values (Table 2). In summary, while the VL decay kinetics and absorbance enhancement for VL+AN and

438 VL+SN were similar, the product analysis supports the participation of ammonium in the aqueous-phase reactions.

439 **3.1.43 Distribution of potential BrC compounds**

440 Figure S11 plots the DBE values vs. number of carbons (n_c) (Lin et al., 2018) for the 50 most abundant products from pH 4

441 experiments under air-saturated conditions, along with reference to DBE values corresponding to fullerene-like hydrocarbons

442 (Lobodin et al., 2012), cata-condensed polycyclic aromatic hydrocarbons (PAHs) (Siegmann and Sattler, 2000), and linear

443 conjugated polyenes with a general formula C_xH_{x+2}. As light absorption by BrC requires uninterrupted conjugation across a

444 significant part of the molecular structure, compounds with DBE/n_C ratios (shaded area in Fig. S11) greater than that of linear

445 conjugated polyenes are potential BrC compounds (Lin et al., 2018). Based on this criterion and the observed absorbance

446 enhancement at > 350 nm (Fig. 3), the majority of the 50 most abundant products from pH 4 experiments under air-saturated

447 conditions were potential BrC chromophores composed of monomers and oligomers up to tetramers. However, as ESI-detected

448 compounds in BB organic aerosols has been reported to be mainly molecules with $n_c < 25$ (Lin et al., 2018), there may be

449 higher oligomers that were not detected in our reaction systems.

450

451 **3.2 Effect of reactants concentration and molar ratios on the direct photosensitized oxidation of VL in the aqueous**
452 **phaseaqueous photo-oxidation of vanillin**

453 To examine the influence of VL and AN nitrate concentration and their molar ratios on the direct photosensitized oxidation of

454 VLVL photo-oxidation, we also characterized the reaction products from lower [VL] (0.01 mM VL*; A10; Table 2), lower

455 [VL] and equal molar ratio of VL/ANnitrate (0.01 mM VL + 0.01 mM AN; A11; Table 2), and lower [VL] and 1:100 molar

456 ratio of VL/ANnitrate (0.01 mM VL + 1 mM AN; A12; Table 2) at pH 4. The normalized abundance of products from low

457 [VL] experiments (A10-A12; Table 2) were up to 1.4 times higher than that of high [VL] experiments (A5 and A7; Table 2).

14

458 Nevertheless, the major products for both low and high [VL] experiments were functionalized monomers (Figs. 1c-d and S12a–

459 c) such as $C_8H_6O_4$ (No. 12~~7~~, Table S2) and $C_{10}H_{10}O_5$ (No. 54, Table S2). For both VL* and VL+AN, the contribution of < 200

460 m/z to the normalized abundance of products was higher at low [VL] than at high [VL], while the opposite was observed for

461 > 300 m/z (Fig. S12d). This indicates that functionalization was favored at low [VL], as supported by the higher <OS_c>, while

462 oligomerization was the dominant pathway at high [VL], consistent with more oligomers or polymeric products reported from

463 high phenols concentration (e.g., 0.1 to 3 mM) (Li et al., 2014; Slikboer et al., 2015; Ye et al., 2019). <u>As the formation</u>

464 <u>mechanism of dimers and higher oligomers during aqueous-phase reactions of phenolic compounds involves the coupling of</u>

465 <u>phenoxy radicals (Kobayashi and Higashimura, 2003; Sun et al., 2010), the enhanced oligomerization at high [VL] can be</u>

466 <u>attributed</u> ~~This is probably due~~ to an increased concentration of phenoxy radicals (in resonance with a carbon-centered

467 cyclohexadienyl radical) at high [VL], promoting radical-radical polymerization (Sun et al., 2010; Li et al., 2014). At low

468 [VL], the contribution of < 200 m/z to the normalized abundance of products was higher for 1:1 than 1:100 VL/<u>AN</u>~~nitrate~~

469 molar ratio, suggesting the prevalence of functionalization for the former. In addition, 1:1 VL/<u>AN</u>~~nitrate~~ (A11; Table 2) had

470 higher <OS_c> than 1:100 VL/<u>AN</u>~~nitrate~~ (A12; Table 2), indicating the formation of more oxidized products, but had fewer N-

471 containing compounds compared to the latter. A possible explanation is that at 1:1 VL/<u>AN</u>~~nitrate~~, VL may compete with NO_2^-

472 for •OH (from nitrate or nitrite photolysis, Reaction 4; Table 1) and indirectly reduce •NO_2. Similarly, hydroxylation has been

473 suggested to be a more important pathway for 1:1 VL/nitrite than in 1:10 VL/nitrite (Pang et al., 2019a). Fragmentation, which

474 leads to the decomposition of previously formed oligomers and generation of small, oxygenated products such as organic acids

475 (Huang et al., 2018), may also occur for the low [VL] experiments. However, its importance would likely be observed at longer

476 irradiation times, similar to the high [VL] experiments.

477 ~~3.3 Participation of ammonium in the aqueous photo-oxidation of vanillin~~

478 ~~Imidazole and imidazole derivatives have been reported to be the major products of glyoxal and ammonium sulfate reactions~~

479 ~~at pH 4 (Galloway et al., 2009; Yu et al., 2011; Sedehi et al., 2013; Gen et al., 2018; Mabato et al., 2019). Here, we compared~~

480 ~~VL+AN and VL+SN at pH 4 in terms of reaction products and oxidative characteristics to confirm the participation of~~

481 ~~ammonium in the aqueous photo-oxidation of VL. The normalized abundance of the products was comparable in both~~

482 ~~experiments (A7 and A9; Table 2), with $C_{10}H_{10}O_5$ (No. 4, Table S2) as the most abundant product (Figs. 1d and S6a), but in~~

483 ~~VL+SN, there was a significant amount of a VL dimer ($C_{15}H_{12}O_8$; No. 8, Table S2). Moreover, the nitrogen-containing~~

484 ~~compounds were distinct. Aside from the potential imidazole derivative ($C_5H_5N_3O_2$; No.5, Table S2), $C_8H_9NO_3$ (No. 2, Table~~

485 ~~S2) was also observed from VL+AN but only under N_2-saturated conditions (Fig. 1b), probably due to further oxidation by~~

486 ~~$^3VL^*$.~~ <u>Relative to VL+AN, the products from VL+SN had higher O:C ratios (e.g., $C_2H_4N_2O_2$; No. 9, Table S2), OS_c, and</u>

487 <u><OS_c> values (Table 2).</u>~~The product analysis suggests the participation of ammonium in the aqueous phase reactions.~~

488 ~~Ammonium salts are an important constituent of atmospheric aerosols particles (Jimenez et al., 2009), and reactions between~~

489 ~~dicarbonyls (e.g., glyoxal) and ammonia or primary amines have been demonstrated to form BrC (De Haan et al., 2009, 2011;~~

490 ~~Nozière et al., 2009; Shapiro et al., 2009; Lee et al., 2013; Powelson et al., 2014; Gen et al., 2018; Mabato et al., 2019).~~

15

491 ~~Relative to VL+AN, the products from VL+SN had higher O:C ratios (e.g., $C_5H_4N_2O_2$; No. 9, Table S2), OS_c, and $<OS_c>$~~
492 ~~values (Table 2).~~

493

3.~~3~~4 Oxidation of guaiacol by photosensitized reactions of ~~vanillin~~ VL~~and photolysis of nitrate~~

495 The oxidation of phenols by $^3C^*$ has been mainly studied using non-phenolic aromatic carbonyls (Anastasio et al., ~~1996~~1997;
496 Smith et al., 2014, 2015; Yu et al., 2014; Chen et al., 2020) and aromatic ketones (Canonica et al., 2000) as triplet precursors.
497 Recently, $^3VL^*$ ha~~ve also~~s been shown to oxidize syringol (Smith et al., 2016), a non-carbonyl phenol, although the reaction
498 products remain unknown. In this section, we discussed the photo-oxidation of guaiacol (GUA), a non-carbonyl phenol that is
499 also a lignocellulosic BB pollutant (Kroflič et al., 2015) ~~that is also a non-carbonyl phenol~~, in the presence of VL (GUA+VL)
500 ~~or nitrate (GUA+AN)~~. The dark experiments did not show any substantial loss of VL or GUA (Fig. S3c). Due to its poor light
501 absorption in the solar range, GUA is not an effective photosensitizer (Smith et al., 2014; Yu et al., 2014). Accordingly, ~~the~~
502 direct GUA photodegradation resulted in minimal decay, which plateaued after ~3 hours. ~~However, I~~in the presence of VL ~~or~~
503 ~~nitrate~~, the GUA decay rate constant was 2.2 times higher ~~by 2.2 (GUA+VL) and 1.3 (GUA+AN) times, respectively,~~ than for
504 ~~direct GUA photodegradation. The enhancement of GUA decay rate constant in the presence of VL is statistically significant~~
505 ~~($p < 0.05$), while that in the presence of AN is not ($p > 0.05$).~~ This enhanced GUA decay rate constant may be due to the
506 oxidation of GUA by $^3VL^*$. ~~As mentioned earlier, $^3VL^*$ chemistry appears to be more important than that of nitrate photolysis~~
507 ~~even at 1:10 molar ratio of VL/nitrate on account of the much higher molar absorptivity of VL compared to that of nitrate (Fig.~~
508 ~~S1) and the high VL concentration (0.1 mM) used in this study. However, the apparent quantum efficiency of GUA~~
509 ~~photodegradation (φ_{GUA}) in the presence of nitrate ($1.3 \times 10^{-2} \pm 2.9 \times 10^{-3}$) is ~14 times larger than that in the presence of VL~~
510 ~~($9.0 \times 10^{-4} \pm 4.0 \times 10^{-4}$), suggesting that nitrate-mediated photo-oxidation of GUA is more efficient than that by photosensitized~~
511 ~~reactions of VL (see Text S7 for more details).~~ The decay rate constant of VL in GUA+VL (A14; Table 2) was 3 times slower
512 than that of VL* (A5; Table 2), which may be due to competition between ground-state VL and GUA for reactions with $^3VL^*$
513 or increased conversion of $^3VL^*$ back to the ground state through the oxidation of GUA (Anastasio et al., ~~1996~~1997; Smith et
514 al., 2014). ~~The corresponding absorbance changes for the GUA experiments (Fig. 3c) were consistent with the observed decay~~
515 ~~trends. The minimal absorbance changes for the direct GUA photodegradation also plateaued after ~3 hours. Moreover, the~~
516 ~~difference between GUA photo-oxidation in the presence of VL or nitrate was more evident, with the former showing much~~
517 ~~higher absorbance enhancement. Yang et al. (2021) also observed greater light absorption during nitrate-mediated photo-~~
518 ~~oxidation relative to direct GUA photodegradation.~~
519 For GUA experiments, ~~the direct GUA photodegradation, GUA+VL, and GUA+AN,~~ the normalized abundance of
520 products was calculated only for GUA+VL (2.2; Table 2)~~,~~ as the GUA signal from the UHPLC-qToF-MS in the positive ion
521 mode was weak, which may introduce large uncertainties during normalization. Nonetheless, the number of products detected
522 from these experiments (178~~, 266,~~ and 844 for ~~the~~ direct GUA photodegradation ~~, GUA+AN,~~ and GUA+VL, respectively)
523 corroborates the kinetics ~~and absorbance~~ results. The major products (Fig. 4a) from ~~the~~ direct GUA photodegradation ~~of GUA~~

16

were $C_{14}H_{14}O_4$ (No. 13~~0~~, Table S2), a typical GUA dimer, and $C_{21}H_{20}O_6$ (No. 14, Table S2), a trimer ~~($C_{21}H_{20}O_6$; No. 11, Table S2)~~ which likely originated from photoinduced O-H bond-breaking (Berto et al., 2016). In general, higher absolute signal intensitie~~s~~s were noted for oligomers (e.g., $C_{14}H_{14}O_4$, No. 13~~0~~ and $C_{21}H_{20}O_6$, No. 14~~1~~, Table S2) and hydroxylated products (e.g., $C_7H_8O_4$) in ~~both~~ GUA+VL ~~and GUA+AN~~, similar to those observed from GUA oxidation by ^{3}~~triplets of 3,4 dimethoxybenzaldehyde (DMB; a non-phenolic aromatic carbonyl)~~DMB* or •OH (from H_2O_2 photolysis) (Yu et al., 2014; Jiang et al., 2021). ~~In contrast to the GUA aqSOA reported by Yu et al. (2014), the photo-oxidation of GUA in this study yielded nitrated compounds (e.g., $C_9H_{14}N_2O_6$, $C_{11}H_{14}N_2O_9$) from GUA+AN and VL dimers (e.g., $C_{16}H_{12}O_8$) from GUA+VL. However, based on a recent work on the aqueous photo-oxidation of guaiacyl acetone (another aromatic phenolic carbonyl) by DMB triplets, the hydroxylation and dimerization of DMB can also contribute to aqSOA (Jiang et al., 2021). The contributions from DMB-participated reactions were only minor due to the low initial DMB concentration (0.005 mM). Relative to GUA+AN, higher signals for dimers such as $C_{14}H_{14}O_4$ (No. 10, Table S2) and $C_{16}H_{12}O_6$ were noted in GUA+VL, possibly due to both GUA and ground-state VL being available as oxidizable substrates for ^{3}VL*.~~ Also, a potential GUA tetramer ($C_{28}H_{26}O_8$, No. 15~~2~~, Table S2) was observed only in GUA+VL, consistent with more efficient ~~higher~~ oligomer formation from the triplet-mediated ~~photo-~~oxidation of phenol~~s~~ies relative to direct photodegradation~~•OH-assisted photo-oxidation~~ (Yu et al., 2014). ~~In general,~~ The ~~the~~ products from the direct GUA photodegradation ~~and,~~ GUA+VL~~, and GUA+AN~~ had mostly similar OS_c values (-0.5 to 0.5) (Figs. 4b–~~c~~d), falling into the criterion of biomass burning organic aerosol (BBOA) and semivolatile oxygenated organic aerosol (SV-OOA) (Kroll et al., 2011). The corresponding absorbance changes for the GUA experiments (Fig. 3c) were consistent with the observed VL and GUA decay trends and detected products. While minimal absorbance changes, which also plateaued after ~3 hours, were observed for direct GUA photodegradation, significant and continuous absorbance enhancement was noted for GUA+VL. ~~In this work, GUA photo-oxidation was observed in the presence of VL or AN, forming aqSOA composed of oligomers, hydroxylated products, and nitrated compounds (for GUA+AN). The higher product signals from GUA+VL compared to GUA+AN is likely due to the availability of both GUA and ground-state VL as aqSOA precursors.~~ Compared to direct GUA photodegradation, GUA oxidation by photosensitized reactions of VL occurred rapidly and yielded higher absolute signal intensities for oligomers and hydroxylated products, which likely contributed to the pronounced absorbance enhancement. These findings indicate that phenol oxidation by ^{3}VL* can also contribute to aqSOA formation.

4 Conclusions and atmospheric implications

In this study, the direct photosensitized oxidation of VL in the absence and presence of AN under atmospherically relevant cloud and fog conditions have been shown to generate aqSOA composed of oligomers, functionalized monomers, oxygenated ring-opening products, and nitrated compounds (from VL+AN). The oligomers from these reaction systems may be rather recalcitrant to fragmentation based on their high normalized abundance, even at the longest irradiation time used in this study.

17

Formatted: Superscript

Nonetheless, the increasing concentration of small organic acids over time implies that fragmentation becomes important at extended irradiation times. The reactions were observed to be influenced by O_2, pH, and reactants concentration and molar ratios. Our results suggest that O_2 could be required for the secondary steps in VL decay (e.g., the reaction of ketyl radical and O_2) via $^3VL^*$ to proceed. Compared to N_2-saturated conditions, $^3VL^*$-initiated reactions under air-saturated conditions (O_2 is present) proceeded rapidly, promoted the formation of more oxidized aqSOA, and generated products (e.g., oligomers, functionalized monomers, and N-containing compounds) with higher normalized abundance which exhibited stronger light absorption. For pH 4 experiments, the presence of both O_2 and nitrate resulted in the highest normalized abundance of products (including N-containing compounds) and $<OS_c>$, which is attributed to O_2 promoting VL nitration. Nevertheless, further work on the effect of O_2 on the reactive intermediates involved in the reactions is necessary to elucidate the mechanisms of direct photosensitized oxidation of VL under air-saturated conditions. Additionally, the formation of oligomers from the direct photosensitized oxidation of VL was promoted at low pH (< 4). Low VL concentration favored functionalization, while oligomerization prevailed at high VL concentration, consistent with past works (Li et al., 2014; Slikboer et al., 2015; Ye et al., 2019). Hydroxylation was observed to be important at equal molar ratios of VL and nitrate, likely due to VL competing with nitrite for $^{\bullet}OH$. Furthermore, the oxidation of guaiacol, a non-carbonyl phenol, via VL photosensitized reactions was shown to form oligomers and hydroxylated products. Aromatic carbonyls and nitrophenols have been reported to be the most significant classes of BrC in cloud water heavily affected by biomass burning in the North China Plain (Desyaterik et al., 2013). Correspondingly, the most abundant products from our reaction systems (pH 4, air-saturated solutions) are mainly potential BrC chromophores. These suggest that aqSOA generated in cloud/fog water from the oxidation of biomass burning aerosols via direct photosensitized reactions and nitrate photolysis products can impact aerosol optical properties and radiative forcing, particularly for areas where biomass burning is intensive.

This study shows that the photo-oxidation of VL via its direct photosensitized reactions and in the presence of nitrate can generate aqSOA composed of oligomers, functionalized monomers, oxygenated ring-opening products, and nitrated compounds (for nitrate-mediated reactions). The characterization of products presented in this work complements earlier studies (e.g., Smith et al. 2014, 2015, 2016) that mainly discussed the kinetics and aqSOA yield of triplet-driven oxidation of phenols. Although Ammonium (and sodium) nitrate was not found to did not substantially affect the VL decay rate constants, likely due to the much higher molar absorptivity of VL than nitrate and high VL concentration used in this work. However, the presence of ammonium (and sodium) nitrate promoted functionalization and nitration, indicating the significance of nitrate photolysis in thfor is aqSOA formation from biomass burning-derived compoundspathway. This work demonstrates that nitration, which is an important process for producing light-absorbing organics or BrC (Jacobson, 1999; Kahnt et al., 2013; Mohr et al., 2013; Laskin et al., 2015; Teich et al., 2017; Li et al., 2020), can also affect the aqueous-phase processing of triplet-generating aromatics. In addition, a potential imidazole derivative observed from VL+AN at pH 4 reveals that ammonium participates in aqSOA formation from the photo-oxidation of phenolic aromatic carbonyls. This observation also suggests that the photosensitized oxidation of phenolic aromatic carbonyls in the presence of AN could be a source of

591 imidazoles in the aqueous phase. It is important to understand the source of imidazoles due to their possible effects on human

592 health, their photosensitizing potential, and their effect on aerosol optical properties as BrC compounds (Teich et al., 2016).

593 A ~~On a related note, a~~ recent work (Ma et al., 2021) mimicking phenol oxidation by ^{3}DMB* (a non-phenolic aromatic

594 carbonyl) ~~triplets~~ in more concentrated conditions of aerosol particles containing high ~~her~~ AN concentration (0.5 M) increased

595 the photodegradation rate constant for guaiacyl acetone (an aromatic phenolic carbonyl with high Henry's law constant, $1.2 \times$

596 10^6 M atm^{-1}; McFall et al., 2020) by > 20 times which was ascribed to $^{\bullet}$OH formation from nitrate photolysis (Brezonik and

597 Fulkerson-Brekken, 1998; Chu and Anastasio, 2003). The same study also estimated that reactions of phenols with high

598 Henry's law constants (10^6 to 10^9 M atm^{-1}) can be important for SOA formation in aerosol particles~~ALW~~, with mechanisms

599 mainly governed by ^{3}C* and ^{1}O$_2$ (Ma et al., 2021). Likewise, Zhou et al. (2019) reported that the direct photodegradation of

600 acetosyringone was faster by about 6 times in the presence of 2 M NaClO$_4$. However, the opposite was noted for the

601 photodegradation of VL in sodium sulfate or sodium nitrate, which would occur slower (~2 times slower in 0.5 M sodium

602 sulfate and ~10 times slower in 0.124 M sodium nitrate) in ~~ALW~~ aerosol particles relative to dilute aqueous phase in clouds

603 (Loisel et al., 2021), implying that ~~. These suggest that~~ the nature of inorganic ions may have an essential role in the

604 photodegradation of organic compounds in the aqueous phase ~~(Loisel et al., 2021)~~.

605 ~~Furthermore, a potential imidazole derivative observed from the VL+AN (A7; Table 2) experiment suggests that~~

606 ~~ammonium may participate in aqSOA formation from the photo-oxidation of phenolic aromatic carbonyls. Also, the oligomers~~

607 ~~from these reaction systems may be rather recalcitrant to fragmentation based on their high abundance, even at the~~

608 ~~longest irradiation time used in this study. Nonetheless, the increasing concentration of small organic acids over time implies~~

609 ~~that fragmentation becomes important at extended irradiation times. Aromatic carbonyls and nitrophenols have been reported~~

610 ~~to be the most important classes of BrC in cloud water heavily affected by biomass burning in the North China Plain~~

611 ~~(Desyaterik et al., 2013). Correspondingly, the most abundant products from our reaction systems (pH 4, air-saturated~~

612 ~~solutions) are mainly potential BrC chromophores. These suggest that aqSOA generated in cloud/fog water from the oxidation~~

613 ~~of biomass burning aerosols via direct photosensitized reactions and nitrate photolysis products can impact aerosol optical~~

614 ~~properties and radiative forcing, particularly for areas where biomass burning is intensive.~~

615 ~~Our results indicate that the photo-oxidation of VL is influenced by O$_2$, pH, and reactants concentration and molar~~

616 ~~ratios. Under N$_2$-saturated conditions, the absence of O$_2$ likely hindered the secondary steps in VL decay (e.g., reaction of~~

617 ~~ketyl radical and O$_2$), regenerating VL as suggested by the minimal VL decay. In contrast, ^{3}VL*-initiated reactions proceeded~~

618 ~~rapidly under air-saturated conditions (O$_2$ is present) as indicated by higher VL decay rate constant and increased normalized~~

619 ~~abundance of products. For pH 4 experiments, the presence of both O$_2$ and nitrate resulted in the highest normalized abundance~~

620 ~~of products (including N-containing compounds) and <OS$_c$>, which may be due to O$_2$ promoting VL nitration. Nevertheless,~~

621 ~~further work is necessary to assess the effect of O$_2$ on the reactive intermediates involved in ^{3}VL*-driven photo-oxidation and~~

622 ~~elucidate the mechanisms of VL photo-oxidation under air-saturated conditions. Additionally, the formation of oligomers from~~

623 ~~VL photo-oxidation was promoted at low pH (< 4). Moreover, low VL concentration favored functionalization, while~~

624 ~~oligomerization prevailed at high VL concentration, consistent with past works (Li et al., 2014; Slikboer et al., 2015; Ye et al.,~~

19

2019). Hydroxylation was observed to be important for equal molar ratios of VL and nitrate, likely due to VL competing with nitrite for •OH. The oxidation of guaiacol, a non-carbonyl phenol, by photosensitized reactions of vanillin was also shown to be less efficient than that by nitrate photolysis products based on its lower apparent quantum efficiency.

In this study, we investigated reactions of VL and nitrate at concentrations in cloud/fog water. The concentrations of VL and nitrate can be significantly higher in aqueous aerosol particles than what we have used to mimic cloud/fog water. As a major component of aerosols, the concentration of nitrate can have concentrations be as high as sulfate (Huang et al., 2014). More studies should then explore the direct photosensitized oxidation and nitrate-mediated photo-oxidation of other biomass burning-derived phenolic aromatic carbonyls, particularly those with high molar absorption coefficients and can generate $^3C^*$. Based on our findings, the presence of nitrate should be considered for examining aqSOA formation from these reactions. The influences of reaction conditions should also be investigated to better understand the oxidation pathways. As aerosols comprise more complex mixtures of organic and inorganic compounds, it is worthwhile to explore the impacts of other potential aerosol constituents on aqSOA formation and photo-oxidation studies. This can also be beneficial in understanding the interplay among different reaction mechanisms during photo-oxidation. Considering that biomass burning emissions are expected to increase continuously, further studies on these aqSOA formation pathways are strongly suggested.

References

Anastasio, C., Faust, B. C., and Rao, C. J.: Aromatic carbonyl compounds as aqueous-phase photochemical sources of hydrogen peroxide in acidic sulfate aerosols, fogs, and clouds. 1. Non-phenolic methoxybenzaldehydes and methoxyacetophenones with reductants (phenols), Environ. Sci. Technol., 31, 218−232, https://doi.org/10.1021/es960359g, ~~1996~~1997.

Arakaki, T., Miyake, T., Hirakawa, T., and Sakugawa, H.: pH dependent photoformation of hydroxyl radical and absorbance of aqueous-phase N(III) (HNO$_2$ and NO$_2^-$), Environ. Sci. Technol., 33, 2561−2565, https://doi.org/10.1021/es980762i, 1999.

Bateman, A. P., Laskin, J., Laskin, A., and Nizkorodov, S. A.: Applications of high-resolution electrospray ionization mass spectrometry to measurements of average oxygen to carbon ratios in secondary organic aerosols, Environ. Sci. Technol., 46, 8315–8324, https://doi.org/10.1021/es3017254, 2012.

Benedict, K. B., McFall, A. S., and Anastasio, C.: Quantum yield of nitrite from the photolysis of aqueous nitrate above 300 nm, Environ. Sci. Technol., 51, 4387−4395, https://doi.org/10.1021/acs.est.6b06370, 2017.

Berto, S., De Laurentiis, E., Tota, T., Chiavazza, E., Daniele, P.G., Minella, M., Isaia, M., Brigante, M., and Vione, D.: Properties of the humic-like material arising from the photo-transformation of L-tyrosine, Sci. Total Environ., 434–444, https://doi.org/10.1016/j.scitotenv.2015.12.047, 2016.

Bianco, A., Minella, M., De Laurentiis, E., Maurino, V., Minero, C., and Vione, D.: Photochemical generation of photoactive compounds with fulvic-like and humic-like fluorescence in aqueous solution, Chemosphere, 111, 529–536, https://doi.org/10.1016/j.chemosphere.2014.04.035, 2014.

Bianco, A., Riva, M., Baray, J.-L., Ribeiro, M., Chaumerliac, N., George, C., Bridoux, M., and Deguillaume, L.: Chemical characterization of cloud water collected at Puy de Dôme by FT-ICR MS reveals the presence of SOA components, ACS Earth Space Chem., 3, 2076–2087, https://doi.org/10.1021/acsearthspacechem.9b00153, 2019.

Bianco, A., Passananti, M., Brigante, M., and Mailhot, G.: Photochemistry of the cloud aqueous phase: a review, Molecules, 25, 423, https://doi.org/10.3390/molecules25020423, 2020.

Birks, J.B.: Organic Molecular Photophysics, John Wiley & Sons, 1973.

Blando, J. D. and Turpin, B. J.: Secondary organic aerosol formation in cloud and fog droplets: a literature evaluation of plausibility, Atmos. Environ., 34, 1623−1632, https://doi.org/10.1016/S1352-2310(99)00392-1, 2000.

Bond, T. C., Streets, D. G., Yarber, K. F., Nelson, S. M., Woo, J-H., and Klimont, Z.: A technology-based global inventory of black and organic carbon emissions from combustion, J. Geophys. Res., 109, https://doi.org/10.1029/2003JD003697, 2004.

Brezonik, P. L. and Fulkerson-Brekken, J.: Nitrate-induced photolysis in natural waters: controls on concentrations of hydroxyl radical photo-intermediates by natural scavenging agents, Environ. Sci. Technol., 32, 3004−3010, https://doi.org/10.1021/es9802908, 1998.

Canonica, S., Hellrung, B., and Wirz, J.: Oxidation of phenols by triplet aromatic ketones in aqueous solution, J. Phys. Chem., 104, 1226–1232, https://doi.org/10.1021/jp9930550, 2000.

21

Canonica, S., Jans, U., Stemmler, K., and Hoigne, J.: Transformation kinetics of phenols in water: photosensitization by dissolved natural organic material and aromatic ketones, Environ. Sci. Technol., 29, 1822–1831, https://doi.org/10.1021/es00007a020, 1995.

Canonica, S., Hellrung, B., and Wirz, J.: Oxidation of phenols by triplet aromatic ketones in aqueous solution, J. Phys. Chem., 104, 1226–1232, https://doi.org/10.1021/jp9930550, 2000.

Chang, J. L. and Thompson, J. E.: Characterization of colored products formed during irradiation of aqueous solutions containing H_2O_2 and phenolic compounds, Atmos. Environ., 44, 541−551, https://doi.org/10.1016/j.atmosenv.2009.10.042, 2010.

Chen, Y., Li, N., Li, X., Tao, Y., Luo, S., Zhao, Z., Ma, S., Huang, H., Chen, Y., Ye, Z., and Ge, X.: Secondary organic aerosol formation from $^3C^*$-initiated oxidation of 4-ethylguaiacol in atmospheric aqueous-phase, Sci. Total Environ., 723, 137953, https://doi.org/10.1016/j.scitotenv.2020.137953, 2020.

Chu, L. and Anastasio, C.: Quantum yields of hydroxyl radical and nitrogen dioxide from the photolysis of nitrate on ice, J. Phys. Chem. A, 107, 9594−9602, https://doi.org/10.1021/jp0349132, 2003.

Collett, J. L. Jr., Hoag, K. J., Sherman, D. E., Bator, A., and Richards, L. W.: Spatial and temporal variations in San Joaquin Valley fog chemistry, Atmos. Environ., 33, 129−140, https://doi.org/10.1016/S1352-2310(98)00136-8, 1998.

De Haan, D. O., Corrigan, A. L., Tolbert, M. A., Jimenez, J. L., Wood, S. E., and Turley, J. J.: Secondary organic aerosol formation by self-reactions of methylglyoxal and glyoxal in evaporating droplets, Environ. Sci. Technol., 43, 8184−8190, https://doi.org/10.1021/es902152t, 2009.

De Haan, D. O., Hawkins, L. N., Kononenko, J. A., Turley, J. J., Corrigan, A. L., Tolbert, M. A., and Jimenez, J. L.: Formation of nitrogen-containing oligomers by methylglyoxal and amines in simulated evaporating cloud droplets, Environ. Sci. Technol., 45, 984−991, https://doi.org/10.1021/es102933x, 2011.

De Haan, D.O., Pajunoja, A., Hawkins, L. N., Welsh, H.G., Jimenez, N. G., De Loera, A., Zauscher, M., Andretta, A. D., Joyce, B. W., De Haan, A. C., Riva, M., Cui, T., Surratt, J. D., Cazaunau, M., Formenti, P., Gratien, A., Pangui, E., and Doussin, J-F.: Methylamine's effects on methylglyoxal-containing aerosol: chemical, physical, and optical changes, ACS Earth Space Chem., 3, 1706–1716, https://doi.org/10.1021/acsearthspacechem.9b00103, 2019.

De Laurentiis, E., Socorro, J., Vione, D., Quivet, E., Brigante, M., Mailhot, G., Wortham, H., and Gligorovski, S.: Phototransformation of 4-phenoxyphenol sensitised by 4-carboxybenzophenone: Evidence of new photochemical pathways in the bulk aqueous phase and on the surface of aerosol deliquescent particles, Atmos. Environ., 81, 569–578, https://doi.org/10.1016/j.atmosenv.2013.09.036, 2013a.

De Laurentiis, E., Sur, B., Pazzi, M., Maurino, V., Minero, C., Mailhot, G., Brigante, M., and Vione, D.: Phenol transformation and dimerisation, photosensitised by the triplet state of 1-nitronaphthalene: a possible pathway to humic-like substances (HULIS) in atmospheric waters, Atmos. Environ., 70, 318–327, https://doi.org/10.1016/j.atmosenv.2013.01.014, 2013b.

Desyaterik, Y., Sun, Y., Shen, X., Lee, T., Wang, X., Wang, T., and Collett, J. L. Jr.: Speciation of "brown" carbon in cloud water impacted by agricultural biomass burning in eastern China, J. Geophys. Res. Atmos., 118, 7389–7399, https://doi.org/10.1002/jgrd.50561, 2013.

Du, Y., Fu, Q. S., Li, Y., and Su, Y.: Photodecomposition of 4-chlorophenol by reactive oxygen species in UV/air system, J. Hazard. Mater., 186, 491–496, https://doi.org/10.1016/j.jhazmat.2010.11.023, 2011.

22

Dzengel, J., Theurich, J., and Bahnemann, D. W.: Formation of nitroaromatic compounds in advanced oxidation processes: photolysis versus photocatalysis, Environ. Sci. Technol., 33, 294–300, https://doi.org/10.1021/es980358j, 1999.

Ervens, B., Turpin, B. J., and Weber, R. J.: Secondary organic aerosol formation in cloud droplets and aqueous particles (aqSOA): a review of laboratory, field and model studies, Atmos. Chem. Phys., 11, 11069−11102, https://doi.org/10.5194/acp-11-11069-2011, 2011.

Fischer, M. and Warneck, P.: Photodecomposition of nitrite and undissociated nitrous acid in aqueous solution, J. Phys. Chem., 100, 18749−18756, https://doi.org/10.1021/jp961692+, 1996.

Fleming, L. T., Lin, P., Laskin, A., Laskin, J., Weltman, R., Edwards, R. D., Arora, N. K., Yadav, A., Meinardi, S., Blake, D. R., Pillarisetti, A., Smith, K. R., and Nizkorodov, S. A.: Molecular composition of particulate matter emissions from dung and brushwood burning household cookstoves in Haryana, India, Atmos. Chem. Phys., 18, 2461–2480, https://doi.org/10.5194/acp-18-2461-2018, 2018.

Foote, C.S.: Definition of type I and type II photosensitized oxidation, Photochem. Photobiol., 54, 659, https://doi.org/10.1111/j.1751-1097.1991.tb02071.x, 1991.

Galloway, M. M., Chhabra, P. S., Chan, A. W. H., Surratt, J. D., Flagan, R. C., Seinfeld, J. H., and Keutsch, F. N.: Glyoxal uptake on ammonium sulphate seed aerosol: reaction products and reversibility of uptake under dark and irradiated conditions, Atmos. Chem. Phys., 9, 3331−3345, https://doi.org/10.5194/acp-9-3331-2009, 2009.

Gelencsér, A., Hoffer, A., Kiss, G., Tombácz, E., Kurdi, R., and Bencze, L.: In-situ formation of light-absorbing organic matter in cloud water, J. Atmos. Chem., 45, 25–33, https://doi.org/10.1023/A:1024060428172, 2003.

Gen, M., Huang, D. D., and Chan, C. K.: Reactive uptake of glyoxal by ammonium-containing salt particles as a function of relative humidity, Environ. Sci. Technol., 52, 6903−6911, https://doi.org/10.1021/acs.est.8b00606, 2018.

Gen, M., Zhang, R., Huang, D. D., Li, Y., and Chan, C. K.: Heterogeneous SO_2 oxidation in sulfate formation by photolysis of particulate nitrate, Environ. Sci. Technol. Lett., 6, 86–91, https://doi.org/10.1021/acs.estlett.8b00681, 2019a.

Gen, M., Zhang, R., Huang, D. D., Li, Y., and Chan, C. K.: Heterogeneous oxidation of SO_2 in sulfate production during nitrate photolysis at 300 nm: eEffect of pH, relative humidity, irradiation intensity, and the presence of organic compounds, Environ. Sci. Technol., 53, 8757–8766, https://doi.org/10.1021/acs.est.9b01623, 2019b.

George, C., Ammann, M., D'Anna, B., Donaldson, D. J., and Nizkorodov, S.A.: Heterogeneous photochemistry in the atmosphere, Chem. Rev., 115, 4218–4258, https://doi.org/10.1021/cr500648z, 2015.

George, C., Brüggemann, M., Hayeck, N., Tinel, L., and Donaldson, D. J.: Interfacial photochemistry: physical chemistry of gas-liquid interfaces, in: Developments in Physical & Theoretical Chemistry, edited by: Faust, J. A. and House, J. E., Elsevier, 435−457, https://doi.org/10.1016/B978-0-12-813641-6.00014-5, 2018.

Gilardoni, S., Massoli, P., Paglione, M., Giulianelli, L., Carbone, C., Rinaldi, M., Decesari, S., Sandrini, S., Costabile, F., Gobbi, G.P., Pietrogrande, M.C., Visentin, M., Scotto, F., Fuzzi, S., and Facchini, M.C.: Direct observation of aqueous secondary organic aerosol from biomass-burning emissions, PNAS., 113, 10013–10018, https://doi.org/10.1073/pnas.1602212113, 2016.

23

Giulianelli, L., Gilardoni, S., Tarozzi, L., Rinaldi, M., Decesari, S., Carbone, C., Facchini, M. C., and Fuzzi, S.: Fog occurrence and chemical composition in the Po valley over the last twenty years, Atmos. Environ., 98, 394–401, https://doi.org/10.1016/j.atmosenv.2014.08.080, 2014.

Goldstein, S. and Czapski, G.: Kinetics of nitric oxide autoxidation in aqueous solution in the absence and presence of various reductants. The nature of the oxidizing intermediates, J. Am. Chem. Soc., 117, 12078–12084, https://doi.org/10.1021/ja00154a007, 1995.

Grosjean, D.: Reactions of o-cresol and nitrocresol with nitrogen oxides (NO_x) in sunlight and with ozone–nitrogen dioxide mixtures in the dark, Environ. Sci. Technol., 19, 968–974, https://doi.org/10.1021/es00140a014, 1985.

Herrmann, H.: On the photolysis of simple anions and neutral molecules as sources of O^-/OH, SO_x^- and Cl in aqueous solution, Phys. Chem. Chem. Phys., 9, 3935-3964, https://doi.org/10.1039/B618565G, 2007.

Herrmann, H., Hoffmann, D., Schaefer, T., Bräuer, P., and Tilgner, A.: Tropospheric aqueous-phase free-radical chemistry: rRadical sources, spectra, reaction kinetics and prediction tools, Chem Phys Chem, 11, 3796−3822, https://doi.org/10.1002/cphc.201000533, 2010.

Hoffer, A., Kiss, G., Blazsó, M., and Gelencsér, A.: Chemical characterization of humic-like substances (HULIS) formed from a lignin-type precursor in model cloud water, Geophys. Res. Lett., 31, https://doi.org/10.1029/2003GL018962, 2004.

Hoffmann, E. H., Tilgner, A., Wolke, R., Böge, O., Walter, A., and Herrmann, H.: Oxidation of substituted aromatic hydrocarbons in the tropospheric aqueous phase: kinetic mechanism development and modelling, Phys. Chem. Chem. Phys., 20, 10960–10977, https://doi.org/10.1039/C7CP08576A, 2018.

Holčapek, M., Jirásko, R., and Lísa, M.: Basic rules for the interpretation of atmospheric pressure ionization mass spectra of small molecules, J. Chromatogr. A, 1217, 3908–3921, https://doi.org/10.1016/j.chroma.2010.02.049, 2010.

Huang, D. D., Zhang, Q., Cheung, H. H. Y., Yu, L., Zhou, S., Anastasio, C., Smith, J. D., and Chan, C. K.: Formation and evolution of aqSOA from aqueous-phase reactions of phenolic carbonyls: comparison between ammonium sulfate and ammonium nitrate solutions, Environ. Sci. Technol., 52, 9215–9224, https://doi.org/10.1021/acs.est.8b03441, 2018.

Huang, R.-J., Zhang, Y., Bozzetti, C., Ho, K.-F., Cao, J.-J., Han, Y., Daellenbach, K. R., Slowik, J. G., Platt, S. M., Canonaco, F., Zotter, P., Wolf, R., Pieber, S. M., Bruns, E. A., Crippa, M., Ciarelli, G., Piazzalunga, A., Schwikowski, M., Abbaszade, G., Schnelle-Kreis, J., Zimmermann, R., An, Z., Szidat, S., Baltensperger, U., El Haddad, I., and Prévôt, A. S. H.: High secondary aerosol contribution to particulate pollution during haze events in China, Nature, 514, 218–222, https://doi.org/10.1038/nature13774, 2014.

Huang, X. H. H., Ip, H. S. S., and Yu, J. Z.: Secondary organic aerosol formation from ethylene in the urban atmosphere of Hong Kong: aA multiphase chemical modeling study, J. Geophys. Res., 116, D03206, https://doi.org/10.1029/2010JD014121, 2011.

Jacobson, M. Z.: Isolating nitrated and aromatic aerosols and nitrated aromatic gases as sources of ultraviolet light absorption, J. Geophys. Res., 104, 3527–3542, https://doi.org/10.1029/1998JD100054, 1999.

Jiang, W., Misovich, M. V., Hettiyadura, A. P. S., Laskin, A., McFall, A. S., Anastasio, C., and Zhang, Q.: Photosensitized reactions of a phenolic carbonyl from wood combustion in the aqueous phase—chemical evolution and light absorption properties of aqSOA, Environ. Sci. Technol., 55, 5199–5211, https://doi.org/10.1021/acs.est.0c07581, 2021.

Jimenez, J. L., Canagaratna, M. R., Donahue, N. M., Prevot, A. S. H., Zhang, Q., Kroll, J. H., DeCarlo, P. F., Allan, J. D., Coe, H., Ng, N. L., Aiken, A. C., Docherty, K. S., Ulbrich, I. M., Grieshop, A. P., Robinson, A. L., Duplissy, J., Smith, J. D., Wilson, K. R., Lanz, V. A., Hueglin, C., Sun, Y. L., Tian, J., Laaksonen, A., Raatikainen, T., Rautiainen, J., Vaattovaara, P., Ehn, M., Kulmala, M., Tomlinson, J. M., Collins, D. R., Cubison, M. J., Dunlea, E., J., Huffman, J. A., Onasch, T. B., Alfarra, M. R., Williams, P. I., Bower, K., Kondo, Y., Schneider, J., Drewnick, F., Borrman, S., Weimer, S., Demerjian, K., Salcedo, D., Cottrell, L., Griffin, R., Takami, A., Miyoshi, T., Hatakeyama, S., Shimono, A., Sun, J. Y., Zhang, Y. M., Dzepina, K., Kimmel, J. R., Sueper, D., Jayne, J. T., Herndon, S. C., Trimborn, A. M., Williams, L. R., Wood, E. C., Middlebrook, A. M., Kolb, C. E., Baltensperger, U., and Worsnop, D. R.: Evolution of organic aerosols in the atmosphere, Science, 326, 1525–1529, https://doi.org/10.1126/science.1180353, 2009.

Kahnt, A., Behrouzi, S., Vermeylen, R., Shalamzari, M. S., Vercauteren, J., Roekens, E., Claeys, M., and Maenhaut, W.: One-year study of nitro-organic compounds and their relation to wood burning in PM_{10} aerosol from a rural site in Belgium, Atmos. Environ., 81, 561−568, https://doi.org/10.1016/j.atmosenv.2013.09.041, 2013.

Kaur, R. and Anastasio, C.: First measurements of organic triplet excited states in atmospheric waters, Environ. Sci. Technol., 52, 5218–5226., https://doi.org/10.1021/acs.est.7b06699, 2018.

Kaur, R., Labins, J. R., Helbock, S. S., Jiang, W., Bein, K. J., Zhang, Q., and Anastasio, C.: Photooxidants from brown carbon and other chromophores in illuminated particle extracts, Atmos. Chem. Phys., 19, 6579–6594, https://doi.org/10.5194/acp-19-6579-2019, 2019.

Kebarle, P. A.: A brief overview of the present status of the mechanisms involved in electrospray mass spectrometry, J. Mass Spectrom., 35, 804−817, https://doi.org/10.1002/1096-9888(200007)35:7<804::AID-JMS22>3.0.CO;2-Qhttps://doi.org/10.1002/9783527628728.ch1, 2000.

Kim, D.-h., Lee, J., Ryu, J., Kim, K., and Choi, W.: Arsenite oxidation initiated by the UV photolysis of nitrite and nitrate, Environ. Sci. Technol., 48, 4030−4037, https://doi.org/10.1021/es500001q, 2014.

Kitanovski, Z., Čusak, A., Grgić, I., and Claeys, M.: Chemical characterization of the main products formed through aqueous-phase photonitration of guaiacol, Atmos. Meas. Tech., 7, 2457–2470, https://doi.org/10.5194/amt-7-2457-2014, 2014.

Klodt, A. L., Romonosky, D. E., Lin, P., Laskin, J., Laskin, A., and Nizkorodov, S. A.: Aqueous photochemistry of secondary organic aerosol of α-pinene and α-humulene in the presence of hydrogen peroxide or inorganic salts, ACS Earth Space Chem., 3, 12, 2736–2746, https://doi.org/10.1021/acsearthspacechem.9b00222, 2019.

Kobayashi, S. and Higashimura, H.: Oxidative polymerization of phenols revisited, Prog. Polym. Sci., 28, 1015–1048, https://doi.org/10.1016/S0079-6700(03)00014-5, 2003.

Kourtchev, I., Fuller, S. J., Giorio, C., Healy, R. M., Wilson, E., O'Connor, I., Wenger, J. C., McLeod, M., Aalto, J., Ruuskanen, T. M., Maenhaut, W., Jones, R., Venables, D. S., Sodeau, J. R., Kulmala, M., and Kalberer, M.: Molecular composition of biogenic secondary organic aerosols using ultrahigh-resolution mass spectrometry: comparing laboratory and field studies, Atmos. Chem. Phys., 14, 2155−2167, https://doi.org/10.5194/acp-14-2155-2014, 2014.

Kroflič, A., Anders, J., Drventić, I., Mettke, P., Böge, O., Mutzel, A., Kleffmann, J., and Herrmann, H.: Guaiacol nitration in a simulated atmospheric aerosol with an emphasis on atmospheric nitrophenol formation mechanisms, ACS Earth Space Chem., 5, 1083−1093, https://doi.org/10.1021/acsearthspacechem.1c00014, 2021.

Kroflič, A., Grilc, M., and Grgić, I.: Unraveling pathways of guaiacol nitration in atmospheric waters: nitrite, a source of reactive nitronium ion in the atmosphere, Environ. Sci. Technol., 49, 9150–9158, https://doi.org/10.1021/acs.est.5b01811, 2015.

Kroflič, A., Anders, J., Drventić, I., Mettke, P., Böge, O., Mutzel, A., Kleffmann, J., and Herrmann, H.: Guaiacol nitration in a simulated atmospheric aerosol with an emphasis on atmospheric nitrophenol formation mechanisms, ACS Earth Space Chem., https://doi.org/10.1021/acsearthspacechem.1c00014, 2021.

Kroll, J. H., Donahue, N. M., Jimenez, J. L., Kessler, S. H., Canagaratna, M. R., Wilson, K. R., Altieri, K. E., Mazzoleni, L. R., Wozniak, A. S., Bluhm, H., Mysak, E. R., Smith, J. D., Kolb, C. E., and Worsnop, D. R.: Carbon oxidation state as a metric for describing the chemistry of atmospheric organic aerosol, Nat. Chem., 3, 133–139, https://doi.org/10.1038/nchem.948, 2011.

Kruve, A., Kaupmees, K., Liigand, J., and Leito, I.: Negative electrospray ionization via deprotonation: predicting the ionization efficiency, Anal. Chem., 86, 4822–4830, https://doi.org/10.1021/ac404066v, 2014.

Laskin, A., Laskin, J., and Nizkorodov, S. A.: Chemistry of atmospheric brown carbon, Chem. Rev., 115, 4335–4382, https://doi.org/10.1021/cr5006167, 2015.

Laskin, J., Laskin, A., Nizkorodov, S. A., Roach, P., Eckert, P., Gilles, M. K., Wang, B., Lee, H. J., and Hu, Q.: Molecular selectivity of brown carbon chromophores, Environ. Sci. Technol., 48, 12047–12055, https://doi:10.1021/es503432r, 2014.

Lathioor, E. C., Leigh, W. J., and St. Pierre, M. J.: Geometrical effects on intramolecular quenching of aromatic ketone (π,π*) triplets by remote phenolic hydrogen abstraction, J. Am. Chem. Soc., 121, 11984–11992, https://pubs.acs.org/doi/abs/10.1021/ja991207z, 1999.

LeClair, J. P., Collett, J. L., and Mazzoleni, L. R.: Fragmentation analysis of water-soluble atmospheric organic matter using ultrahigh-resolution FT-ICR mass spectrometry, Environ. Sci. Technol., 46, 4312–4322, https://doi.org/10.1021/es203509b, 2012.

Lee, A. K. Y., Herckes, P., Leaitch, W. R., Macdonald, A. M., and Abbatt, J. P. D.: Aqueous OH oxidation of ambient organic aerosol and cloud water organics: Formation of highly oxidized products, Geophys. Res. Lett., 38, L11805, https://doi.org/10.1029/2011GL047439, 2011.

Lee, A. K. Y., Zhao, R., Li, R., Liggio, J., Li, S.-M., and Abbatt, J. P. D.: Formation of light absorbing organo-nitrogen species from evaporation of droplets containing glyoxal and ammonium sulfate, Environ. Sci. Technol., 47, 12819−12826, https://doi.org/10.1021/es402687w, 2013.

Lee, H. J., Aiona, P. K., Laskin, A., Laskin, J., and Nizkorodov, S. A.: Effect of solar radiation on the optical properties and molecular composition of laboratory proxies of atmospheric brown carbon, Environ. Sci. Technol., 48, 10217–10226, https://doi.org/10.1021/es502515r, 2014.

Lee, P. C. C. and Rodgers, M. A. J.: Laser flash photokinetic studies of Rose Bengal sensitized photodynamic interactions of nucleotides and DNA, Photochem. Photobiol., 45, 79–86, https://doi.org/10.1111/j.1751-1097.1987.tb08407.x, 1987.

Leito, I., Herodes, K., Huopolainen, M., Virro, K., Künnapas, A., Kruve, A., and Tanner, R.: Towards the electrospray ionization mass spectrometry ionization efficiency scale of organic compounds, Rapid Commun. Mass Sp., 22, 379–384, https://doi.org/10.1002/rcm.3371, 2008.

Li, F., Tang, S., Tsona, N. T., and Du, L.: Kinetics and mechanism of OH-induced α-terpineol oxidation in the atmospheric aqueous phase, Atmos. Environ., 237, 117650, https://doi.org/10.1016/j.atmosenv.2020.117650, 2020.

951
952 Li, P., Li, X., Yang, C., Wang, X., Chen, J., and Collett, J. L. Jr.: Fog water chemistry in Shanghai, Atmos. Environ., 45,
953 4034−4041, https://doi.org/10.1016/j.atmosenv.2011.04.036, 2011.
954
955 Li, Y. J., Huang, D. D., Cheung, H. Y., Lee, A. K. Y., and Chan, C. K.: Aqueous-phase photochemical oxidation and direct
956 photolysis of vanillin - a model compound of methoxy phenols from biomass burning, Atmos. Chem. Phys., 14, 2871−2885,
957 https://doi.org/10.5194/acp-14-2871-2014, 2014.
958
959 Liang, Z., Zhang, R., Gen, M., Chu, Y., and Chan, C. K.: Nitrate photolysis in mixed sucrose–nitrate–sulfate particles at
960 different relative humidities, J. Phys. Chem. A, 125, 3739–3747, https://doi.org/10.1021/acs.jpca.1c00669, 2021.
961
962 Liigand, P., Kaupmees, K., Haav, K., Liigand, J., Leito, I., Girod, M., Antoine, R., and Kruve, A.: Think negative: finding the
963 best electrospray ionization/MS mode for your analyte, Anal. Chem., 89, 5665–5668,
964 https://doi.org/10.1021/acs.analchem.7b00096 https://doi.org/10.1021/acs.analchem.7, 2017.
965
966 Lim, Y. B., Tan, Y., Perri, M. J., Seitzinger, S. P., and Turpin, B. J.: Aqueous chemistry and its role in secondary organic
967 aerosol (SOA) formation, Atmos. Chem. Phys., 10, 10521−10539, https://doi.org/10.5194/acp-10-10521-2010, 2010.
968
969 Lin, P., Bluvshtein, N., Rudich, Y., Nizkorodov, S. A., Laskin, J., and Laskin, A.: Molecular chemistry of atmospheric brown
970 carbon inferred from a nationwide biomass burning event, Environ. Sci. Tech., 51, 11561–
971 11570, https://doi.org/10.1021/acs.est.7b02276, 2017.
972
973
974 Lin, P., Fleming, L. T., Nizkorodov, S. A., Laskin, J., and Laskin, A.: Comprehensive molecular characterization of
975 atmospheric brown carbon by high resolution mass spectrometry with electrospray and atmospheric pressure photoionization,
976 Anal. Chem., 90, 12493–12502, https://doi.org/10.1021/acs.analchem.8b02177, 2018.
977
978 Lin, P., Yu, J. Z., Engling, G., and Kalberer, M.: Organosulfates in humic-like substance fraction isolated from aerosols at
979 seven locations in East Asia: a study by ultra-high-resolution mass spectrometry, Environ. Sci. Technol., 46, 13118–13127,
980 https://doi.org/10.1021/es303570v, 2012.
981
982 Liu, C., Liu, J., Liu, Y., Chen, T., and He, H.: Secondary organic aerosol formation from the OH-initiated oxidation of guaiacol
983 under different experimental conditions, Atmos. Environ., 207, 30–37, https://doi.org/10.1016/j.atmosenv.2019.03.021, 2019.
984
985 Lobodin, V. V., Marshall, A. G., and Hsu, C. S.: Compositional space boundaries for organic compounds, Anal. Chem., 84,
986 3410–3416, https://doi.org/10.1021/ac300244f, 2012.
987
988 Loisel, G., Mekic, M., Liu, S., Song, W., Jiang, B., Wang, Y., Deng, H., and Gligorovski, S.: Ionic strength effect on the
989 formation of organonitrate compounds through photochemical degradation of vanillin in liquid water of aerosols, Atmos.
990 Environ., 246, 118140, https://doi.org/10.1016/j.atmosenv.2020.118140, 2021.
991
992 Ma, L., Guzman, C., Niedek, C., Tran, T., Zhang, Q., and Anastasio, C.: Kinetics and mass yields of aqueous secondary organic
993 aerosol from highly substituted phenols reacting with a triplet excited state, Environ. Sci. Technol., 55, 5772–5781,
994 https://doi.org/10.1021/acs.est.1c00575, 2021.
995
996 Mabato, B. R. G., Gen, M., Chu, Y., and Chan, C. K.: Reactive uptake of glyoxal by methylaminium-containing salts as a
997 function of relative humidity, ACS Earth Space Chem., 3, 150–157, https://doi.org/10.1021/acsearthspacechem.8b00154, 2019.
998

27

Machado, F. and Boule, P.: Photonitration and photonitrosation of phenolic derivatives induced in aqueous solution by excitation of nitrite and nitrate ions, J. Photochem. Photobiol. A: Chem., 86, 73–80, https://doi.org/10.1016/1010-6030(94)03946-R, 1995.

Mack, J. and Bolton, J. R.: Photochemistry of nitrite and nitrate in aqueous solution: a review, J. Photochem. Photobiol. ~~-~~ ~~Chem.~~A, 128, 1–13, https://doi.org/10.1016/S1010-6030(99)00155-0, 1999.

Mazzoleni, L. R., Saranjampour, P., Dalbec, M. M., Samburova, V., Hallar, A. G., Zielinska, B., Lowenthal, D. H., and Kohl, S.: Identification of water-soluble organic carbon in non-urban aerosols using ultrahigh-resolution FT-ICR mass spectrometry: organic anions, Environ. Chem., 9, 285−297, https://doi.org/10.1071/EN11167, 2012.

McFall, A. S., Johnson, A. W., and Anastasio, C.: Air–water partitioning of biomass-burning phenols and the effects of temperature and salinity, Environ. Sci. Technol., 54, 3823–3830, https://doi.org/10.1021/acs.est.9b06443, 2020.

McNally, A. M., Moody, E. C., and McNeill, K.: Kinetics and mechanism of the sensitized photodegradation of lignin model compounds, Photochem. Photobiol. Sci., 4, 268−274, https://doi.org/10.1039/B416956E, 2005.

Minella, M., Romeo, F., Vione, D., Maurino, V., and Minero, C.: Low to negligible photoactivity of lake-water matter in the size range from 0.1 to 5 μm, Chemosphere, 83, 1480–1485, https://doi.org/10.1016/j.chemosphere.2011.02.093, 2011.

Minero, C., Bono, F., Rubertelli, F., Pavino, D., Maurino, V., Pelizzetti, E., and Vione, D.: On the effect of pH in aromatic photonitration upon nitrate photolysis, Chemosphere, 66, 650−656, https://doi.org/10.1016/j.chemosphere.2006.07.082, 2007.

Misovich, M. V., Hettiyadura, A. P. S., Jiang, W., Zhang, Q., and Laskin, A.: Molecular-level study of the photo-oxidation of aqueous-phase guaiacyl acetone in the presence of $^3C^*$: formation of brown carbon products, ACS Earth Space Chem., 5, 1983−1996, https://doi.org/10.1021/acsearthspacechem.1c00103, 2021.

Mohr, C., Lopez-Hilfiker, F. D., Zotter, P., Prévôt, A. S. H., Xu, L., Ng, N. L., Herndon, S. C., Williams, L. R., Franklin, J. P., Zahniser, M. S., Worsnop, D. R., Knighton, W. B., Aiken, A. C., Gorkowski, K. J., Dubey, M. K., Allan, J. D., and Thornton, J. A.: Contribution of nitrated phenols to wood burning brown carbon light absorption in Detling, United Kingdom during winter time, Environ. Sci. Technol., 47, 6316–6324, https://doi.org/10.1021/es400683v, 2013.

Munger, J. W., Jacob, D. J., Waldman, J. M., and Hoffmann, M. R.: Fogwater chemistry in an urban atmosphere, J. Geophys. Res. Oceans, 88, 5109–5121, https://doi.org/10.1029/JC088iC09p05109, 1983.

Neumann, M. G., De Groote, R. A. M. C., and Machado, A. E. H.: Flash photolysis of lignin: Part 1. Deaerated solutions of dioxane-lignin, Polym. Photochem., 7, 401–407, https://doi.org/10.1016/0144-2880(86)90007-2, 1986a.

Neumann, M. G., De Groote, R. A. M. C., and Machado, A. E. H.: Flash photolysis of lignin: II. Oxidative photodegradation of dioxane-lignin, Polym. Photochem., 7, 461–468, https://doi.org/10.1016/0144-2880(86)90015-1, 1986b.

Ning, C., Gao, Y., Zhang, H., Yu, H., Wang, L., Geng, N., Cao, R., and Chen, J.: Molecular characterization of dissolved organic matters in winter atmospheric fine particulate matters (PM$_{2.5}$) from a coastal city of northeast China, Sci. Total Environ., 689, 312–321, https://doi.org/10.1016/j.scitotenv.2019.06.418, 2019.

Nolte, C. G., Schauer, J. J., Cass, G. R., and Simoneit, B. R. T.: Highly polar organic compounds present in wood smoke and in the ambient atmosphere, Environ. Sci. Technol., 35, 1912−1919, https://doi.org/10.1021/es001420r, ~~1912–1919,~~ 2001.

Nozière, B., Dziedzic, P., and Córdova, A.: Products and kinetics of the liquid-phase reaction of glyoxal catalyzed by ammonium ions (NH$_4^+$), J. Phys. Chem. A, 113, 231−237, https://doi.org/10.1021/jp8078293, 2009.

28

Nozière, B., Dziedzic, P., and Córdova, A.: Inorganic ammonium salts and carbonate salts are efficient catalysts for aldol condensation in atmospheric aerosols, Phys. Chem. Chem. Phys., 12, 3864−3872, https://doi.org/10.1039/B924443C, 2010.

Nozière, B., Fache, F., Maxut, A., Fenet, B., Baudouin, A., Fine, L., and Ferronato, C.: The hydrolysis of epoxides catalyzed by inorganic ammonium salts in water: kinetic evidence for hydrogen bond catalysis, Phys. Chem. Chem. Phys., 20, 1583−1590, https://doi.org/10.1039/C7CP06790A, 2018.

Pang, H., Zhang, Q., Lu, X. H., Li, K. , Chen, H., Chen, J. , Yang, X., Ma, Y., Ma, J., and Huang, C.: Nitrite-mediated photooxidation of vanillin in the atmospheric aqueous phase, Environ. Sci. Technol., 53, 14253−14263, https://doi.org/10.1021/acs.est.9b03649, 2019a.

Pang, H., Zhang, Q., Wang, H., Cai, D., Ma, Y., Li, L., Li, K., Lu, X., Chen, H., Yang, X., and Chen, J.: Photochemical aging of guaiacol by Fe(III)-oxalate complexes in atmospheric aqueous phase, Environ. Sci. Technol., 53, 127−136, https://doi.org/10.1021/acs.est.8b04507, 2019b.

Perry, R. H., Cooks, R. G., and Noll, R. J.: Orbitrap mass spectrometry: instrumentation, ion motion and applications, Mass Spectrom. Rev., 27, 661–699, https://doi.org/10.1002/mas.20186, 2008.

Powelson, M. H., Espelien, B. M., Hawkins, L. N., Galloway, M. M., and De Haan, D. O.: Brown carbon formation by aqueous-phase carbonyl compound reactions with amines and ammonium sulfate, Environ. Sci. Technol., 48, 985−993, https://doi.org/10.1021/es4038325, 2014.

Pye, H., Nenes, A., Alexander, B., Ault, A. P., Barth, M. C., Clegg, S. L., Collett, J. L. Jr., Fahey, K. M., Hennigan, C. J., Herrmann, H., Kanakidou, M., Kelly, J. T., Ku, I.-T., McNeill, V. F., Riemer, N., Schaefer, T., Shi, G., Tilgner, A., Walker, J. T., Wang, T., Weber, R., Xing, J., Zaveri, R. A., and Zuend, A.: The acidity of atmospheric particles and clouds, Atmos. Chem. Phys., 20, 4809–4888, https://doi.org/10.5194/acp-20-4809-2020, 2020.

Qi, L., Chen, M., Stefenelli, G., Pospisilova, V., Tong, Y., Bertrand, A., Hueglin, C., Ge, X., Baltensperger, U., Prévôt, A. S. H., and Slowik, J.G.: Organic aerosol source apportionment in Zurich using an extractive electrospray ionization time-of-flight mass spectrometer (EESI-TOF-MS) — Part 2: Biomass burning influences in winter, Atmos. Chem. Phys., 19, 8037–8062, https://doi.org/10.5194/acp-19-8037-2019, 2019.

Rogge, W. F., Hildemann, L. M., Mazurek, M. A., and Cass, G. R., and Simoneit, B. R. T.: Sources of fine organic aerosol. 9. Pine, oak, and synthetic log combustion in residential fireplaces, Environ. Sci. Technol., 32, 13−22, https://doi.org/10.1021/es960930b, 1998.

Romonosky, D. E., Li, Y., Shiraiwa, M., Laskin, A., Laskin, J., and Nizkorodov, S. A.: Aqueous photochemistry of secondary organic aerosol of α-Pinene and α-Humulene oxidized with ozone, hydroxyl radical, and nitrate radical, J. Phys. Chem. A, 121, 1298–1309, https://doi.org/10.1021/acs.jpca.6b10900, 2017.

Scharko, N. K., Berke, A. E., and Raff, J. D.: Release of nitrous acid and nitrogen dioxide from nitrate photolysis in acidic aqueous solutions, Environ. Sci. Technol., 48, 20, 11991–1200, https://doi.org/10.1021/es503088x, 2014.

Schauer, J. J., Kleeman, M. J., Cass, G. R., and Simoneit, B. R. T.: Measurement of emissions from air pollution sources. 3. C_1−C_{29} organic compounds from fireplace combustion of wood, Environ. Sci. Technol., 35, 1716−1728, https://doi.org/10.1021/es001331e, 2001.

Schmidt, A-C., Herzschuh, R., Matysik, F-M., and Engewald, W.: Investigation of the ionisation and fragmentation behaviour of different nitroaromatic compounds occurring as polar metabolites of explosives using electrospray ionisation tandem mass spectrometry, Rapid Commun. Mass Sp., 20, 2293–2302, https://doi.org/10.1002/rcm.2591, 2006.

Sedehi, N., Takano, H., Blasic, V. A., Sullivan, K. A., and De Haan, D. O.: Temperature- and pH-dependent aqueous-phase kinetics of the reactions of glyoxal and methylglyoxal with atmospheric amines and ammonium sulfate, Atmos. Environ., 77, 656−663, https://doi.org/10.1016/j.atmosenv.2013.05.070, 2013.

Shapiro, E. L., Szprengiel, J., Sareen, N., Jen, C. N., Giordano, M. R., and McNeill, V. F.: Light-absorbing secondary organic material formed by glyoxal in aqueous aerosol mimics, Atmos. Chem. Phys., 9, 2289−2300, https://doi.org/10.5194/acp-9-2289-2009, 2009.

Siegmann, K. and Sattler, K. D.: Formation mechanism for polycyclic aromatic hydrocarbons in methane flames, J. Chem. Phys., 112, 698–709, https://doi.org/10.1063/1.480648, 2000.

Slikboer, S., Grandy, L., Blair, S. L., Nizkorodov, S. A., Smith, R. W., and Al-Abadleh, H. A.: Formation of light absorbing soluble secondary organics and insoluble polymeric particles from the dark reaction of catechol and guaiacol with Fe(III), Environ. Sci. Technol., 49, 7793–7801, https://doi.org/10.1021/acs.est.5b01032, 2015.

Smith, J. D., Sio, V., Yu, L., Zhang, Q., and Anastasio, C.: Secondary organic aerosol production from aqueous reactions of atmospheric phenols with an organic triplet excited state, Environ. Sci. Technol., 48, 1049–1057, https://doi.org/10.1021/es4045715, 2014.

Smith, J. D., Kinney, H., and Anastasio, C.: Aqueous benzene-diols react with an organic triplet excited state and hydroxyl radical to form secondary organic aerosol, Phys. Chem. Chem. Phys., 17, 10227–10237, https://doi.org/10.1039/C4CP06095D, 2015.

Smith, J. D., Kinney, H., and Anastasio, C.: Phenolic carbonyls undergo rapid aqueous photodegradation to form low-volatility, light-absorbing products, Atmos. Environ., 126, 36−44, https://doi.org/10.1016/j.atmosenv.2015.11.035, 2016.

Smith, J. D., Sio, V., Yu, L., Zhang, Q., and Anastasio, C.: Secondary organic aerosol production from aqueous reactions of atmospheric phenols with an organic triplet excited state, Environ. Sci. Technol., 48, 1049–1057, https://doi.org/10.1021/es4045715, 2014.

Song, J., Li, M., Jiang, B., Wei, S., Fan, X., and Peng, P.: Molecular characterization of water-soluble humic like substances in smoke particles emitted from combustion of biomass materials and coal using ultrahigh-resolution electrospray ionization Fourier transform ion cyclotron resonance mass spectrometry, Environ. Sci. Technol., 52, 2575–2585, https://doi.org/10.1021/acs.est.7b06126, 2018.

Sun, Y. L., Zhang, Q., Anastasio, C., and Sun, J.: Insights into secondary organic aerosol formed via aqueous-phase reactions of phenolic compounds based on high resolution mass spectrometry, Atmos. Chem. Phys., 10, 4809−4822, https://doi.org/10.5194/acp-10-4809-2010, 2010.

Teich, M., van Pinxteren, D., Kecorius, S., Wang, Z., and Herrmann, H.: First quantification of imidazoles in ambient aerosol particles: potential photosensitizers, brown carbon constituents, and hazardous components, Environ. Sci. Technol., 50, 1166–1173, https://doi.org/10.1021/acs.est.5b05474, 2016.

Teich, M., van Pinxteren, D., Wang, M., Kecorius, S., Wang, Z., Müller, T., Močnik, G., and Herrmann, H.: Contributions of nitrated aromatic compounds to the light absorption of water-soluble and particulate brown carbon in different atmospheric environments in Germany and China, Atmos. Chem. Phys., 17, 1653–1672, https://doi.org/10.5194/acp-17-1653-2017, 2017.

1148
1149   Tratnyek, P. G. and Hoigne, J.: Oxidation of substituted phenols in the environment: a QSAR analysis of rate constants for
1150   reaction with singlet oxygen, Environ. Sci. Technol., 25, 1596−1604, https://doi.org/10.1021/es00021a011, 1991.
1151
1152   Turro, N., Ramamurthy, V., and Scaiano, J.C.: Modern Molecular Photochemistry, University Science Books, 2010.
1153
1154   Vione, D., Albinet, A., Barsotti, F., Mekic, M., Jiang, B., Minero, C., Brigante, M., and Gligorovski, S.: Formation of
1155   substances with humic-like fluorescence properties, upon photoinduced oligomerization of typical phenolic compounds
1156   emitted by biomass burning, Atmos. Environ., 206, 197−207, https://doi.org/10.1016/j.atmosenv.2019.03.005, 2019.
1157
1158   Vione, D., Maurino, V., Minero, C., and Pelizzetti, E.: Phenol photonitration upon UV irradiation of nitrite in aqueous solution
1159   I: effects of oxygen and 2-propanol, Chemosphere, 45, 893–902, https://doi.org/10.1016/S0045-6535(01)00035-2, 2001.
1160
1161   Vione, D., Maurino, V., Minero, C., and Pelizzetti, E.: Reactions induced in natural waters by irradiation of nitrate and nitrite
1162   ions, in: The Handbook of Environmental Chemistry Vol. 2M - Environmental Photochemistry Part II, Springer, Berlin,
1163   Heidelberg, Germany, 221−253, https://doi.org/10.1007/b138185, 2005.
1164
1165   Vione, D., Maurino, V., Minero, C., Pelizzetti, E., Harrison, M. A. J., Olariu, R., and Arsene, C.: Photochemical reactions in
1166   the tropospheric aqueous phase and on particulate matter, Chem. Soc. Rev., 35, 441−453, https://doi.org/10.1039/B510796M,
1167   2006.
1168
1169   Vione, D., Albinet, A., Barsotti, F., Mekic, M., Jiang, B., Minero, C., Brigante, M., and Gligorovski, S.: Formation of
1170   substances with humic-like fluorescence properties, upon photoinduced oligomerization of typical phenolic compounds
1171   emitted by biomass burning, Atmos. Environ., 206, 197−207, https://doi.org/10.1016/j.atmosenv.2019.03.005, 2019.
1172
1173   Volkamer, R., Ziemann, P. J., and Molina, M. J.: Secondary organic aerosol formation from acetylene (C_2H_2): seed effect
1174   on SOA yields due to organic photochemistry in the aerosol aqueous phase, Atmos. Chem. Phys., 9, 1907−1928,
1175   https://doi.org/10.5194/acp-9-1907-2009, 2009.
1176
1177   Wang, K., Huang, R-J., Brüggemann, M., Zhang, Y., Yang, L., Ni, H., Guo, J., Wang, M., Han, J., Bilde, M., Glasius, M., and
1178   Hoffmann, T.: Urban organic aerosol composition in eastern China differs from north to south: molecular insight from a liquid
1179   chromatography–mass spectrometry (Orbitrap) study, Atmos. Chem. Phys., 21, 9089–9104, https://doi.org/10.5194/acp-21-
1180   9089-2021, 2021.
1181
1182   Wang, X., Hayeck, N., Brüggemann, M., Yao, L., Chen, H., Zhang, C., Emmelin, C., Chen, J., George, C., and Wang, L.:
1183   Chemical characterization of organic aerosols in Shanghai: A study by ultrahigh-performance liquid chromatography
1184   coupled   with   orbitrap   mass   spectrometry,   J.   Geophys.   Res.   Atmos.,   122,   11703–11722,
1185   https://doi.org/10.1002/2017JD026930, 2017.
1186
1187   Xiao, H.-W., Wu, J.-F., Luo, L., Liu, C., Xie, Y.-J., and Xiao, H.-Y.: Enhanced biomass burning as a source of aerosol
1188   ammonium   over   cities   in   Central   China   in   autumn,   Environ.   Pollut.,   266,   art.   no.   115278,
1189   https://doi.org/10.1016/j.envpol.2020.115278, 2020.
1190
1191   Xie, Q., Su, S., Chen, S., Xu, Y., Cao, D., Chen, J., Ren, L., Yue, S., Zhao, W., Sun, Y., Wang, Z., Tong, H., Su, H., Cheng,
1192   Y., Kawamura, K., Jiang, G., Liu, C-Q., and Fu, P.: Molecular characterization of firework-related urban aerosols using Fourier
1193   transform ion cyclotron resonance mass spectrometry, Atmos. Chem. Phys., 20, 6803–6820, 10.5194/acp-2019-1180,
1194   https://doi.org/10.5194/acp-20-6803-2020, 2020.
1195

Yang, J., Au, W. C., Law, H., Lam, C. H., and Nah, T.: Formation and evolution of brown carbon during aqueous-phase nitrate-mediated photooxidation of guaiacol and 5-nitroguaiacol, Atmos. Environ., 254, 118401, https://doi.org/10.1016/j.atmosenv.2021.118401 https://doi.org/10.1016/j.atmosenv.2020.118140, 2021.

Yaws, C. L.: Handbook of vapor pressure: Volume 3: Organic compounds C_8 to C_{28}, Gulf Professional Publishing, USA, 1994.

Ye, Z., Qu, Z., Ma, S., Luo, S., Chen, Y., Chen, H., Chen, Y., Zhao, Z., Chen, M., and Ge, X.: A comprehensive investigation of aqueous-phase photochemical oxidation of 4-ethylphenol, Sci. Total Environ., 685, 976–985, https://doi.org/10.1016/j.scitotenv.2019.06.276, 2019.

Yee, L. D., Kautzman, K. E., Loza, C. L., Schilling, K. A., Coggon, M. M., Chhabra, P. S., Chan, M. N., Chan, A. W. H., Hersey, S. P., Crounse, J. D., Wennberg, P. O., Flagan, R. C., and Seinfeld, J. H.: Secondary organic aerosol formation from biomass burning intermediates: phenol and methoxyphenols, Atmos. Chem. Phys., 13, 8019−8043, https://doi.org/10.5194/acp-13-8019-2013, 2013.

Yu, G., Bayer, A. R., Galloway, M. M., Korshavn, K. J., Fry, C. G., and Keutsch, F. N.: Glyoxal in aqueous ammonium sulfate solutions: products, kinetics and hydration effects, Environ. Sci. Technol., 45, 6336−6342, https://doi.org/10.1021/es200989n, 2011.

Yu, L., Smith, J., Laskin, A., Anastasio, C., Laskin, J., and Zhang, Q.: Chemical characterization of SOA formed from aqueous-phase reactions of phenols with the triplet excited state of carbonyl and hydroxyl radical, Atmos. Chem. Phys., 14, 13801−13816, https://doi.org/10.5194/acp-14-13801-2014, 2014.

Zhang, Q. and Anastasio, C.: Conversion of fogwater and aerosol organic nitrogen to ammonium, nitrate, and NO_x during exposure to simulated sunlight and ozone, Environ. Sci. Technol., 37, 3522–3530, https://doi.org/10.1021/es034114x, 2003.

Zhang, R., Gen, M., Fu, T-M., and Chan, C. K.: Production of formate via oxidation of glyoxal promoted by particulate nitrate photolysis, Environ. Sci. Technol., 55, 5711–5720, https://doi.org/10.1021/acs.est.0c08199, 2021.

Zhang, R., Gen, M., Huang, D. D., Li, Y., and Chan, C. K.: Enhanced sulfate production by nitrate photolysis in the presence of halide ions in atmospheric particles, Environ. Sci. Technol., 54, 3831–3839, https://dx.doi.org/10.1021/acs.est.9b06445, 2020.

Zhao, R., Lee, A. K. Y., Huang, L., Li, X., Yang, F., and Abbatt, J. P. D.: Photochemical processing of aqueous atmospheric brown carbon, Atmos. Chem. Phys., 15, 6087–6100, https://doi.org/10.5194/acp-15-6087-2015, 2015.

Zhao, Y., Hallar, A. G., and Mazzoleni, L. R.: Atmospheric organic matter in clouds: exact masses and molecular formula identification using ultrahigh-resolution FT-ICR mass spectrometry, Atmos. Chem. Phys. 13, 12343–12362, https://doi.org/10.5194/acp-13-12343-2013, 2013.

Zhou, W., Mekic, M., Liu, J., Loisel, G., Jin, B., Vione, D., and Gligorovski, S.: Ionic strength effects on the photochemical degradation of acetosyringone in atmospheric deliquescent aerosol particles, Atmos. Environ., 198, 83–88, https://doi.org/10.1016/j.atmosenv.2018.10.047, 2019.

Zielinski, T., Bolzacchini, E., Cataldi, M., Ferrero, L., Graßl, S., Hansen, G., Mateos, D., Mazzola, M., Neuber, R., Pakszys, P., Posyniak, M., Ritter, C., Severi, M., Sobolewski, P., Traversi, R., and Velasco-Merino, C.: Study of chemical and optical properties of biomass burning aerosols during long-range transport events toward the Arctic in summer 2017, Atmosphere, 11, 84, https://doi.org/10.3390/atmos11010084, 2020.

1246
1247

33
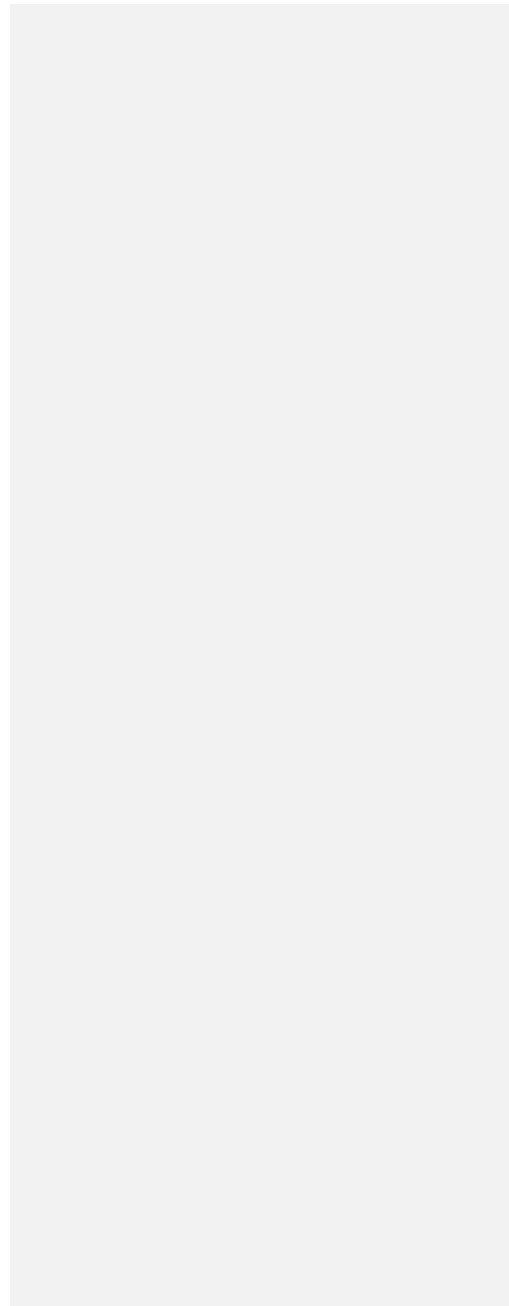
1248   **Table 1**. List of reactions involving reactive species relevant to this study.

No.	Reactions	References
1	$NO_3^- + h\nu \rightarrow {}^{\bullet}NO_2 + O^-$; $\phi = 0.01$	Vione et al., 2006; Benedict et al., 2017
2	$O^- + H_3O^+ \leftrightarrow {}^{\bullet}OH + H_2O$	
3	$NO_3^- + h\nu \rightarrow NO_2^- + O(^3P)$; $\phi = 0.011$	
4	$NO_2^- + {}^{\bullet}OH \rightarrow {}^{\bullet}NO_2 + OH^-$ ($k = 1.0 \times 10^{10}$ M^{-1} s^{-1})	Mack and Bolton, 1999; Pang et al., 2019a
5	$O_2^{\bullet -} + NO_2^- + 2H^+ \rightarrow {}^{\bullet}NO_2 + H_2O_2$	Vione et al., 2001; Pang et al., 2019a
6	$NO_2^- + h\nu \rightarrow {}^{\bullet}NO + O^-$; $\phi_{OH,300} = 6.7\ (\pm 0.9)\%$	Fischer and Warneck, 1996; Mack and Bolton, 1999; Pang et al., 2019a
7	${}^{\bullet}NO + O_2 \leftrightarrow {}^{\bullet}ONOO$	Goldstein and Czapski, 1995; Pang et al., 2019a
8	${}^{\bullet}ONOO + {}^{\bullet}NO \rightarrow ONOONO$	
9	$ONOONO \rightarrow 2{}^{\bullet}NO_2$	
10	$HNO_2 + {}^{\bullet}OH \rightarrow {}^{\bullet}NO_2 + H_2O$ ($k = 2.6 \times 10^9$ M^{-1} s^{-1})	Kim et al., 2014; Pang et al., 2019a

1249
1250
1251
1252
1253
1254
1255
1256
1257
1258
1259
1260
1261
1262
1263
1264
1265
1266
1267
1268
1269
1270
1271
1272
1273
1274
1275
1276
1277
1278

34

Table 2. Reaction conditions, initial VL (and GUA) decay rate constants, normalized abundance of products, and average carbon oxidation state ($<OS_c>$) in each experiment. Except where noted, the reaction systems consisted of VL (0.1 mM); GUA (0.1 mM), AN (1 mM); ~~sodium nitrate (~~SN~~)~~ (1 mM) under air-saturated conditions after 6 h of simulated sunlight irradiation. Analyses were performed using UHPLC-qToF-MS equipped with an ESI source and operated in the positive ion mode.

Exp no.	pH	Reaction conditions	Initial VL (and GUA) decay rate constants (min^{-1})[b]	Ratio of 50 most abundant products to total products[c]	Normalized abundance of products[d]	Normalized abundance of N-containing compounds[d]	$<OS_c>$[e] (OS$_c$ of VL: -0.25; OS$_c$ of GUA: -0.57)
A1		VL*	$2.0 \times 10^{-2} \pm 5.8 \times 10^{-5}$	0.59	1.7 ± 0.16	N/A	-0.05
A2	2.5	VL+AN	$1.7 \times 10^{-2} \pm 7.3 \times 10^{-4}$	0.63	1.4 ± 0.19	5.3×10^{-2}	-0.04
A3		VL*	$1.5 \times 10^{-2} \pm 4.2 \times 10^{-4}$	0.53	1.9 ± 0.33	N/A	-0.04
A4	3	VL+AN	$1.5 \times 10^{-2} \pm 2.3 \times 10^{-4}$	0.56	1.9 ± 0.30	3.6×10^{-2}	-0.05
A5		VL*	$1.2 \times 10^{-2} \pm 5.9 \times 10^{-4}$	0.58	0.26 ± 0.42	N/A	-0.16
A6		VL* (N$_2$-saturated)	$3.2 \times 10^{-3} \pm 1.1 \times 10^{-3}$	0.96	$4.7 \times 10^{-2} \pm 0.0027$	N/A	-0.24
A7		VL+AN	$1.2 \times 10^{-2} \pm 8.8 \times 10^{-4}$	0.53	0.37 ± 0.38	1.7×10^{-2}	-0.13
A8		VL+AN (N$_2$-saturated)	$1.9 \times 10^{-3} \pm 9.2 \times 10^{-5}$	0.89	0.12 ± 0.0095	6.3×10^{-3}	-0.21
A9		VL+SN	$1.3 \times 10^{-2} \pm 3.5 \times 10^{-4}$ ~~N/A~~	0.51	0.42 ± 0.33	1.7×10^{-2}	-0.07
A10	4	VL* (0.01 mM)[a]	N/A	0.90	0.37 ± 0.018	N/A	-0.07
A11		VL (0.01 mM) + AN (0.01 mM)	N/A	0.77	0.40 ± 0.074	8.6×10^{-3}	0.12
A12		VL (0.01 mM) + AN	N/A	0.42	0.45 ± 0.025	1.2×10^{-2}	-0.06
A13		GUA only	$6.2 \times 10^{-3} \pm 2.5 \times 10^{-4}$	0.77	N/A	N/A	-0.28
A14		GUA+VL	GUA: $1.4 \times 10^{-2} \pm 4.0 \times 10^{-4}$ VL: $4.3 \times 10^{-3} \pm 2.2 \times 10^{-4}$	0.60	2.2 ± 0.47	N/A	-0.27
~~A15~~		~~GUA+AN~~	~~$8.0 \times 10^{-3} \pm 2.9 \times 10^{-3}$~~	~~0.77~~	~~N/A~~	~~N/A~~	~~-0.26~~

[a]Irradiation time for VL* (0.01 mM, A10) was 3 h. [b]The data fitting was performed in the initial linear region. Each value is the average of results from triplicate experiments. Errors represent one standard deviation. Kinetic measurements were not performed for experiments marked with N/A. [c]Ratio of the normalized abundance of the 50 most abundant products to that of total products, except for direct GUA photodegradation and ~~,~~ GUA+VL ~~, and GUA+AN~~ (A13–1~~5~~4) whose ratios are based on the absolute signals of products. [d]The normalized abundance of products was calculated using Eq. 2. The samples for experiments without nitrate (marked with N/A) were not analyzed for N-containing compounds. For the GUA experiments, the normalized abundance of products was calculated only for GUA+VL as the GUA signal from the UHPLC-qToF-MS in

1299   the positive ion mode was weak, which may introduce large uncertainties during normalization. [e]$\langle OS_c \rangle$ of the 50 most
1300   abundant products.
1301
1302
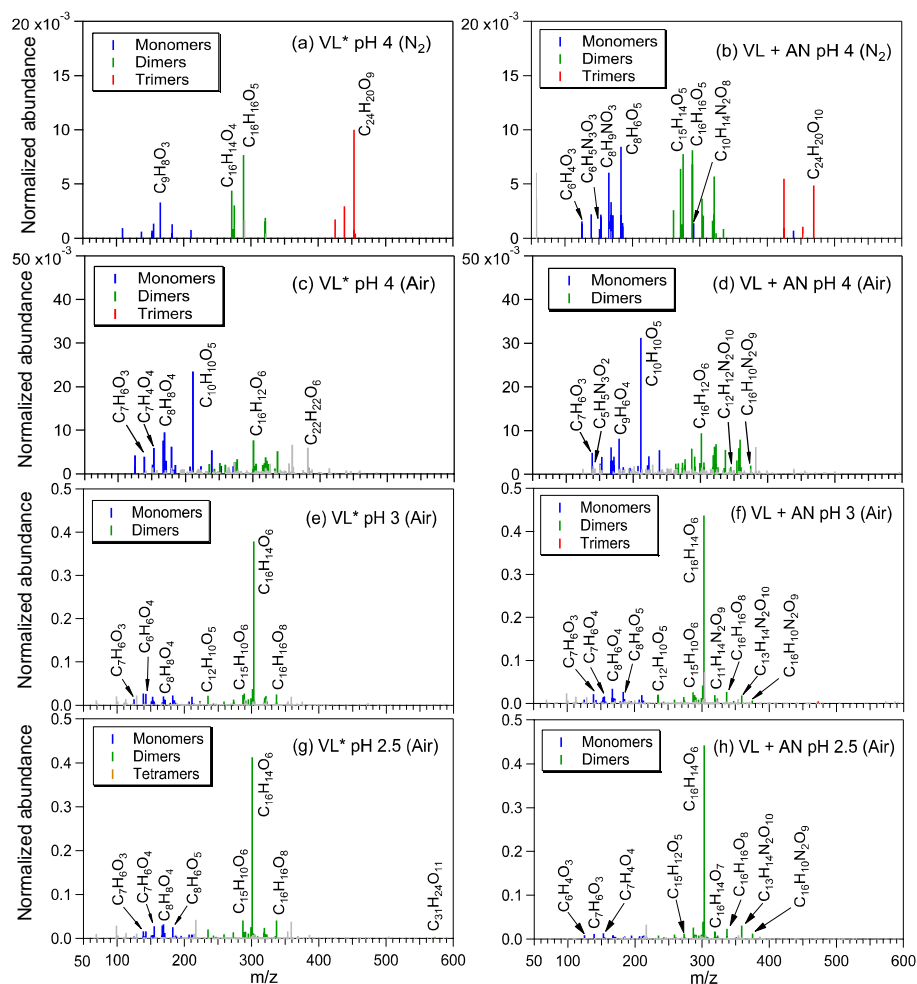
Figure 1. Reconstructed mass spectra of assigned peaks from (a) VL* pH 4 (N$_2$-saturated; A6), (b) VL+AN pH 4 (N$_2$-saturated; A8), (c) VL* pH 4 (air-saturated; A5), (d) VL+AN pH 4 (air-saturated; A7), (e) VL* pH 3 (air-saturated; A3), (f) VL+AN pH 3 (air-saturated; A4), (g) VL* pH 2.5 (air-saturated; A1), and (h) VL+AN pH 2.5 (air-saturated; A2) after 6 h of simulated

1307 sunlight irradiation. The normalized abundance of products was calculated using ~~from the ratio of the peak area of the product~~
1308 ~~to that of VL~~ (Eq. 2~~)~~. The 50 most abundant products contributed more than half of the total normalized abundance of products,
1309 and they were identified as monomers (blue), dimers (green), trimers (red), and tetramers (orange). Grey peaks denote peaks
1310 with low abundance or unassigned formula. Examples of high-intensity peaks were labeled with the corresponding neutral
1311 formulas. Note the different scales on the y-axes.
1312
1313
1314
1315
1316
1317
1318
1319
1320
1321
1322
1323
1324
1325
1326
1327
1328
1329

1330
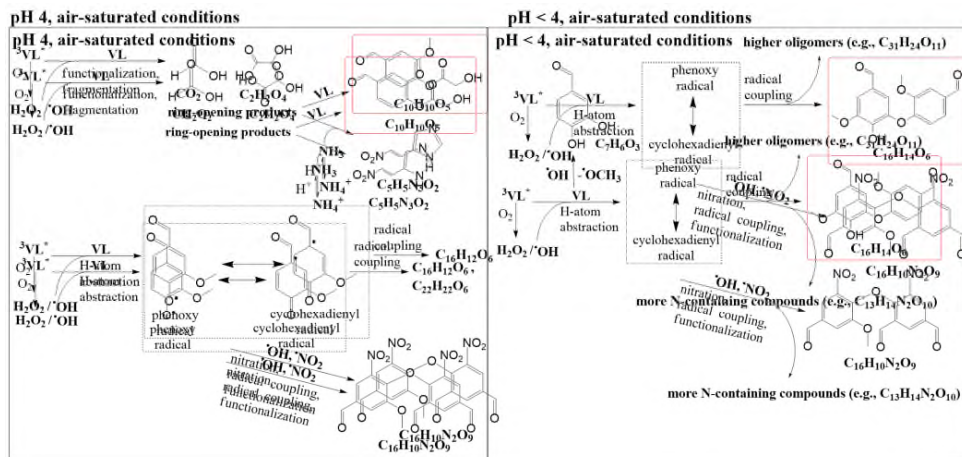
1331
1332
1333
1334 **Figure 2.** Potential aqSOA formation pathways via the direct photosensitized oxidation of VL in the absence (VL*) and
1335 presence of and ammonium nitrate (VL+AN) mediated VL photo oxidation at pH 4 and pH < 4 under air-saturated conditions.
1336 Product structures were proposed based on the molecular formulas, DBE values, and MS/MS fragmentation patterns. The
1337 molecular formulasstructures presented were the major products detected using UHPLC-qToF-MS in positive ESI mode. The
1338 highlighted structures are the most abundant product for each condition.

1339
1340
1341
1342
1343
1344
1345
1346
1347
1348
1349
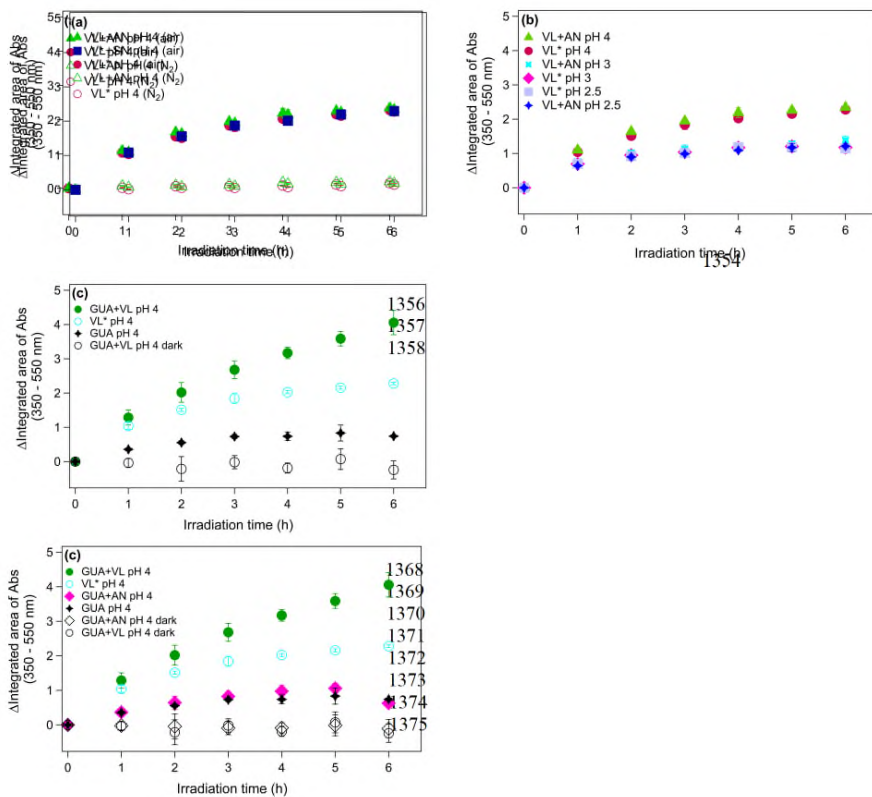
Figure 3. (a–c) Increase in light absorption under different experimental conditions for direct photosensitized oxidation of VL in the absence (VL*) and ~~nitrate-mediated VL photo-oxidation~~ presence of ammonium nitrate (VL+AN): (a) VL* and VL+AN at pH 4 under N_2- (A6, A8) and air-saturated (A5, A7) conditions. Direct photosensitized oxidation of VL in the presence of sodium nitrate (VL+SN) at pH 4 under air-saturated condition (A9). (b) Effect of pH on VL* and VL+AN at pH 2.5 (A1, A2), 3 (A3, A4), and 4 (A5, A7) under air-saturated conditions. ——(c) Increase in light absorption during direct GUA

40

1385 photodegradation (A13) and ~~photo-~~oxidation of GUA ~~in the presence of VL~~via photosensitized reactions of VL (GUA+VL;
1386 A14) ~~or nitrate (GUA+AN; A15)~~ at pH 4 under air-saturated conditions after 6 h of simulated sunlight irradiation. Error bars
1387 represent one standard deviation; most error bars are smaller than the markers.
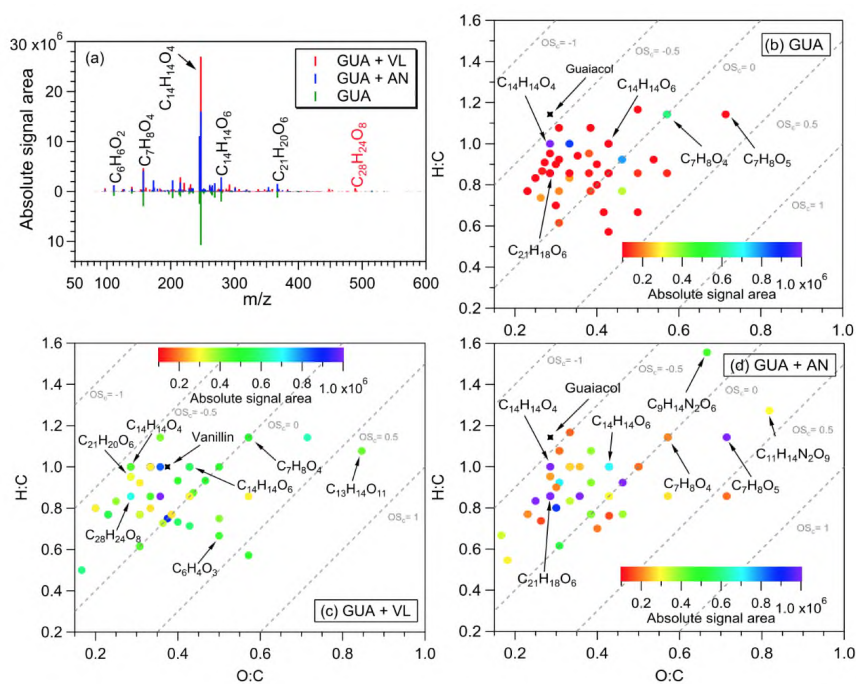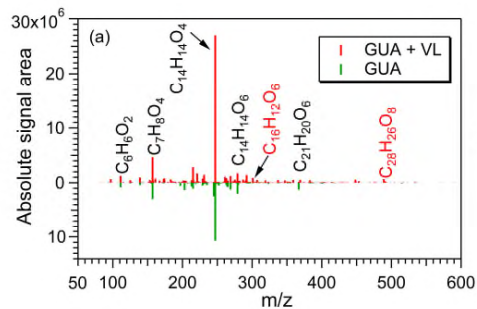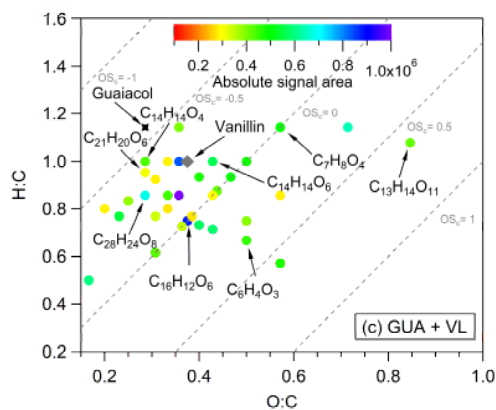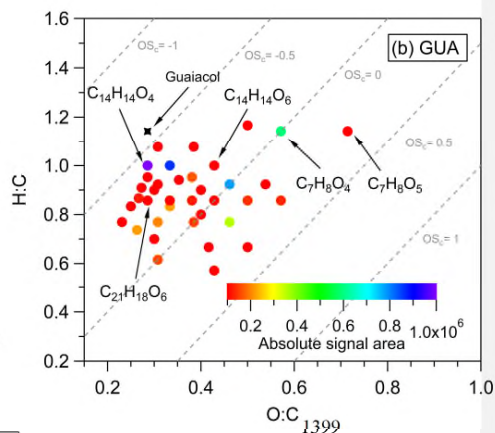
Figure 4. (a) Reconstructed mass spectra of assigned peaks from the direct GUA photodegradation (A13) and ~~photo-~~oxidation of GUA <u>via photosensitized reactions</u> ~~in the presence~~ of VL (GUA+VL; A14) ~~or nitrate (GUA+AN; A15)~~ at pH 4 under air-saturated conditions after 6 h of simulated sunlight irradiation. The y-axis is the absolute signal area of the products. Examples of high-intensity peaks were labeled with the corresponding neutral formulas. <u>The formulas in red text correspond to products observed only from GUA+VL.</u> (b-c~~d~~) van Krevelen diagrams of the 50 most abundant products from the (b) direct photodegradation of GUA (A13) <u>and</u> ~~,~~ (c) GUA+VL (A14) ~~, and (d) GUA+AN (A15)~~ at pH 4 under air-saturated conditions

1419   after 6 h of simulated sunlight irradiation. The color bar denotes the absolute signal area. The grey dashed lines indicate the

1420   carbon oxidation state values (e.g., OS_c =-1, 0, and 1).
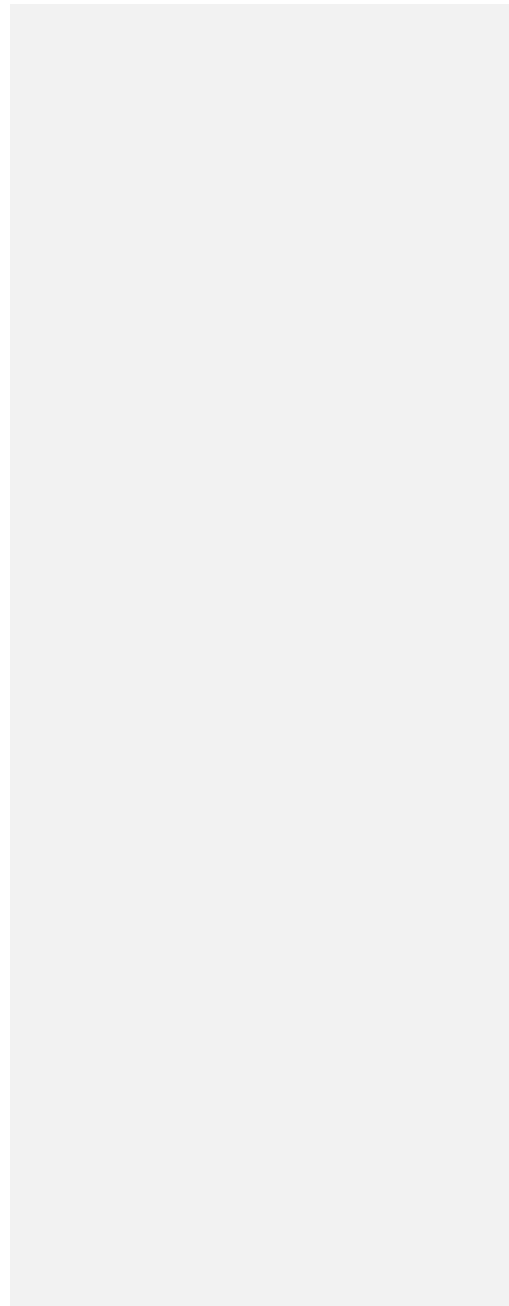
1 **Supplementary material**

2

3 **Aqueous SOA formation from the direct photosensitized
4 oxidation of vanillin in the absence and presence of ammonium
5 nitrate<s style="color:red">: Direct photosensitized reactions and nitrate-mediated</s>
6 <s style="color:red">reactions</s>**

7

8 Beatrix Rosette Go Mabato[1], Yan Lyu[1], Yan Ji[1], Yong Jie Li[2], Dan Dan Huang[3], Xue Li[4], Theodora

9 Nah[1], Chun Ho Lam[1], and Chak K. Chan[1]*

10

11 [1]School of Energy and Environment, City University of Hong Kong, Hong Kong, China

12 [2]Department of Civil and Environmental Engineering, and Centre for Regional Ocean, Faculty of

13 Science and Technology, University of Macau, Macau, China

14 [3]Shanghai Academy of Environmental Sciences, Shanghai 200233, China

15 [4]Institute of Mass Spectrometry and Atmospheric Environment, Jinan University No. 601

16 Huangpu Avenue West, Guangzhou 510632, China

17

18 *Correspondence to*: Chak K. Chan (Chak.K.Chan@cityu.edu.hk)

19

20

21

22

23

24

25

Text S1. Materials.

Initial solutions of 0.1 mM vanillin (VL, Acros Organics, 99%, pure), 0.1 mM guaiacol (GUA,

Sigma Aldrich, $\geq$ 98.0%), 1 mM ammonium nitrate (AN, Acros Organics, 99+%, for analysis),

and 1 mM sodium nitrate (SN, Sigma-Aldrich, $\geq$ 99.5%) were prepared in Milli-Q water. The pH

values of the samples were adjusted using sulfuric acid (H_2SO_4; Acros Organics, ACS reagent, 95%

solution in water).

Text S2. UV-Vis spectrophotometric analyses.

The absorbance changes for all samples were characterized using a UV-Vis

spectrophotometer (UV-3600, Shimadzu Corp., Japan). The absorbance values from 200 to 700

nm were recorded instantly after sample collection, and measurements were done in triplicate.

Absorbance enhancements were calculated as the change in the integrated area of absorbance from

350 to 550 nm. The increase of light absorption at this wavelength range, where VL and GUA did

not initially absorb light, suggests the formation of light-absorbing compounds (Zhou et al., 2019).

Text S3. UHPLC-PDA analyses.

An ultra-high performance liquid chromatography system (UHPLC, Waters Acquity H-

Class, Waters, Milford, USA) coupled to a photodiode array (PDA) detector (Waters, Milford,

USA) was used for the quantification of VL and GUA concentrations. The drawn solutions were

first filtered through a 0.2 μm Chromafil ®Xtra PTFE filter (Macherey-Nagel GmbH & Co. KG,

Germany). Briefly, the separation of products was performed using an Acquity HSS T3 column

(1.8 μm, 2.1 mm × 100 mm; Waters Corp.). The column oven was held at 30 ℃, and the

autosampler was cooled at 4 ℃. The injection volume was set to 5 μL. The binary mobile phase

52 consisted of A (water) and B (acetonitrile). The gradient elution was performed at a flow rate of

53 0.2 mL/min: 0–1 min, 10% eluent B; 1–25 min, linear increase to 90% eluent B; 25–29.9 min,

54 hold 90% eluent B; 29.9–30 min, decrease to 10% eluent B; 30–35 min, re-equilibrate at 10%

55 eluent B for 5 min. Standard solutions of VL and GUA ranging from 10 to 130 µM were analyzed

56 along with samples and blanks using the channels with UV absorption at 300 and 274 nm,

57 respectively. The calibration curves for VL and GUA standard solutions are shown in Figure S2.

58
59 **Text S4.** IC analyses of small organic acids.
60
61   The small organic acids were analyzed using an ion chromatography system (IC, Dionex

62 ICS-1100, Sunnyvale, CA) equipped with a Dionex AS-DV autosampler (Sunnyvale, CA). The

63 separation was achieved using an IonPac^{TM} AS15 column (4 × 250 mm) with an AG15 guard

64 column (4 × 50 mm). The isocratic gradient was applied at a flow rate of 1.2 mL/min with 38 mM

65 sodium hydroxide (NaOH) as the eluent. The total run time was set at 20 min. The standard

66 solutions (1–50 µM) of formic, succinic, and oxalic acid were analyzed three times along with the

67 samples and water blank. Formic, succinic, and oxalic acid had retention times of 3.6 min, 8.3 min,

68 and 11.9 min, respectively.

69
70 **Text S5.** UHPLC-qToF-MS analyses.
71
72   The characterization of reaction products was performed using a UHPLC system

73 (ExionLC^{TM} AD, ABSciex, Concord, Canada) coupled to a quadrupole time-of-flight mass

74 spectrometer (qToF-MS) (TripleTOF 6600+, ABSciex). The settings (e.g., column, mobile phase,

75 gradient, oven temperature) in the UHPLC system were the same as those used in UHPLC-PDA

76 (Text S3). The mass spectrometer was equipped with an electrospray ionization (ESI) source and

77 operated in the positive ion mode (the negative ion mode signals were too low for our analyses) at

78 a resolving power (full width at half-maximum (fwhm) at m/z 300) of 30000 in MS and 30000 in

79 MS/MS (high-resolution mode). Information-dependent acquisition (IDA) scanning was adapted

80 for product identification. The acquisition using IDA consisted of a ToF-MS scan and information-

81 dependent trigger events. The ToF-MS scan had an accumulation time of 250 ms and covered a

82 mass range of m/z 30–700 with a declustering potential (DP) of 40 and collision energy (CE) of

83 10 eV. The accumulation time for the IDA experiment was 100 ms, and the MS/MS scan range

84 was set from m/z 30–700 in high-resolution mode. The IDA criteria were as follows: 5 most intense

85 ions (number of IDA experiments) with an intensity threshold above 50 cps, isotope exclusion was

86 switched off, and dynamic background subtraction was switched on. The automated calibration

87 device system (CDS) was set to perform an external calibration every four samples. The ESI source

88 conditions were as follows: temperature, 500 °C; curtain gas (CUR), 25 psi; ion source gas 1 at 50

89 psi; ion source gas 2 at 50 psi; and ion-spray voltage floating (ISVF) at 4.5 kV.

90   All parameters in the liquid chromatography system and mass spectrometer were controlled

91 using Analyst TF Software 1.8 (ABSciex). The high-resolution LC-MS data were processed with

92 PeakView and Analyst in the SCIEX OS software 1.5 (ABSciex). Peaks from the blank sample

93 were subtracted from the sample signals. In addition to a minimum signal-to-noise ratio of 30, a

94 peak was determined as a product if the difference in peak area between the samples before and

95 after irradiation is ≥ 10 times. The formula assignments were carried out using the MIDAS

96 molecular formula calculator (http://magnet.fsu.edu/~midas/) with the following constraints: C ≤

97 35, H ≤ 70, N ≤ 5, O ≤ 20, Na ≤ 1, and the mass error was initially set a~~ts~~ 10 ppm. The nitrogen

98 atom was removed in the constraints for the experiments without AN or SN. The detected adducts

99 in ESI positive ion mode have several types (e.g., [M+H]$^+$, [M+Na]$^+$), and their formation can be

100 influenced by the sample matrix (Erngren et al., 2019). For simplification purposes, we mainly

101 considered [M+H]$^+$ adducts for formula assignments, except for specific experiments with AN or

102 SN in which [M+NH$_4$]$^+$ adducts and [M+Na]$^+$ adducts were observed. The final assigned formulas

103 were constrained by a mass error of mostly < 5 ppm, which is a requirement for product

104 identification using positive ion mode (Roemmelt et al., 2015). The double bond equivalent (DBE)

105 values and carbon oxidation state (OS$_c$) of the neutral formulas were calculated using the following

106 equations (Koch and Dittmar, 2006):

107 DBE = C − H/2 + N/2 + 1   (Eq. S1)

108 OS$_c$ = 2 × O/C − H/C

109 (Eq. S2)

110

111

112

113 where C, H, O, and N correspond to the number of carbon, hydrogen, oxygen, and nitrogen atoms

114 in the neutral formula, respectively. Based on the identified products, the average oxygen to carbon

115 (O:C) ratios, <O:C>: ($< O:C >= \sum_i(\text{abundance}_i)O_i/\sum_i(\text{abundance}_i)C_i$) and average hydrogen

116 to carbon (H:C) ratios, <H:C>: ($< H:C >= \sum_i(\text{abundance}_i)H_i/\sum_i(\text{abundance}_i)C_i$) after the

117 reactions were further estimated using the signal-weighted method (Bateman et al., 2012). The

118 average OS$_c$ (<OS$_c$>) was calculated as follows:

119 <OS$_c$> = 2 × <O:C> − <H:C>   (Eq. S3)

120

121 Based on the typical MS/MS fragmentation behavior for individual functional groups (Table S1)

122 and DBE values, examples of structures for products detected~~identified~~ from VL (and GUA)

123 photo-oxidation experiments were proposed (Table S2).

124

Text S6. Photon flux measurements.

126

In this work, 2-nitrobenzaldehyde (2NB), a chemical actinometer, was used to determine the photon flux in the aqueous photoreactor. Briefly, the photolysis of 50 μM 2NB in the reactor was monitored by determining its concentration every 5 min for a total of 35 min, during which 2NB was almost completely decayed. The concentration of 2NB was measured using UHPLC-PDA, and the settings (e.g., column, mobile phase, gradient, oven temperature) were the same as those for VL decay analysis (Text S3). The channel with UV absorption at 254 nm was used for the quantification of 2NB. The concentration of 2NB in the reactor followed exponential decay, and its decay rate constant was determined using the following equation:

$$ln\left(\frac{[2NB]_t}{[2NB]_0}\right) = -j(2NB) \times t \qquad \text{(Eq. S4)}$$

136

where $[2NB]_t$ and $[2NB]_0$ are the 2NB concentrations at time t and 0, respectively. The calculated 2NB decay rate constant, $j(2NB)$, was 0.0026 s^{-1}. The following equation can also be used to calculate $j(2NB)$:

$$j(2NB) = 2.303 \times (10^3 \text{ cm}^3 \text{ L}^{-1} \times 1 \text{ mol}/N_A \text{ mlc}) \times \Sigma\left(I'_\lambda \times \Delta\lambda \times \varepsilon_{2NB,\lambda} \times \Phi_{2NB}\right) \qquad \text{(Eq. S5)}$$

where N_A is Avogadro's number, I'_λ is the actinic flux (photons cm^{-2} s^{-1} nm^{-1}), $\Delta\lambda$ is the wavelength interval between actinic flux data points (nm), and $\varepsilon_{2NB,\lambda}$ and $\Phi_{2NB,\lambda}$ are the base-10 molar absorptivity (M^{-1} cm^{-1}) and quantum yield (molecule photon^{-1}) for 2NB, respectively. Values of $\varepsilon_{2NB,\lambda}$ (in water) at each wavelength under 298 K and a wavelength-independent Φ_{2NB} value of 0.41 were adapted from Galbavy et al. (2010). Similar to Smith et al. (2014, 2016), we measured the spectral shape of the photon output of our illumination system (i.e., the relative flux at each wavelength) using a high-sensitivity spectrophotometer (Brolight Technology Co. Ltd,

148   Hangzhou, China). Using a scaling factor (SF), this measured relative photon output, $I_\lambda^{\text{relative}}$, is

149   related to I_λ' as follows (Hullar et al., 2020):

150      $I_\lambda' = I_\lambda^{\text{relative}} \times \text{SF}$ (Eq. S6)

151

152

153   Substitution of Eq. S6 into Eq. S5 and rearrangement yields:

154

155

156      $\text{SF} = \dfrac{j(2\text{NB})}{2.303 \times (10^3 \text{ cm}^3 \text{ L}^{-1} \times 1 \text{ mol/N}_A \text{ mlc}) \times \sum(I_\lambda^{\text{relative}} \times \Delta\lambda \times \varepsilon_{2\text{NB},\lambda} \times \Phi_{2\text{NB}})}$ (Eq. S7)

157

158

159

160

161   and substitution of Eq. S6 into Eq. S7 yields:

162

163

164      $I_\lambda' = I_\lambda^{\text{relative}} \dfrac{j(2\text{NB})}{2.303 \times (10^3 \text{ cm}^3 \text{ L}^{-1} \times 1 \text{ mol/N}_A \text{ mlc}) \times \sum(I_\lambda^{\text{relative}} \times \Delta\lambda \times \varepsilon_{2\text{NB},\lambda} \times \Phi_{2\text{NB}})}$ (Eq. S8)

165

166

167   Finally, I_λ' was estimated through Eq. S8. The estimated photon flux in the aqueous reactor is shown

168   in Fig. S1. The actinic flux during a haze event over Beijing (40º N, 116º E) on January 12,

169   2013, at 12:00 pm (GMT+8) (Che et al., 2014) estimated using the National Center for

170   Atmospheric Research —Tropospheric Ultraviolet-Visible (TUV) Radiation Model

171   (http://cprm.acom.ucar.edu/Models/TUV/Interactive_TUV/) is also shown in Figure S2. The

172   parameters used for the Quick TUV calculator were: Overhead Ozone Column: 300 du; Surface

173   Albedo: 0.1; Ground Elevation: 0 km asl; Measured Altitude: 0 km asl; Clouds optical depth: 0,

174   base: 4, top: 5; Aerosols optical depth: 2.5, single scattering albedo: 0.9, Angstrom exponent: 1;

175   Sunlight direct beam, diffuse down, diffuse up: 1; 4 streams transfer model. For clear days, the

176   actinic flux was estimated over Beijing (at the same date and time) using the default parameters.

177

Text S7. Estimation of the apparent quantum efficiency of guaiacol photodegradation.

The apparent quantum efficiency of GUA photodegradation (φ_{GUA}) in the presence of either VL or nitrate during simulated sunlight illumination can be defined as (Anastasio et al., 1996; Smith et al., 2014, 2016):

$$\Phi_{GUA} = \frac{\text{mol GUA destroyed}}{\text{mol photons absorbed}} \hspace{4cm} \text{(Eq. S9)}$$

Φ_{GUA} was calculated using the measured rate of GUA decay and rate of light absorption by either VL or nitrate through the following equation:

$$\Phi_{GUA} = \frac{\text{rate of GUA decay}}{\text{rate of light absorption by VL or nitrate}} = \frac{k'_{GUA} \times [GUA]}{\sum [(1-10^{-\varepsilon_\lambda [C] l}) \times I_\lambda^t]} \hspace{2cm} \text{(Eq. S10)}$$

where k'_{GUA} is the pseudo-first-order rate constant for GUA decay, [GUA] is the concentration of GUA (M), ε_λ is the base-10 molar absorptivity ($M^{-1} \cdot cm^{-1}$) of VL or nitrate at wavelength λ, [C] is the concentration of VL or nitrate (M), l is the pathlength of the illumination cell (cm), and I'_λ is the volume-averaged photon flux (mol-photons $L^{-1} \cdot s^{-1} \cdot nm^{-1}$) determined from 2NB actinometry:

$$j(2NB) = 2.303 \times \Phi_{2NB} \times l \times \sum_{300\,nm}^{350\,nm} (\varepsilon_{2NB,\lambda} \times I'_\lambda \times \Delta\lambda) \hspace{2cm} \text{(Eq. S11)}$$

202

203

204

Table S1. Typical fragmentation behavior observed in MS/MS spectra for individual functional groups from Holčapek et al. (2010).
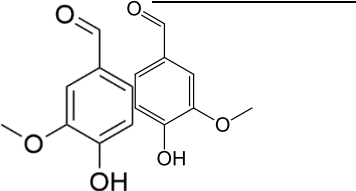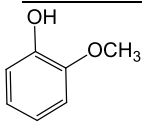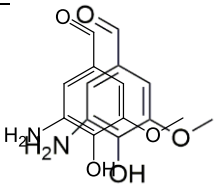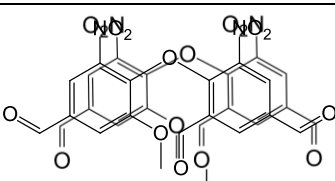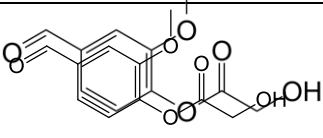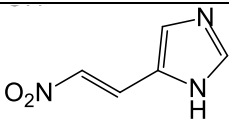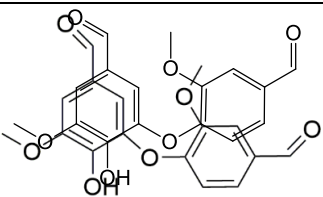
Functional group	Fragment ions	MS/MS loss
Nitro (RNO_2)	$[M+H-OH]^{+\bullet}$	-OH
	$[M+H-H_2O]^+$	$-H_2O$
	$[M+H-NO]^{+\bullet}$	-NO
	$[M+H-NO_2]^{+\bullet}$	$-NO_2$
Nitroso (RNO)	$[M+H-NO]^+$	-NO
Carboxylic acid (ROOH)	$[M+H-H_2O]^+$	$-H_2O$
	$[M+H-CO_2]^+$	$-CO_2$
	$[M+H-H_2O-CO]^+$	$-H_2O-CO$
Phenol (ROH)	$[M+H-H_2O]^+$	$-H_2O$
	$[M+H-CO]^+$	-CO
Methoxy ($ROCH_3$)	$[M+H-CH_3]^{+\bullet}$	$-CH_3$
	$[M+H-CH_3O]^{+\bullet}$	$-CH_3O$
	$[M+H-CH_3OH]^+$	$-CH_3OH$
	$[M+H-HCOH]^+$	-HCOH
Ester (R^1COOR^2)	$[M+H-R^2OH]^+$	$-R^2OH$
	$[M+H-R^2OH-CO]^+$	$-R^2OH-CO$
Amine	$[M+H-NH_3]^+$	$-NH_3$
Aldehyde (RCHO)	$[M+H-CO]^+$	-CO

221

222

223

224

225

226

227

228

229

230
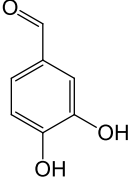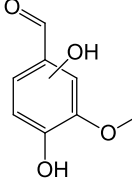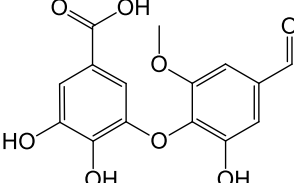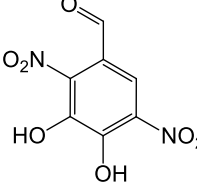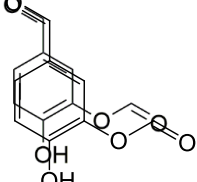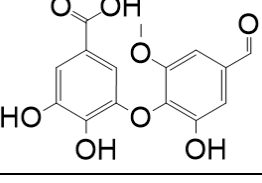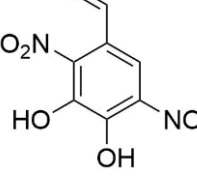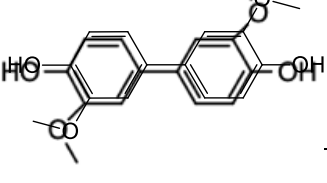
231
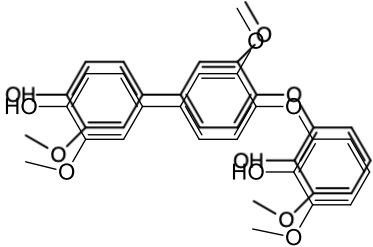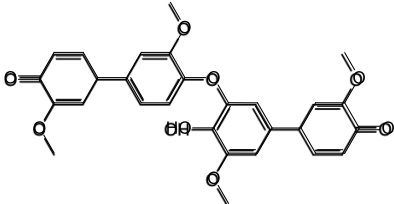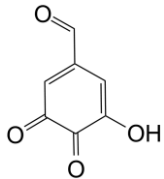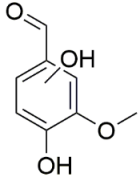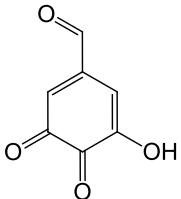
232

233

234 **Table S2.** Examples of proposed ~~molecular~~ structures for products <u>detected</u> ~~identified~~ from
235 vanillin (and guaiacol) -photo-oxidation experiments in this study.

236
237

No.	Formula	DBE	Proposed structure	MS/MS fragment ions		
1	$C_8H_8O_3$ (VL; <u>triplet and</u>~~the~~ aqSOA precursor)	5		-CO-CH$_3$OH	-CO	-CO-CH$_3$OH-CO
<u>2</u>	<u>$C_7H_8O_2$ (GUA; aqSOA precursor)</u>	<u>4</u>				
<u>3</u>~~2~~	$C_8H_9NO_3$	5		-CO-CH$_3$	-NH$_3$	
<u>4</u>~~3~~	$C_{16}H_{10}N_2O_9$	13		-NO$_2$		
<u>5</u>~~4~~	$C_{10}H_{10}O_5$	6		-CH$_3$OH	-CH$_3$OH-CO	
6	$C_5H_5N_3O_2$	5		-NH		
<u>7</u>~~6~~	$C_{16}H_{14}O_6$	10		-CO-CH$_3$OH-CO	-CO-CH$_3$OH-CO-CH$_3$OH	-CO-CH$_3$OH-CO-CO

S10

8	$C_7H_6O_3$	5				
9	$C_8H_8O_4$	5		-CO-CH$_3$OH	-CO	-H$_2$O
10	$C_{15}H_{12}O_8$	10		-COOH		
11	$C_7H_4N_2O_7$	7				
12~~7~~	$C_8H_6O_4$	6		-CO	-CO-CO	
~~8~~	~~$C_{15}H_{12}O_8$~~	~~10~~		~~-COOH~~		
~~9~~	~~$C_7H_4N_2O_7$~~	~~7~~				
13~~0~~	$C_{14}H_{14}O_4$	8				

14	$C_{21}H_{20}O_6$	12				
15	$C_{28}H_{26}O_8$	16				
~~13~~	~~$C_7H_4O_4$~~	~~6~~		~~-CO~~	~~-CO-CO~~	
~~14~~	~~$C_8H_8O_4$~~	~~5~~		~~-CO-CH_3OH~~	~~-CO~~	~~-H_2O~~
16	$C_7H_4O_4$	6		-CO	-CO-CO	

238
239
240
241
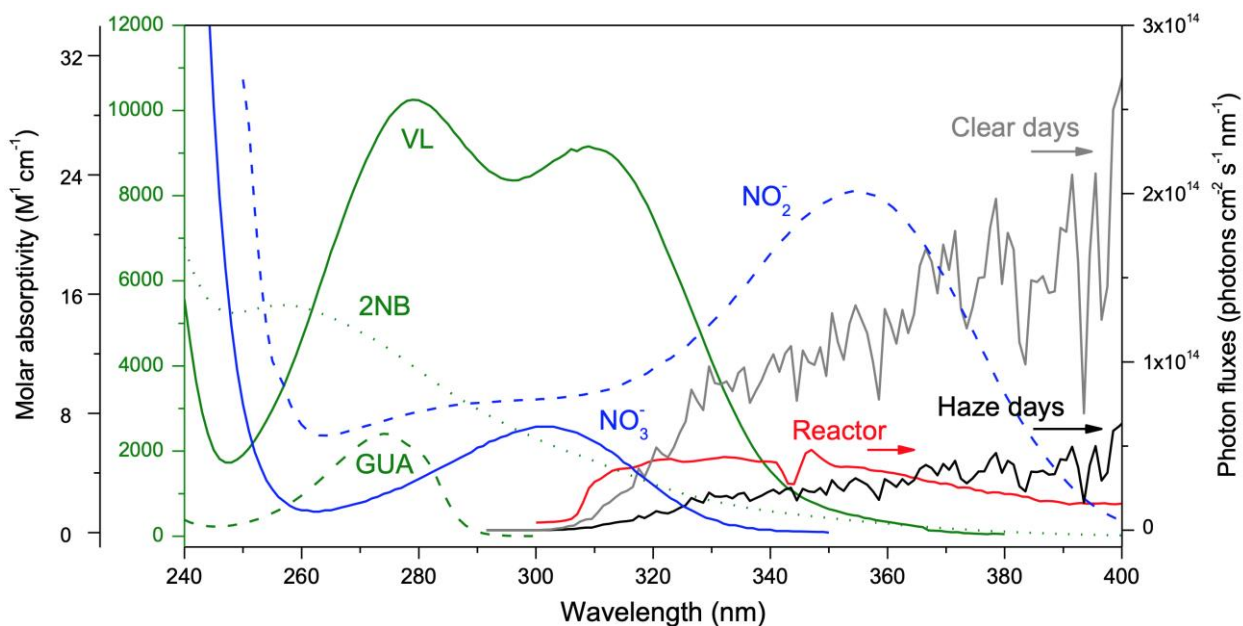
Figure S1. The base-10 molar absorptivities (ε, M^{-1} cm^{-1}) of vanillin (VL, green solid line), 2-nitrobenzaldehyde (2NB, green dotted line), guaiacol (GUA, green dashed line), NO$_2^-$ (blue dashed line), NO$_3^-$ (blue solid line), and photon flux in the aqueous reactor (red line) during typical haze days (black line) or clear days (grey line) in Beijing, China. The ε values for 2NB and NO$_2^-$ were adapted from Galbavy et al. (2010) and Chu and Anastasio (2007), respectively.

247

248
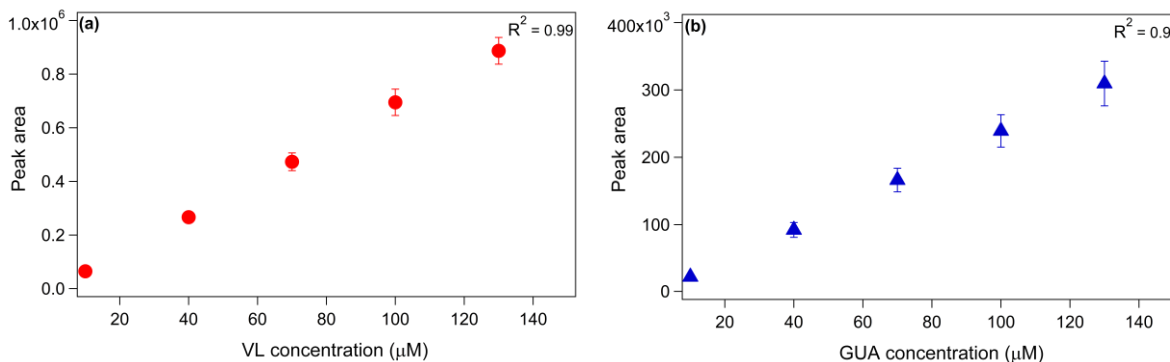
251
252

Figure S2. Calibration curves for (a) VL and (b) GUA standard solutions (10–130 µM). Error bars represent one standard deviation.

255

256

257

258

259

260

261

262

263

264

265

266

267

268

269

270

271
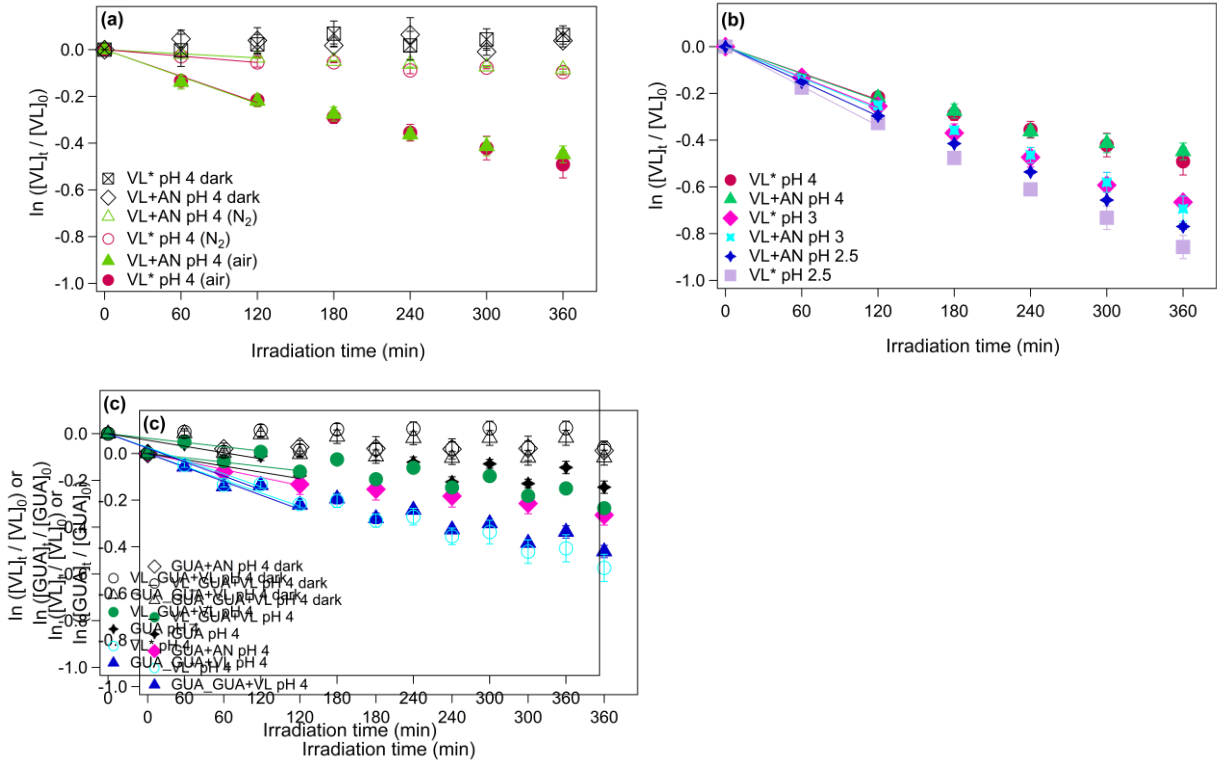
272 **Figure S3.** (a–c) The decay of VL under different experimental conditions for direct
273 photosensitized oxidation of VL in the absence (VL*) and presence of ammonium nitrate mediated
274 VL photo-oxidation (VL+AN): (a) VL* and VL+AN at pH 4 under N_2- (A6, A8) and air-saturated
275 (A5, A7) conditions. No statistically significant difference ($p > 0.05$) was noted between VL+AN
276 (A7) and VL+SN (A9; not shown here). (b) Effect of pH on VL* and VL+AN at pH 2.5 (A1, A2),
277 3 (A3, A4), and 4 (A5, A7) under air-saturated conditions. (c) The decay of VL (and GUA) during
278 direct GUA photodegradation (A13) and photo-oxidation of GUA in the presence via
279 photosensitized reactions of VL (GUA+VL; A14) or nitrate (GUA+AN; A15) at pH 4 under air-
280 saturated conditions after 6 h of simulated sunlight irradiation. Error bars represent one standard
281 deviation; most error bars are smaller than the markers.

282

283

284
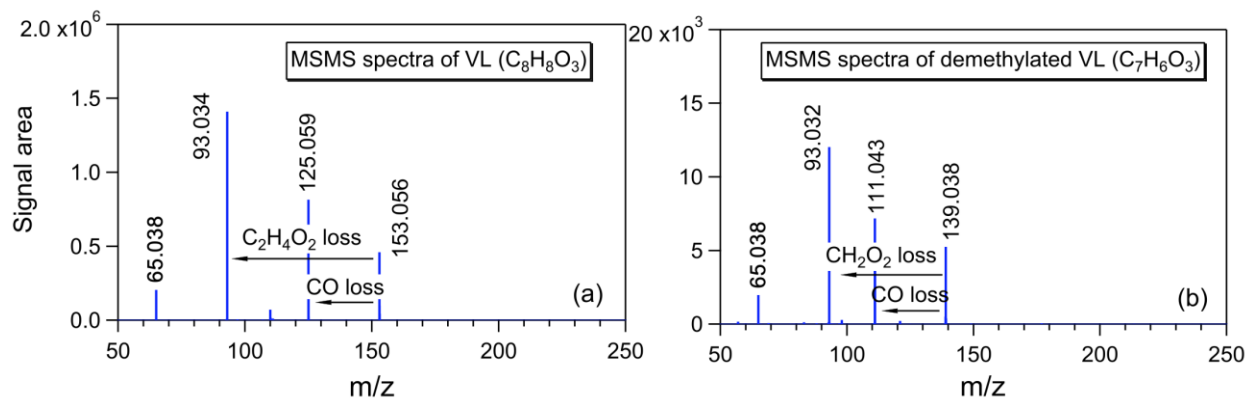
Figure S4. MS/MS spectra of (a) VL and (b) demethylated VL. The arrows indicate possible fragmentation pathways of VL and demethylated VL.

287

288

289
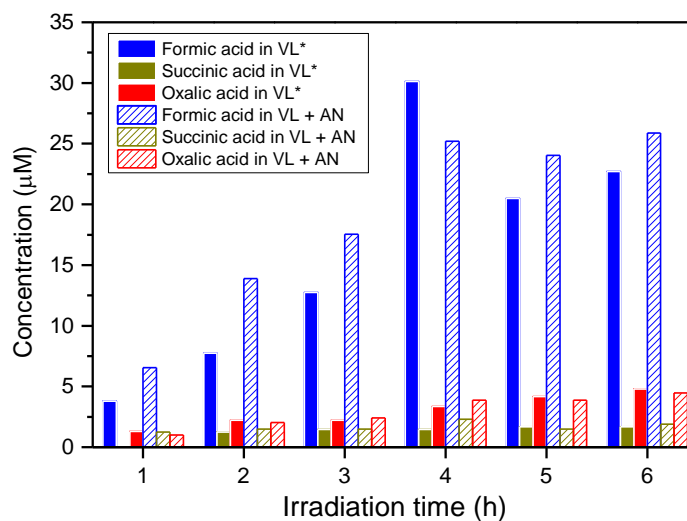
Figure S5. The concentration of formic, oxalic, and succinic acid at different reaction times for VL* (A5) and VL+AN (A7) at pH 4 under air-saturated conditions.

292

293

294
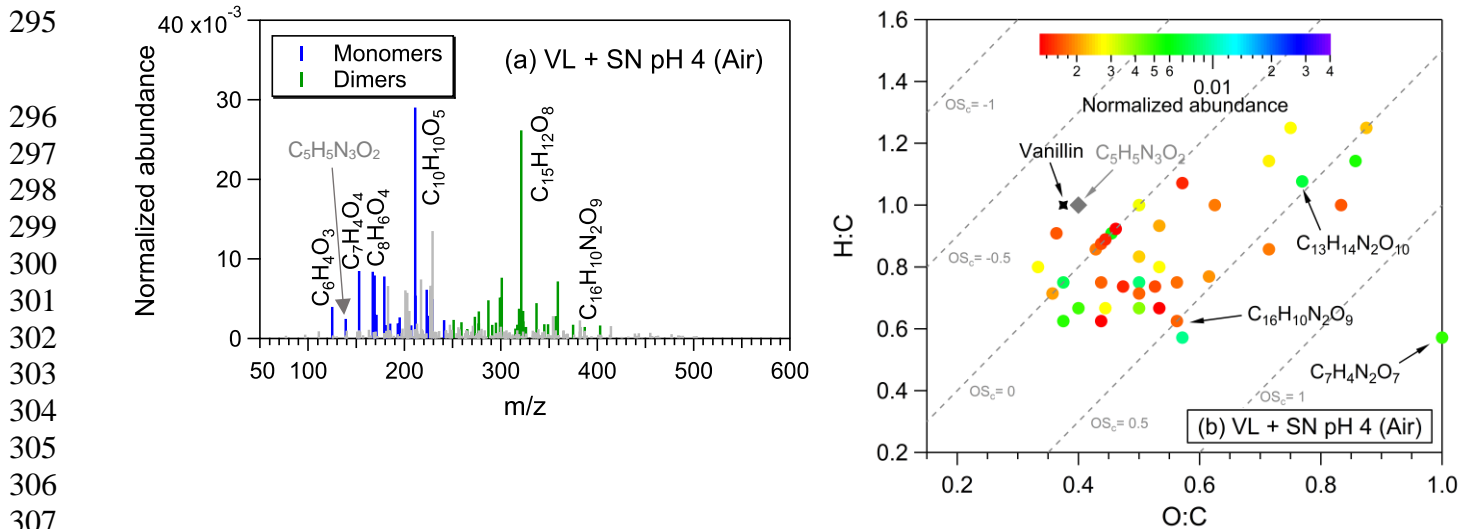
295
296
297
298
299
300
301
302
303
304
305
306
307
308
309
310 **Figure S6.** (a) Reconstructed mass spectra of assigned peaks and (b) van Krevelen diagram of the
311 50 most abundant products from VL+SN (A9) at pH 4 under air-saturated conditions after 6 h of
312 simulated sunlight irradiation. The normalized abundance of products was calculated ~~from the~~
313 ~~ratio of the peak area of the product to that of VL~~using (Eq. 2~~)~~. The 50 most abundant products
314 contributed more than half of the total normalized abundance of products, and they were identified
315 as monomers (blue) and dimers (green). Grey peaks denote peaks with low abundance or
316 unassigned formula. The grey arrows show where the potential imidazole derivative ($C_5H_5N_3O_2$)
317 from VL+AN (A7) was observed. Examples of high-intensity peaks were labeled with the
318 corresponding neutral formulas. The color bar denotes the normalized abundance of products. The
319 grey dashed lines indicate the carbon oxidation state values (e.g., OS_c = -1, 0, and 1). ~~The grey~~
320 ~~arrows show where the potential imidazole derivative ($C_5H_5N_3O_2$) from VL+AN was observed.~~
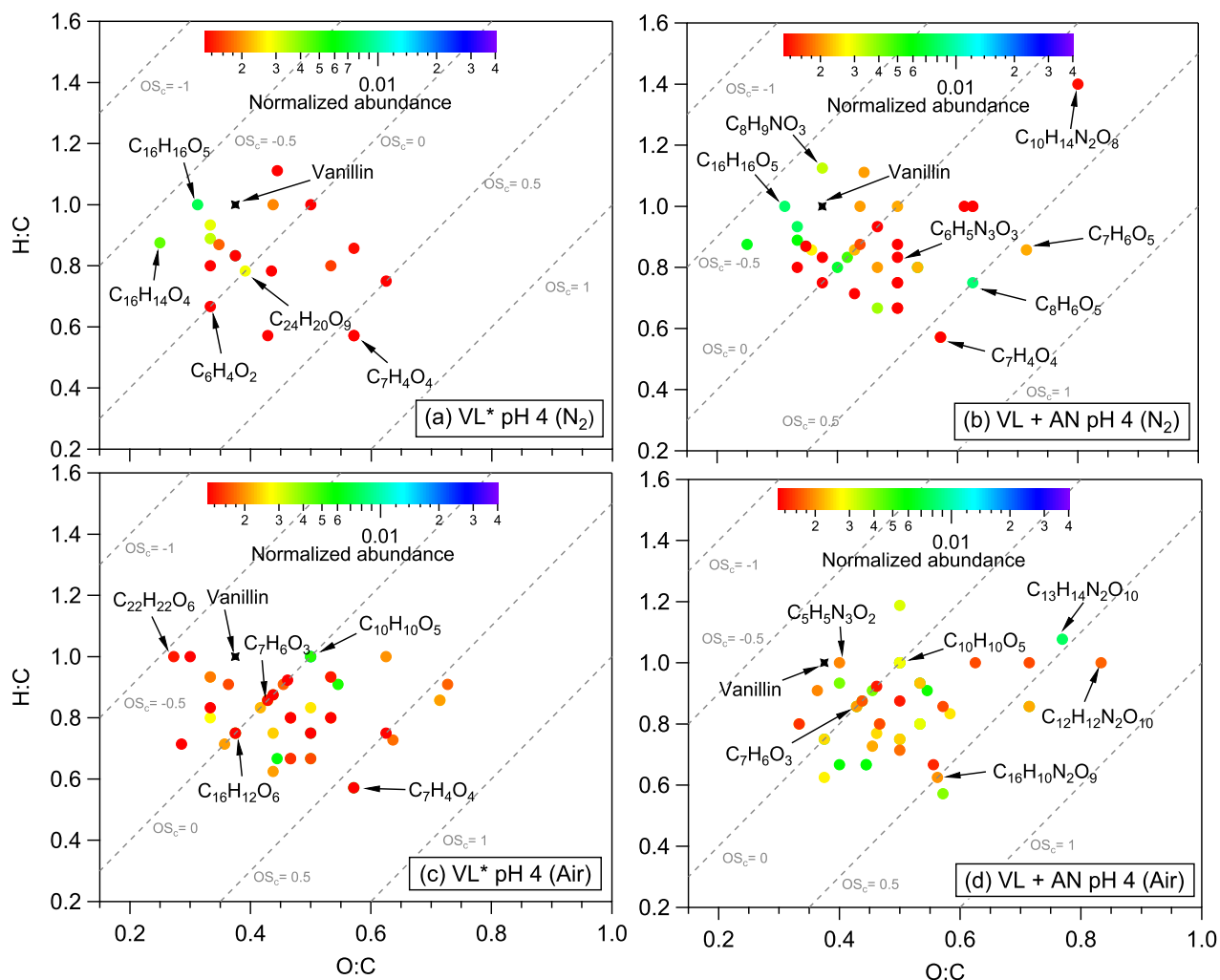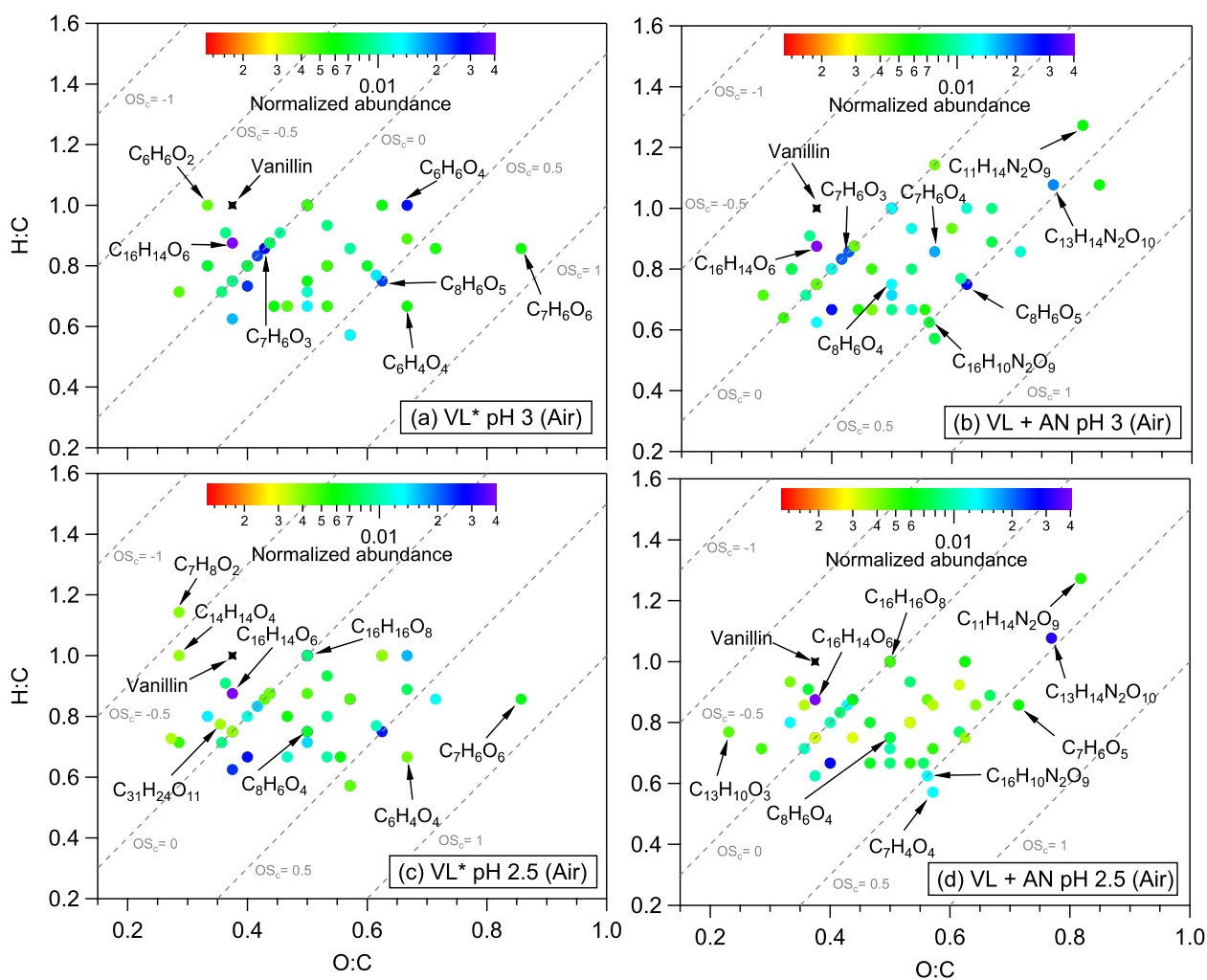
Figure S7. van Krevelen diagrams of the 50 most abundant products from (a) VL* (N_2-saturated; A6), (b) VL+AN (N_2-saturated; A8), (c) VL* (air-saturated; A5), and (d) VL+AN (air-saturated; A7) at pH 4 after 6 h of simulated sunlight irradiation. The color bar denotes the normalized abundance of products. The grey dashed lines indicate the carbon oxidation state values (e.g., OS_c = -1, 0, and 1).

333

334

335

336

337

338

339
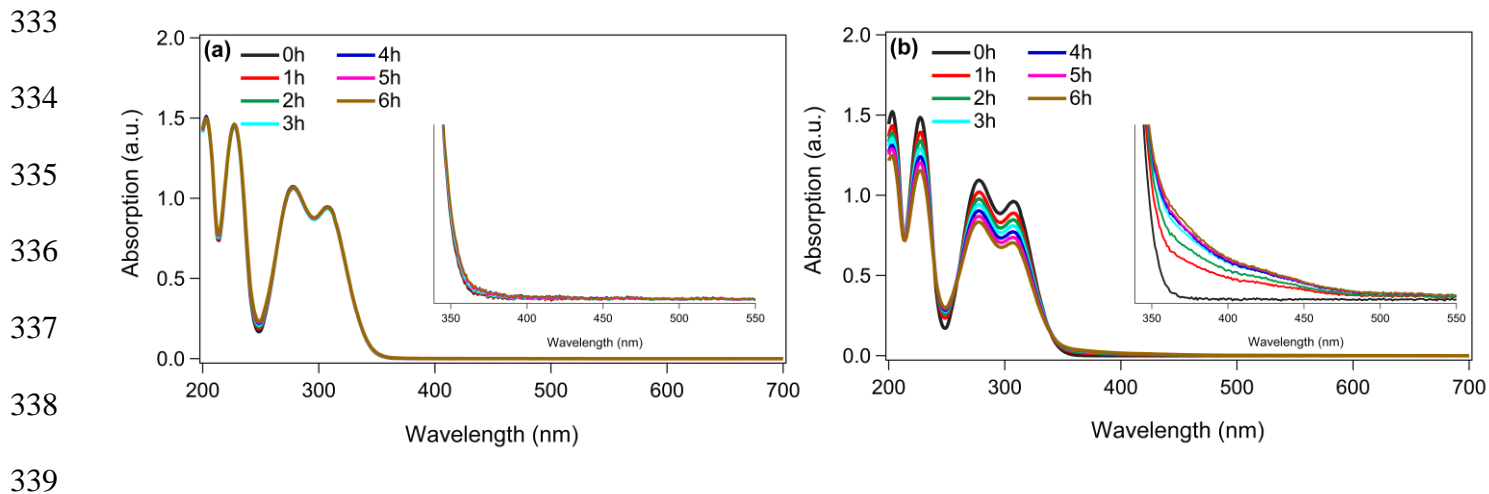
340 **Figure S8.** UV–Vis absorption spectra of VL* (A6, A5; pH 4) under (a) N_2- and (b) air-saturated
341 conditions at different time intervals. The insets show the absorbance enhancement from 350 to
342 550 nm.

343

Figure S9. van Krevelen diagrams of the 50 most abundant products from (a) VL* pH 3 (A3), (b) VL+AN pH 3 (A4), (c) VL* pH 2.5 (A1), and (d) VL+AN pH 2.5 (A2) under air-saturated conditions after 6 h of simulated sunlight irradiation. The color bar denotes the normalized abundance of products. The grey dashed lines indicate the carbon oxidation state values (e.g., OS_c =-1, 0, and 1).
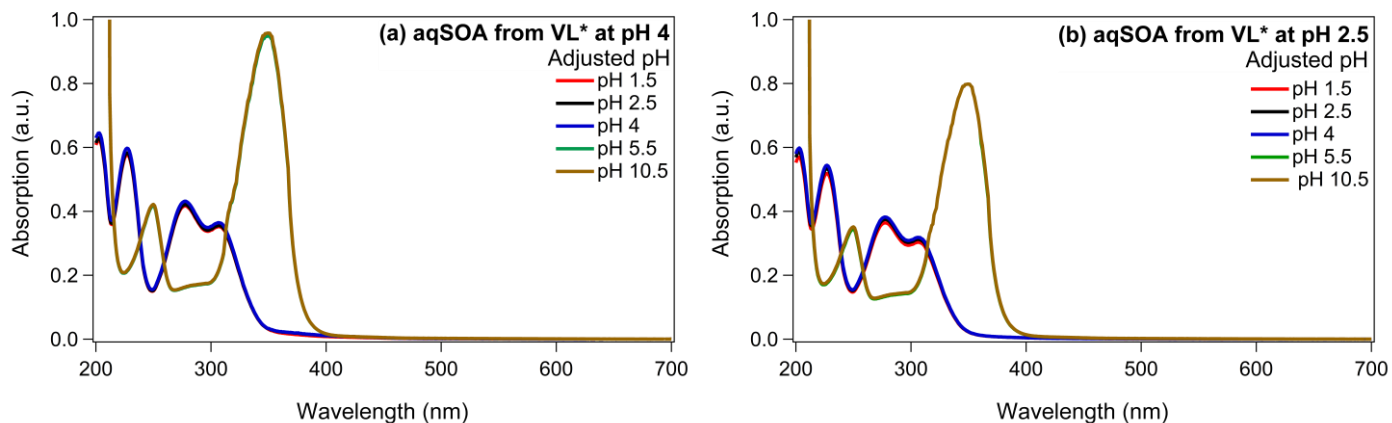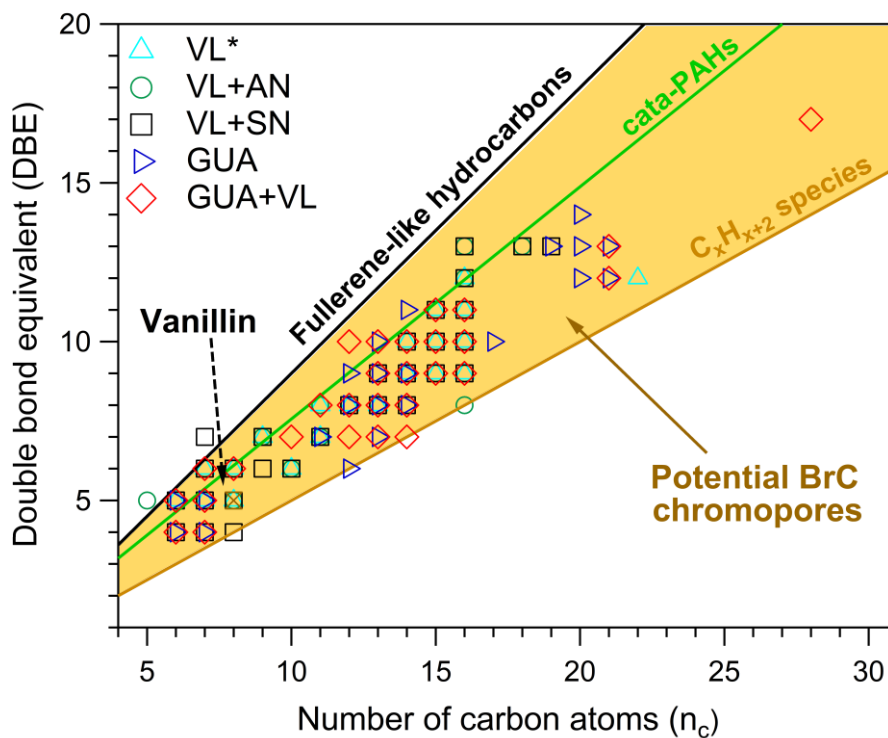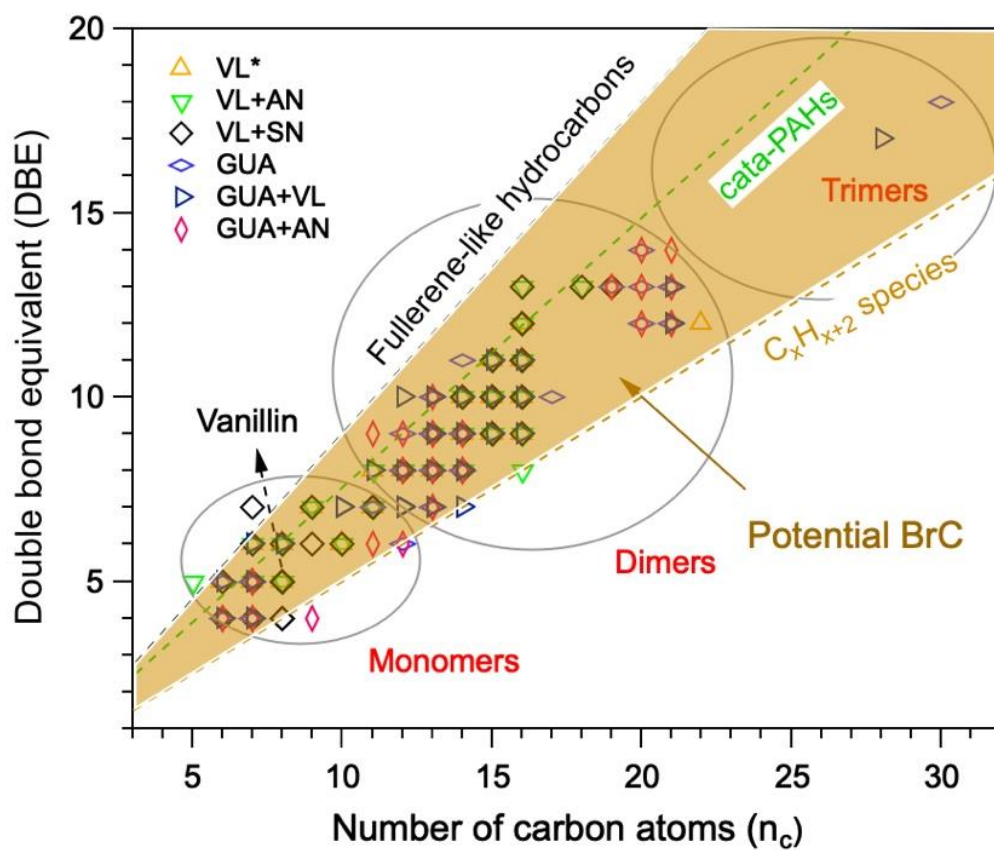
357
358 **Figure S10**. UV–Vis absorption spectra of VL*-derived aqSOA formed at (a) pH 4 and (b) pH 2.5
359 over a range of pH conditions from 1.5 to 10.5.
360
361
362
363
364
365
366
367
368

Figure S11. The plot of the double bond equivalent (DBE) values vs. number of carbon atoms (n_c) (Lin et al., 2018) for the 50 most abundant products from pH 4 experiments under air-saturated

398 conditions. Dashed lines indicate DBE reference values of fullerene-like hydrocarbons (black solid
399 line; Lobodin et al., 2012) (black dashed line), cata-condensed polycyclic aromatic hydrocarbons
400 (PAHs) ((green solid line; Siegmann and Sattler, 2000) (green dashed line), and linear conjugated
401 polyenes (general formula C_xH_{x+2}) (brown dashed solid line). Data points within the shaded area
402 are potential BrC chromophores. Light grey circles show the classification of the data points as
403 monomers, dimers, trimers, or tetramers.
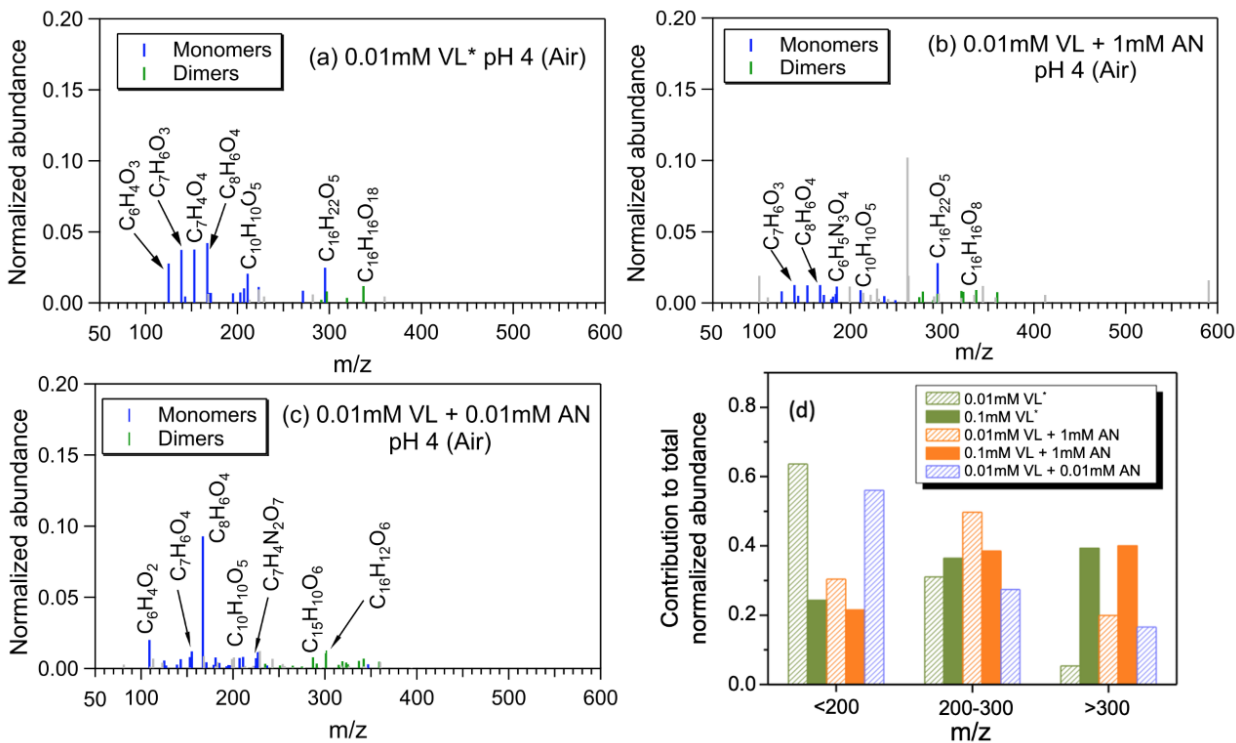
404

405

406 **Figure S12.** Reconstructed mass spectra of assigned peaks from (a) 0.01 mM VL* (A10), (b) 0.01
407 mM VL + 1 mM AN (A121), and (c) 0.01 mM VL + 0.01 mM AN (A112) at pH 4 under air-
408 saturated conditions after 6 h of simulated sunlight irradiation. The normalized abundance of
409 products was calculated from the ratio of the peak area of the product to that of VLusing (Eq. 2).
410 The 50 most abundant products contributed more than half of the total normalized abundance of
411 products, and they were identified as monomers (blue) and dimers (green). Grey peaks denote
412 peaks with low abundance or unassigned formula. Examples of high-intensity peaks were labeled
413 with the corresponding neutral formulas. (d) Contributions of different m/z ranges to the
414 normalized abundance of products from experiments with low [VL] = 0.01 mM (A10–A12) and
415 high [VL] = 0.1 mM (A5 and A7) at pH 4 under air-saturated conditions after 6 h of simulated
416 sunlight irradiation.

417
418
419
420

421
422
423
424
425
426
427
428
429
430
431
432
433
434
435
436
437
438

References

~~Anastasio, C., Faust, B. C., and Rao, C. J.: Aromatic carbonyl compounds as aqueous-phase photochemical sources of hydrogen peroxide in acidic sulfate aerosols, fogs, and clouds. 1. Non-phenolic methoxybenzaldehydes and methoxyacetophenones with reductants (phenols), Environ. Sci. Technol., 31, 218–232, https://doi.org/10.1021/es960359g, 1996.~~

Bateman, A. P., Laskin, J., Laskin, A., and Nizkorodov, S. A.: Applications of high-resolution electrospray ionization mass spectrometry to measurements of average oxygen to carbon ratios in secondary organic aerosols, Environ. Sci. Technol., 46, 8315–8324, https://doi.org/10.1021/es3017254, 2012.

Che, H., Xia, X., Zhu, J., Li, Z., Dubovik, O., Holben, B., Goloub, P., Chen, H., Estelles, V., Cuevas-Agulló, E., Blarel, L., Wang, H., Zhao, H., Zhang, X., Wang, Y., Sun, J., Tao, R., Zhang, X., and Shi, G.: Column aerosol optical properties and aerosol radiative forcing during a serious haze-fog month over North China Plain in 2013 based on ground-based sunphotometer measurements, Atmos. Chem. Phys., 14, 2125–2138, https://doi.org/10.5194/acp-14-2125-2014, 2014.

Chu, L. and Anastasio, C.: Temperature and wavelength dependence of nitrite photolysis in frozen and aqueous solutions, Environ. Sci. Technol., 41, 3626–3632, https://doi.org/10.1021/es062731q, 2007.

Erngren, I., Haglöf, J., Engskog, M. K. R., Nestor, M., Hedeland, M., Arvidsson, T., and Pettersson, C.: Adduct formation in electrospray ionisation-mass spectrometry with hydrophilic interaction liquid chromatography is strongly affected by the inorganic ion concentration of the samples, J. Chromatogr. A, 1600, 174–182, https://doi.org/10.1016/j.chroma.2019.04.049, 2019.

466

467 Galbavy, E. S., Ram, K., and Anastasio, C.: 2-Nitrobenzaldehyde as a chemical actinometer for
468 solution and ice photochemistry, J. Photochem. Photobiol. A, 209, 186–192,
469 https://doi.org/10.1016/j.jphotochem.2009.11.013, 2010.

471 Holčapek, M., Jirásko, R., and Lísa, M.: Basic rules for the interpretation of atmospheric pressure
472 ionization mass spectra of small molecules, J. Chromatogr. A, 1217, 3908–3921,
473 https://doi.org/10.1016/j.chroma.2010.02.049, 2010.

475 Hullar, T., Bononi, F. C., Chen, Z., Magadia, D., Palmer, O., Tran, T., Rocca, D., Andreussi, O.,
476 Donadio, D., and Anastasio, C.: Photodecay of guaiacol is faster in ice, and even more rapid on
477 ice, than in aqueous solution, Environ. Sci.: Processes Impacts, 22, 1666–
478 1677, https://doi.org/10.1039/d0em00242a, 2020.

480 Koch, B. P. and Dittmar, T.: From mass to structure: an aromaticity index for high-resolution mass
481 data of natural organic matter, Rapid Commun. Mass Spectrom., 20, 926–932,
482 https://doi.org/10.1002/rcm.2386~~https://doi.org/10.1002/rcm.7433,~~ 2006.

484 Lin, P., Fleming, L. T., Nizkorodov, S. A., Laskin, J., and Laskin, A.: Comprehensive molecular
485 characterization of atmospheric brown carbon by high resolution mass spectrometry with
486 electrospray and atmospheric pressure photoionization, Anal. Chem., 90, 12493–12502,
487 https://doi.org/10.1021/acs.analchem.8b02177, 2018.

489 Lobodin, V. V., Marshall, A. G., and Hsu, C. S.: Compositional space boundaries for organic
490 compounds, Anal. Chem., 84, 3410–3416, https://doi.org/10.1021/ac300244f, 2012.

492 Roemmelt, A. T., Steuer, A. E., and Kraemer, T.: Liquid chromatography, in combination with a
493 quadrupole time-of-flight instrument, with sequential window acquisition of all theoretical
494 fragment-ion spectra acquisition: validated quantification of 39 antidepressants in whole blood as
495 part of a simultaneous screening and quantification procedure, Anal. Chem., 87, 9294–9301,
496 https://doi.org/10.1021/acs.analchem.5b02031, 2015.

498 Siegmann, K. and Sattler, K. ~~D.~~: Formation mechanism for polycyclic aromatic hydrocarbons in
499 methane flames, J. Chem. Phys., 112, 698–709, https://doi.org/10.1063/1.480648, 2000.

501 Smith, J. D., Kinney, H., and Anastasio, C.: Phenolic carbonyls undergo rapid aqueous
502 photodegradation to form low-volatility, light-absorbing products, Atmos. Environ., 126, 36−44,
503 https://doi.org/10.1016/j.atmosenv.2015.11.035, 2016.

506 Smith, J. D., Sio, V., Yu, L., Zhang, Q., and Anastasio, C.: Secondary organic aerosol production
507 from aqueous reactions of 973 atmospheric phenols with an organic triplet excited state, Environ.
508 Sci. Technol., 48, 1049–1057, https://doi.org/10.1021/es4045715, 2014.

510 ~~Smith, J. D., Kinney, H., and Anastasio, C.: Phenolic carbonyls undergo rapid aqueous~~
511 ~~photodegradation to form low-volatility, light-absorbing products, Atmos. Environ., 126, 36−44,~~
512 ~~https://doi.org/10.1016/j.atmosenv.2015.11.035, 2016.~~

513
514 Zhou, W., Mekic, M., Liu, J., Loisel, G., Jin, B., Vione, D., and Gligorovski, S.: Ionic strength
515 effects on the photochemical degradation of acetosyringone in atmospheric deliquescent aerosol
516 particles, Atmos. Environ., 198, 83–88, https://doi.org/10.1016/j.atmosenv.2018.10.047, 2019.